Control of Endocytic Trafficking and Recycling Pathways by Phosphatidylserine in *S. cerevisiae*

by

David G. Sapp

Submitted in partial fulfilment of the requirements
for the degree of Masters of Science

at

Dalhousie University
Halifax, Nova Scotia
June 2024

Dalhousie University is located in Mi'kma'ki, the
ancestral and unceded territory of the Mi'kmaq.
We are all Treaty people.

TABLE OF CONTENTS

List of Tables

List of Figures

Abstract

Phosphatidylserine (PS) is the most abundant anionic phospholipid in cells. Consequently, it plays important roles in intracellular function, including in the endocytic trafficking pathway. Specifically, PS is involved in retrograde transport pathways that facilitate recycling from endosomes to the trans Golgi network (TGN). The role of PS in retrograde transport from early endosomes to TGN has been studied in some detail, however, its role in transport from late endosomes to TGN, a pathway mediated by the retromer complex, has been less well studied. This work characterizes the effects of PS-deficiency in *S. cerevisiae* on proteins involved in retrograde transport from late endosomes to the TGN. Protein localization data show that the retromer system is dysfunctional in PS-deficient cells. Additionally, PS transport and distribution in the cell is largely mediated by the lipid transfer proteins, Osh6 and Osh7. This work characterises the effects of Osh6 and Osh7 on PS distribution and metabolism and shows that there are compensatory mechanisms for distributing PS.

List of Abbreviations Used

ANOVA	Analysis of Variance	Opi	Phospholipid methyltransferase
AP	Adaptor protein	Osh	Oxysterol-binding protein
Atg27	Autophagy related 27	PA	Phosphatidic acid
BAR	Bin-Amphiphysin-Rvs	PBS	Phosphate-buffered saline
Bem1	Bud Emergence 1	PC	Phosphatidylcholine
BSA	Bovine Serum Albumin	PCR	polymerase chain reaction
Can1	Canavanine resistance 1	PDE	Phosphatidyldimethylethanolamine
Cdc42	Cell division cycle 42	PE	Phosphatidylethanolamine
Cho1	Phosphatidylserine synthase	PI	Phosphatidylinositol
Cho2	PE methyltransferase	PM	Plasma membrane
CL	Cardiolipin	PME	Phosphatidylmonomethylethanolamine
CM	Chloroform: methanol	PMSF	phenylmethylsulfonyl fluoride
CPY	Carboxypeptidase Y	PS	Phosphatidylserine
DAG	Diacylglycerol	Pss1	Phosphatidylserine synthase 1
DMSO	Dimethyl sulfoxide	Pss2	Phosphatidylserine synthase 2
DNA	Deoxyribonucleic acid	PVDF	polyvinylidene fluoride
Dnf1	Drs2 Neo1 Family 1/2	PX	Phox homology
Dnf2	Drs2 Neo1 Family 2	RIPA	Radio-Immunoprecipitation Assay
dNTP	Deoxynucleotide triphosphate	SC	synthetic complete
DPM	Disintegrations per minute	Sec1	Secretory 1
Drs2	Deficiency in ribosomal subunits 2	Sec6	Secretory 6
DTT	Dithiothreitol	SNARE	Soluble NSF attachment protein receptor
EDTA	Ethylenediaminetetraacetic acid	Snc1	Suppressor of the Null allele of CAP 1
EE	Early endosomes	SNX-BAR	Sorting Nexin-Bar Domain
EGFR	Epidermal growth factor receptor	SOC	Super Optimal broth with Catabolite repression
ER	Endoplasmic Reticulum	Ste2	Sterile 2
ERMES	ER-mitochondria encounter structure	TAE	Tris-acetate-EDTA
GFP	Green Fluorescent Protein	TBST	Tris buffered saline-Tween
HRP	Horse Radish Protein	TE	Tris-EDTA
Ist2	Increased sodium tolerance protein 2	Tfr	Transferrin receptor
Lact-C2	C2 domain of lactadherin	TGN	Trans Golgi network
LB	Luria Broth	TLC	thin layer chromatography
LDL	Low density lipoprotein	VINE	Vps9 GEF-interacting sorting nexin
Ldlr	Low density lipoprotein receptor	Vps	Vacuolar sorting protein
LE	Late endosomes	Wsc1	Synthetic lethal with GAP 1
LSC	Liquid scintillation counting	WT	Wild type

MAM	Mitochondrial-associated membrane	YPD	Yeast extract-peptone-dextrose
Mrl1	Mannose 6-phosphate Receptor Like 1	YPT	Yeast Protein Two

Acknowledgements

Thank you to all who have helped me through the past two years and in the years before helping to prepare me for an MSc. Thank you to my supervisor, Dr. Gregory Fairn for your support and sharing your depth of knowledge and experience. Similarly, thank you to my committee members who helped guide me through this project. Thank you, the members of my lab, for their support and help wading through all the new techniques and experiment protocols. Thank you Jayatee for sharing the burden of being an MSc student for the past two years. Thank you, Arezoo, for the constant offers of support and the much-needed check-ins. Thank you, Haggag, for your help in the learning process.

Thank you to my family, and especially parents, who offer more support than I manage to accept. Thank you to the friends who spent long hours in the library helping me get through the writing process, especially Emily. Thank you especially to Mitchell who indulges me in just about anything and gets me motivated to do a little better each day. Support from friends and family is how I finished writing this thesis in the tight timeline created by my next step in life.

CHAPTER 1 Introduction

1.1 Composition of eukaryotic membranes

Lipid membranes are a fundamental component of life. In eukaryotic cells, discrete compartments, including the cell itself, and its organelles, are separated by lipid bilayers. Lipid bilayers are primarily comprised of phospholipids, sterols, and proteins. The emergence of subcellular membrane compartments marks a major evolutionary branching point, introducing eukaryotes and facilitating the development of functional complexity (Gould, 2018). The cell membrane has been described by a "mosaic model," which is generally applicable to all cell membranes. This model describes the fluidity and diverse composition of the membrane. While lipid bilayers form semi-permeable barriers that prevent most molecules from crossing (other than small hydrophobic molecules and gases), the components of the membranes themselves diffuse longitudinally. The relative composition of membrane components determines the physical properties and membrane identity of the lipid bilayers (Holthius & Menon, 2014).

Phospholipids are both necessary and sufficient for the formation of a lipid membrane; they self-assemble into a lipid bilayer in an aqueous environment in a process driven by their molecular structure. Phospholipids have fatty acid lipid tails, which aggregate, and polar head groups, which form a surface interacting with aqueous environments. The consequent structure is a lipid bilayer with the polar head groups occluding the lipid tails from water (Wenk. 2005). The two major classes of phospholipids are glycerophospholipids and phosphosphingolipids/sphingomyelins. Glycerophospholipids have a glycerol backbone esterified to fatty acids and a phosphate head group, which may by bound to a defining head group (Shevchenko & Simons. 2010). Similarly, phosphosphingolipids have a ceramide backbone with fatty acid tails and a head group (Quinville *et al*., 2021). The spectrum of phospholipids forms the base of all lipid membranes in eukaryotic cells.

Sterols are another major lipid component of cellular membranes. In vertebrates, cholesterol is the primary sterol component, however, fungi, including *S. cerevisiae*, have ergosterol as the primary sterol component (Zinser *et al*., 1993). Sterols are characterised by a complex structure comprised of four rigid carbon rings with a hydroxyl group on the first ring. Ergosterol is structurally similar to cholesterol, with two additional double bonds and one additional methyl group. It is a hydrophobic molecule that resides in the hydrophilic core of the lipid bilayer. Fundamentally, its roles in lipid membranes are to increase membrane fluidity and to act as a buffer, maintaining membrane fluidity across a range of temperatures.

The protein component of lipid membranes is diverse and membrane specific. The three main classes of membrane proteins are peripheral proteins, monotopic integral membrane proteins, and transmembrane proteins. A membrane protein's characteristics facilitate membrane specific interactions and functions. For example, transmembrane receptor proteins on the plasma membrane (PM) can trigger signaling cascades that result in transcriptional and translational regulation. Membrane associated proteins can also affect the structure, permeability, signaling, and enzymatic activity of membranes.

1.2 GLYCEROPHOSPHOLIPIDS

Glycerophospholipids are the predominant form of phospholipids in yeast membranes. The four main glycerophospholipids in yeast are phosphatidylinositol (PI), phosphatidylethanolamine (PE), phosphatidylcholine (PC), and phosphatidylserine (PS) (Figure 1.1). Each of these glycerophospholipids are derived from phosphatidic acid (PA) (Figure 1.1). The common features of glycerophospholipids are all present in PA. Every glycerophospholipid has a fatty acid tail, a glycerol backbone, and a phosphoester head group.

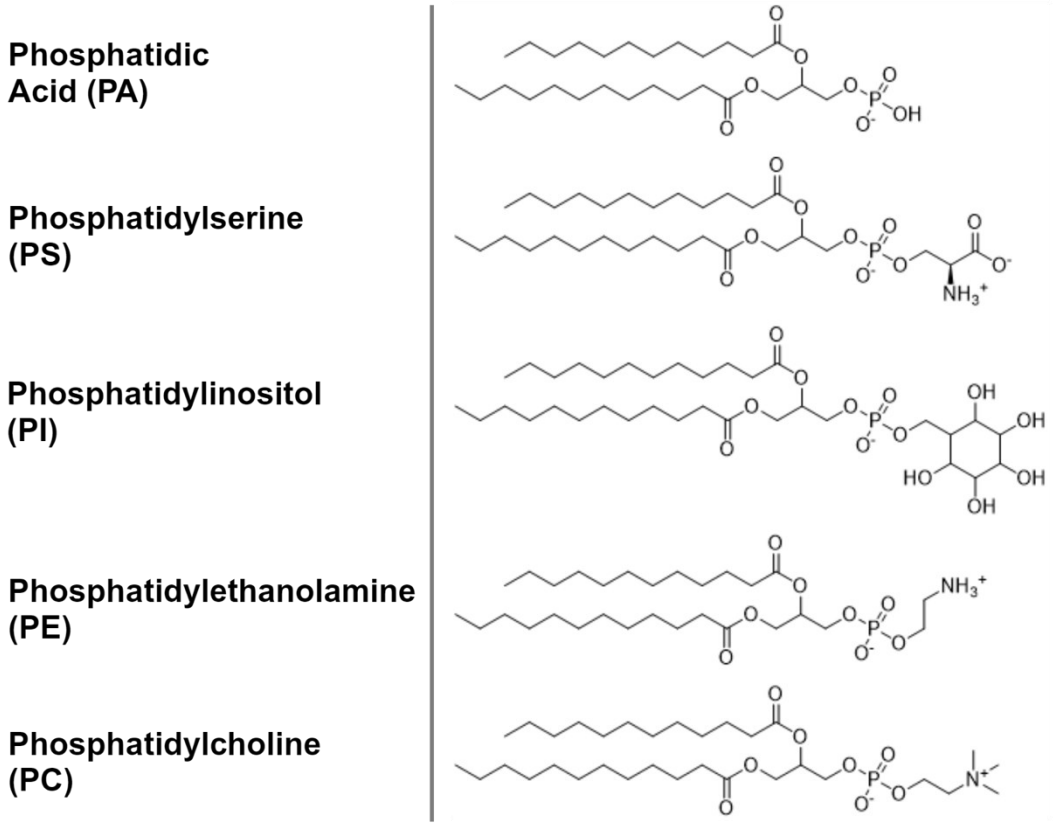

Figure 1.1. Chemical structures of glycerophospholipids in *S. cerevisiae*.

In the single celled eukaryotic model organism, *S. cerevisiae*, PC is the most abundant phospholipid comprising 17-48 % of the total phospholipids in different subcellular fractions (Zinser *et al*., 1991). It has a cylindrical shape, allowing it to act as the bulk structural element of lipid membranes. The second most abundant phospholipid in *S. cerevisiae* is PE, which comprises 19-33 % of the total phospholipids in different subcellular fractions (Zinser *et al*., 1991). The conic structure of PE promotes negative/concave curvature of the lipid membrane on the head group face. PI is also a major phospholipid component in *S. cerevisiae*, making up 7.5-19 % of the total phospholipids in different subcellular fractions (Zinser *et al*., 1991). The inositol head group of PI can be phosphorylated at three different sites, comprising isoforms of phosphoinositides. These molecules act as cellular signals and provide membrane identity based on their relative presence in the membrane.

1.3 PHOSPHATIDYLSERINE

PS is the most abundant anionic phospholipid, comprising 2-10% of total phospholipids depending on cell type (Vance, 2008). It has functional roles in blood clotting, apoptosis, viral infection, and localisation of polybasic proteins, such as the oncogene Kras. On a cellular level, its asymmetric subcellular and transleaflet distribution are important features regulating its cellular processes. These features are exaggerated in *S. cerevisiae* with PS making up 34 % total phospholipids in the PM, 13 % total phospholipids in secretory vesicles, and only 4 % total phospholipids in vacuoles (Zinser *et al*., 1991). PS also exhibits transbilayer asymmetry, with nearly 100% of PS on the PM (PM) on the cytosolic leaflet of yeast, making up over 60% of the total phospholipids on this leaflet. PS acts as a recognition site for enzymes and adaptors that typically associate with its negative charge. Upon addition of cationic membrane components or calcium influx, strongly cationic proteins that typically localise to the cytosolic surface of the PM are redistributed to endocytic compartments (Yeung *et al*., 2008). The basis of a PS specific molecular probe, Lactadherin is a glycoprotein involved in a variety of biological and physiological systems that binds PS in a calcium-independent fashion. Specifically, the C2 domain of lactadherin (Lact-C2) is a discoidin-like fold that binds specifically to PS (Kamińska *et al*., 2018). The Lact-C2 domain has been repurposed as a biosensor to study the subcellular distribution of PS using the pRS plasmid vector (Yeung *et al*., 2008; Sikorski & Hieter, 1989). Subsequent studies have used this probe to investigate the distribution of PS, showing that it is concentrated in recycling endosomes (Uchida *et al*., 2011) and at sites of cell polarity (Fairn *et al*., 2011).

1.4 PHOSPHOINOSITIDES

As described above, PI is a major lipid component of lipid membranes. PI also comes in various phosphorylated forms, known as phosphinositides. The inositol head group of PI has three readily phosphorylated hydroxyl groups at positions D3, D4, and D5. There are seven isoforms of

phosphoinositides for each combination of phosphorylated hydroxyl groups (PI3P, PI4P, PI5P, $PI_{3,4}P_2$, $PI_{4,5}P_2$, $PI_{3,5}P_2$ and PIP_3). While phosphoinositides are a minority population of anionic phospholipids, they can play important roles in signaling, acting as molecular switches (Lolicato *et al*., 2024). The localised interconversion between phosphoinositide species can regulate specific activities by protein binding. Furthermore, cellular membranes have characteristic phosphoinositide compositions, facilitating organelle specific targeting. Consequently, phosphoinositides have considerable depth of function including in ion channel regulation, growth signaling, and endocytic regulation. In humans, hundreds of potential phosphoinositide binding domains are known between pleckstrin homology (PH) domains, C2 domains, and Phox homology (PX) domains (Lemmon, 2008). Like PS, creation of phosphoinositide-specific markers has aided in determining their roles in cellular processes. Due to the similarity between the phosphoinositides, creating biosensors that target a single phosphoinositide species has been challenging. In particular, the role of $PI_{3,4}P_2$ has been largely unexplored, and even attributed to PIP_3 due to a lack of accurate biosensors and the non-specific effect of Class I PI3K inhibition, until recently (Ray *et al*., 2024).

The primary mechanism of phosphoinositide regulation is through the action of kinases and phosphatases. These enzymes can convert between phosphoinositides by addition or removal of phosphate groups, respectively. The regulation of phosphoinositides is then regulated by the localisation of these enzymes to specific membranes or organelles. In the case of $PI_{3,4}P_2$, $PI_{4,5}P_2$ is converted to PIP_3 by PI3K class I, which is then converted to $PI_{3,4}P_2$ by SHIP1/SHIP2. $PI_{3,4}P_2$ can then be degraded by either PTEN or INPP4A/B for the down regulation $PI_{3,4}P_2$ mediated signaling (Ray *et al*., 2024).

1.5 Metabolism and cellular distribution of phospholipids

Metabolism of phospholipids (Figure 1.2B) in *S. cerevisiae* is mostly carried out by enzymes that are common to mammalian cells, however, PS is an exception (Carman & Henry, 1999). PA is the

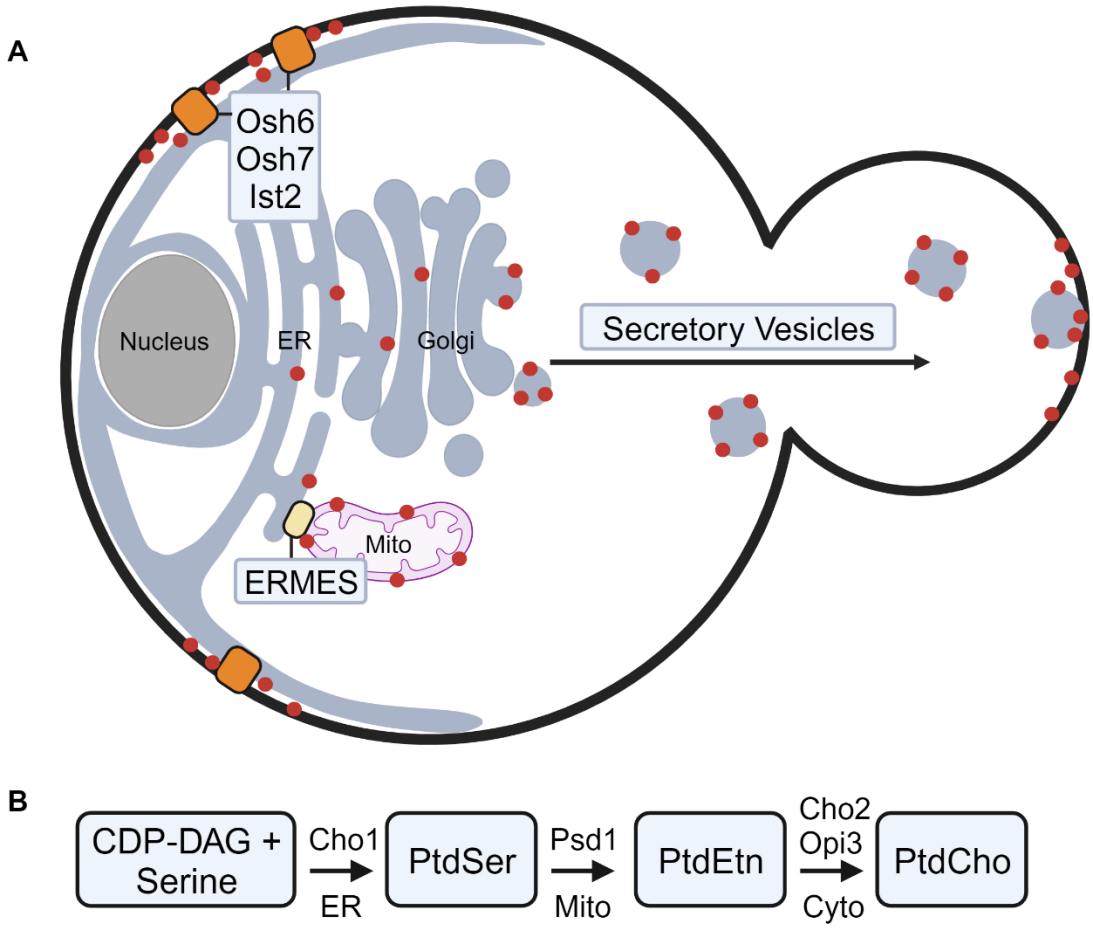

Figure 1.2. Mechanisms of Phosphatidylserine Distribution in *S. cerevisiae*. **A**. PtdSer is distributed through the cell from the ER, where it is synthesized, via secretory vesicles and lipid transfer proteins. The transfer of phosphatidylserine at the ER-PM contact sites is mediated by the protein tether Ist2 and lipid transfer proteins Osh6 and Osh7. ERMES complex forms contact sites between the ER and the mitochondria. **B**. PtdSer is metabolized according to this pathway. Cho1 synthesises PtdSer from CDP-DAG and serine in the ER. PtdSer is converted to PtdEtn by Psd1 in the mitochondria. Finally, Cho2 and Opi3 convert PtdEtn to PtdCho in the cytosol. ER: endoplasmic reticulum, Mito: mitochondria, Cyto: cytosol, PtdSer: phosphatidylserine, PtdEtn: phosphatidylethanolamine, PtdCho: phosphatidylcholine. Created using BioRender.com.

building block for the other major phospholipids. It is synthesized in the endoplasmic reticulum (ER). Downstream from PA production, there are two phospholipid production pathways, the CDP-DAG pathway and the Kennedy pathway (Kennedy & Weiss, 1956). The CDP-DAG pathway begins with the conversion of PA to CDP-diacylglycerol (DAG). CDP-DAG can be converted directly to PI, indirectly to cardiolipin (CL), or to PS by the phosphatidylserine synthase (Cho1) enzyme on mitochondrial-associated membrane (MAM) (Vance, 1990). Subsequently, PS is

converted to PE by either PS decarboxylase 1/2 (Psd1/2). Psd1 is in the inner mitochondrial membrane and accounts for up to 70 % of the total PS decarboxylation activity (Bürgermeister *et al*., 2004).

Psd2 localises to either trans Golgi network (TGN) or endosomal compartments, also producing a lesser component of PE (Calzada *et al*., 2019). The production of PC from PE is a three-step process starting with the transformation of PE into phosphatidylmonomethylethanolamine (PME) by PE methyltransferase (Cho2), then PME is converted to phosphatidyldimethylethanolamine (PDE) by phospholipid methyltransferase (Opi3), which also converts PDE to PC.

The Kennedy pathway provides an alternate route for production of PE and PC that bypasses CDP-DAG and PS production. Instead, PA is converted to DAG which can act as a direct precursor to either PE or PC. CDP-ethanolamine or CDP-choline are added directly to DAG to form PE or PC, respectively. For ethanolamine to be transferred to DAG, ethanolamine is phosphorylated by ethanolamine kinase, then phosphoethanolamine cytidylyltransferase catalyses the second step, in which CDP-ethanolamine is formed from CTP and phosphoethanolamine. Finally, ethanolamine phosphotransferase transfers ethanolamine from CDP-ethanolamine onto DAG, synthesizing PE. By an equivalent mechanism, choline kinase, phosphocholine cytidylyltransferase, and choline phosphotransferase synthesize PC from DAG (Carman & Henry. 1999). Notably, the Kennedy pathway is non-essential to cell viability because both PE and PC can be produced by the CDP-DAG pathway. These two pathways comprise independent mechanisms for the production of major phospholipids in *S. cerevisiae*.

1.6 METABOLISM OF PHOSPHATIDYLSERINE

In mammalian cells, PS is produced by two enzymes, phosphatidylserine synthase 1 and 2 (Pss1/2). Pss1 and Pss2 act by exchanging the head group of PC or PE, respectively, for PS (Vance & Steenbergen. 2005). Conversely, in *S. cerevisiae*, PS is upstream in the metabolic pathway of PC

and PE. Yeast only have a single PS synthase enzyme, Cho1, which exchanges CMP from CDP-DAG with serine. In the yeast model, the Kennedy pathway provides an opportunity to specifically investigate the role of PS. Deletion of the *cho1* gene is non-lethal, but ethanolamine or choline auxotrophic (Atkinson *et al*., 1980). This is because PE or PC are essential and in the absence of ethanolamine, they cannot be produced by the CDP-DAG pathway, however, ethanolamine supplementation enables the Kennedy pathway to bypass the CDP-DAG pathway and produce PE and PC. Consequently, the *cho1Δ* strain produces all phospholipids except PS, and has increased PI and PC synthesis (Atkinson *et al*., 1980). This model strain has been highly valuable for studying the role of PS in *S. cerevisiae*.

1.7 Distribution of phosphatidylserine

As described earlier, PS has an asymmetric distribution between leaflets of lipid membranes and along the endocytic pathway. PS distribution varies between organelles in a manner that has been well described in mammalian cells (Yang *et al*., 2018; Figure 1.3). However, this differs from the distribution in *S. cerevisiae*, which has a higher concentration of PS in the PM and is overall less described (Zinser *et al*., 1991). These distribution patterns are maintained and modified by flippases, scramblases, lipid transfer proteins, and vesicular transport.

Maintenance of PS distribution and function depend on protein binding to PS. Proteins bind to PS based on either electrostatics or “lock and key” specific binding. The negative charge of PS facilitates non-specific electrostatics-driven binding of proteins including polybasic sequences (Cho & Stahelin, 2005; Mulgrew-Nesbitt *et al*., 2006). This includes many proteins that bind to the cytosolic face of the PM such as Kras, which has a polybasic domain containing six consecutive

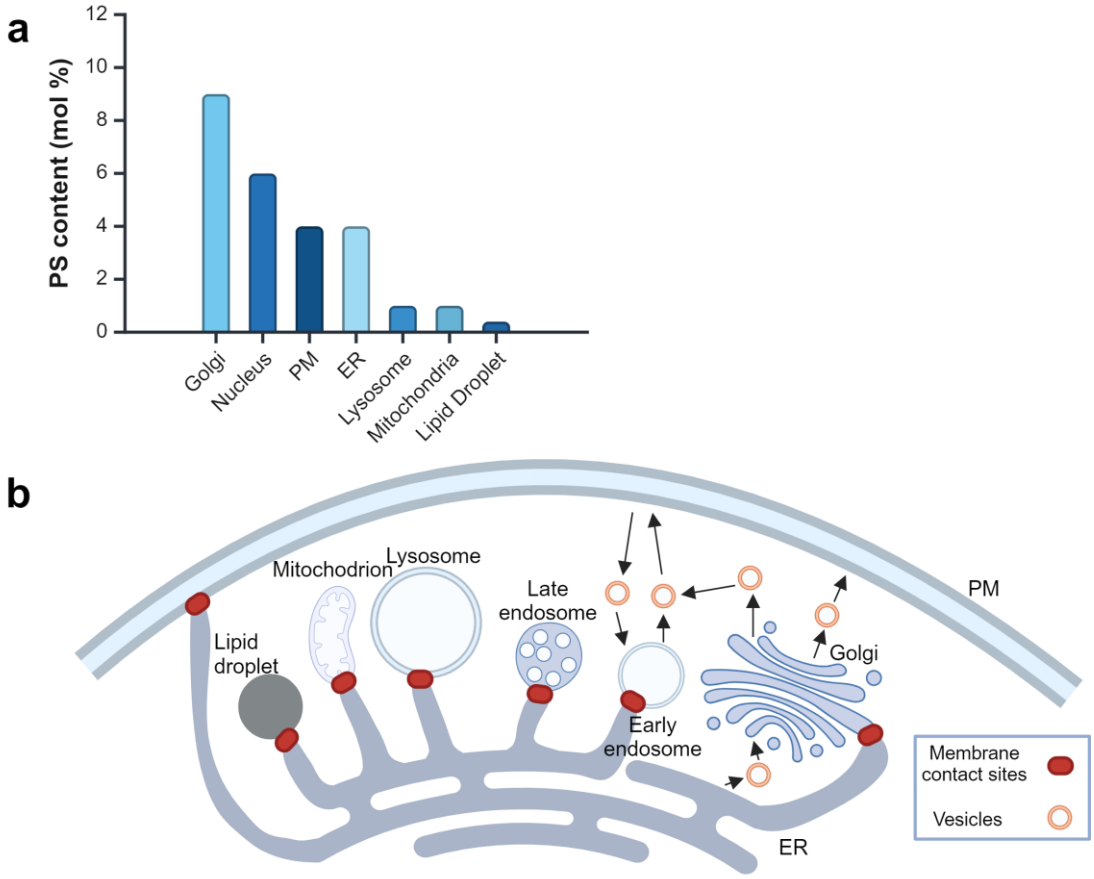

Figure 1.3. Distribution of phospholipids in mammalian cells. Adapted from Yang et al., 2018. **a.** PS content of membranes in rat hepatocytes (murine hepatocytes for lipid droplets). **b**. Mechanisms of phospholipid distribution in mammalian cells. Phospholipids are primarily transferred by vesicles or at membrane contact sites. PM: plasma membrane; ER: endoplasmic reticulum.

lysine residues (Hancock *et al*., 1990) and (non-discoidin-like) C2 domain-containing proteins Annexin V, Protein kinase C α, and Protein kinase C β (Leventis & Grinstein, 2010). Alternatively, PS can bind specifically via "lock and key" binding. Discoidin-like C2 domain-containing proteins such as Lactadherin and Coagulation factor V bind with stereospecificity to L-serine in phosphatidylserine (Leventis & Grinstein, 2010), while Oxysterol-binding protein (Osh) proteins can transfer PS specifically by binding a single molecule at a time (Maeda *et al*., 2013).

Flippases are ATP-dependent enzymes that transfer either PS or PE from the luminal to cytoplasmic leaflet. In *S. cerevisiae*, Deficiency in ribosomal subunits 2 (Drs2) and its homologs, Drs2 Neo1

Family 1/2 (Dnf1/2) create and maintain PS trans-membrane asymmetry (Yang *et al*., 2018). The enzymes' activity corresponds to their location, with Drs2 primarily in the TGN, while Dnf1 and Dnf2 both localise to the PM (Pomorski *et al*., 2003; Natarajan *et al*., 2004).Transbilayer asymmetry of PS also has a role in generating membrane curvature and vesicular trafficking (Xu *et al*., 2013). In *S. cerevisiae*, Drs2 is necessary for formation of clathrin-coated vesicles on the TGN (Gall *et al*., 2002), while Dnf1, Dnf2, and Drs2 all have a role in budding of endocytic vesicles (Pomorski *et al*., 2003).

Scramblases enable energy-independent exchange of phospholipids between the leaflets. Activation of flippases on the PM is important for some of PS's well known functions—blood coagulation signaling in platelets (Bevers *et al*., 1989) and signaling for cell clearance by phagocytes in apoptosis (Fadok *et al*., 2001). In both cases, flippase activation causes PS to be transferred to the extracellular leaflet, acting as a signal to the surrounding environment. Unless stimulated, these flippases remain inactive, allowing the PS to remain on the cytosolic leaflet. Xkr8 is one scramblase that is activated during apoptosis. It contains a caspase cleavage site that, upon cleave, activates the scramblase activity. Conversely, ATP11C is an Atpase with a caspase cleavage site that prevents the return of PS to the intracellular leaflet following cleavage. Together, the externalisation of PS results in an In apoptosis, scramblases TEMEM16 and Xkr8 are activated resulting in anti-inflammatory signaling and removal of the apoptotic cells (Birge *et al*., 2016).

PS is synthesised on the ER and transported at membrane-membrane contact sites or by secretory vesicles (Figure 1.2A). Membrane-membrane contact sites are where two lipid bilayers within the cell are tethered together by proteins and remain in proximity. At these sites, lipid transfer proteins can transport phospholipids between the membranes. The secretory pathway in yeast begins at the ER where COPII vesicles form and are transported to the TGN. COPII vesicles are coated in a layered protein scaffold, which remodels the membrane into a spherical vesicle for transport and

facilitates membrane fission (Melero *et al*., 2022). Vesicles for secreted proteins continue to the PM and vesicle membrane fuses with the PM in a process mediated by soluble NSF attachment protein receptor (SNARE) proteins (Burri & Lithgow, 2004). The process of membrane fusion also results in phospholipid transport as a by-product.

Osh6 and Osh7 in *S. cerevisiea* are lipid transfer proteins that transfer PS to the PM at ER-PM contact sites, however they do not contain membrane-targeting motifs. Consequently, they function in conjunction with ER-PM tethering protein, Increased sodium tolerance protein 2 (Ist2). Ist2 contains an Osh6 binding motif that is necessary for PS transfer to the PM by lipid transfer proteins (D'Ambrosio *et al*., 2020). This has a major contribution to the high concentration of PS on the PM. *osh6Δ /osh7Δ* strain has an abnormal PS distribution and less total cell PS relative to other phospholipids (Maeda *et al*., 2013). However, alternative data shows the abnormal phenotype present in a minority of cells when tested in two different genetic backgrounds (SEY6210 & BY4741) (Yang, unpublished). The consequences of *osh6Δosh7Δ* remains unclear.

The ER-mitochondria encounter structure (ERMES) complex mediates ER-Mitochondrion contact sites, where PS transfer to the mitochondria occurs, however, the ERMES complex is not directly involved in the process of PS transport between the membranes (Nguyen *et al*., 2012). Once PS is transferred to the mitochondrial membrane, it is decarboxylated into PE by Psd1.

Secretory vesicles play an essential role in transport of PS to sites of cell polarity, such as mating projections and budding sites. Secretory vesicles containing PS form from the ER and are transported to sites of cell polarity. Conversely, knockout of Secretory 1 (Sec1) or Sec6 prevents secretory vesicle fusion to the PM and results in accumulation of PS containing secretory vesicles in buds (Fairn *et al*., 2011). Furthermore, *cho1Δ* has substantial functional consequences on cell polarity. Cell division cycle 42 (Cdc42) is an essential GTPase involved in cell polarity, bud

growth, and mating. In the *cho1Δ* strain, Cdc42 localisation was defective as well as the ability to form mating projections and to localise the scaffold protein Bud Emergence 1 (Bem1) to bud emergence sites (Fairn *et al*., 2011). These results support PS playing an important role in the secretory pathway for establishing cell polarity through a range of cellular functions.

1.8 ENDOCYTOSIS AND ENDOCYTIC TRAFFICKING

Endocytosis is a key cellular process integrated into nearly all elements of cellular life. In the endocytic pathway, external factors are internalised into membrane-bound compartments and sorted for use, recycling, or degradation. This process mediates the interactions between a cell and its environment by regulation of the features presented on the extracellular leaflet of the PM and by uptake of components from the environment into the cell. Broadly, the endocytic pathway is comprised of multidirectional transport from the PM the lysosome or, the equivalent organelle in *S. cerevisiae*, the vacuole. The TGN feeds into the pathway through exchange with the intermediate components—early and late endosomes. While there are distinct labels for each of the compartments along the endocytic pathway, there is substantial overlap between their features (Huatari & Helenius, 2011). Endocytosis begins with invagination of the PM to internalise external components. This can occur by many different mechanisms, including clathrin-mediated endocytosis, phagocytosis, and micropinocytosis. The early endosomes are characterised by the Rab GTPase, Rab5 in mammalian cells and Ypt52 in *S. cerevisiae* (Zerial & McBride, 2001; Singer-Krüger *et al*., 1994) and PI3P, produced by Vacuolar sorting protein 34 (Vps34) contributes to the membrane identity (Behnia & Munro, 2005). Early endosomes are also typically smaller structures with many tubules, participating in cargo sorting (Huatari & Helenius, 2011). Proteins and lipids in early endosomes are sorted for further transport or recycling by endosomal sorting complex required for transport (ESCRT) machinery (Schuh & Audhya, 2014). Subsequently, early endosomes mature into late endosomes in a process mediated by Rab5 and complex interactions with its replacement

GTPase, Rab7 and each of their resepective guanine nucleotide exchange factors and GTPase-activating proteins (Castro *et al*., 2021). In *S. cerevisiae*, Ypt7 is the Rab7 homolog and plays a role in recruiting effector proteins to late endosomes and is involved in recruiting fusion machinery in late endosomes and the vacuole (Haas *et al*., 1995; Ostrowicz *et al*., 2008). Some key characteristics of late endosomes are the exchange of Rab5 for Rab7, formation of intraluminal vesicles within the late endosomes, a decrease in the luminal pH, and conversion of PI3P to $PI_{3,5}P_2$. Late endosomes are also rounder and larger than early endosomes (Huatari & Helenius, 2011). Finally, Late endosomes fuse with the terminal compartment of the endocytic pathway—the lysosome or vacuole. The vacuole, in yeast, is a large compartment that performs bulk degradation of proteins, lipids, and other molecules. Importantly, acidity increases along the endocytic pathway as the pH drops from 6.8-6.1 in early endosomes, to 6.0-4.8 in late endosomes, and finally to ~4.5 in lysosomes (Maxfield & Yamashiro, 1987). The acidification of these compartments is mediated by V-ATPases, which pump protons into the lipid compartment. The change in pH contributes to organelle identity, but also to degradation.

1.9 Retrograde endocytic trafficking

The PM of mammalian cells has 50-180 % of its membrane turned over by exocytosis and endocytosis every hour (Steinman *et al*., 1983). Consequently, recycling of internalized material is essential. In yeast, transport from endosomes to TGN is termed retrograde, while transport from endosomes to PM is called membrane recycling (Ma & Burd. 2020). Cargo within endosomes can be directed into distinct trafficking pathways in signal-dependent manner (Nothwehr *et al*., 1999; Nothwehr *et al*., 2000). The factors that mediate this sorting process include ESCRT machinery, sorting nexins, and the retromer complex.

Low density lipoprotein receptor (Ldlr) and Transferrin receptor (Tfr) are well studied membrane protein receptors in mammalian cells that are internalised and recycled. Ldlr binds and internalises

low density lipoprotein (LDL) via clathrin-mediated endocytosis, then brings LDL to sorting endosomes. The low pH environment of the sorting endosome triggers the release of LDL. Ldlr is then recycled back to the PM. Tfr transports its cargo, diferric transferrin, to sorting endosomes by the same mechanism, however, the low pH of the sorting endosome only results in the release of the two iron molecules from the transferrin. Tfr, with transferrin still bound, is then recycled back to the PM, where transferrin is finally released (Maxfield & McGraw, 2004). Another well-studied membrane receptor, epidermal growth factor receptor (EGFR), must be degraded to prevent continuous receptor activation. Activated EGFR is internalised and ubiquitinated by an E3 ubiquitin ligase. Following ubiquitination, EGFR is trafficked to intraluminal vesicles of multivesicular bodies/late endosomes by ESCRT complexes and finally transported the vacuole for degradation (Sapmaz & Erson-Bensan, 2023). The selective retrograde trafficking and degradation pathways are essential to maintaining signaling homeostasis within the cell.

Sorting Nexin-BAR domain proteins in endocytic trafficking

Sorting Nexin-Bar Domain (SNX-BAR) proteins are a family of sorting nexins that play an important role in membrane tubulation and linking sorting compartments to the cytoskeletal elements for transport in the endocytic trafficking pathway (van Weering *et al*., 2010). SNX-BAR proteins form dimers and they have two key features: a crescent-shaped Bin-Amphiphysin-Rvs (BAR) domain comprised of three helices, with basic residues on the concave surface and a PX domain, classically known to bind the negatively charged PI3P. Consequently, these proteins preferentially bind to negatively charged curved membranes. Furthermore, members of this protein family assemble into a helical lattice that stabilises the formation of membrane tubules and vesicles (Frost *et al*., 2008). Thus, when vesicles form from endocytic compartments, with a lipid tubule that extrudes from the subcellular structure, the SNX-BAR proteins form part of a protein coat that facilitates this process. Membrane scission allows the tubule to become a vesicle that can be

transported through the cell along the cytoskeletal components. In *S. cerevisiae*, there are six members of the SNX-BAR protein sub-family: Vps5, Vps17, Mvp1, Snx4, Snx41, and Snx42 (Chi *et al*., 2015). Vps5 and Vps17 are components of the retromer complex, which mediates retrograde transport from late endosomes to TGN. Snx4 forms heterodimers with either Snx41 or Snx42. Snx4-Snx42 heterodimer has a distinct role in trafficking the v-SNARE protein, suppressor of the Null allele of CAP 1 (Snc1). The Snx4-Snx41 heterodimer mediates retrograde sorting of the membrane protein Autophagy related 27 (Atg27) from the vacuole to endosomes (Ma *et al*., 2016; Hettema *et al*., 2003). In mammalian cells, the precise residue composition of the PX domain localised to the inner lining of the curved protein determines the specific phosphoinositide binding. In *S. cerevisiae*, there is a smaller population of phosphoinositides and a greater prevalence of PS, which is also negatively charged.

Retromer complex in endocytic trafficking

The retromer complex is a sorting machinery that coats lipid tubules during vesicle formation and mediates specific retrograde transport from late endosomes to TGN. The complex was first described in *S. cerevisiae* (Seaman *et al*., 1997; Seaman *et al*., 1998) and is largely like its mammalian counterpart. The yeast retromer is a pentameric protein complex comprised of two subcomplexes: the cargo selective complex and the SNX-BAR dimer. The dimer is comprised of the SNX-BAR proteins, Vps5 and Vps17, which form a dimer that binds to the lipid membrane (Hurley & Johannes, 2019). The cargo selective complex is made of Vps26, Vps29, and Vps35, which determine cargo selection (Figure 1.4) (Seaman, 2012). Retromer function begins with binding of the SNX-BAR dimer to the endosomal membrane. Then the cargo selective complex is recruited and retromer cargo are sequestered to the retromer complex. Yeast Protein Two 7 (YPT7), a Rab family GTPase, is activated and associates with the cargo selective complex. This results in the formation of the lipid tubule and subsequent export of retromer coated vesicles (Liu *et al*., 2012).

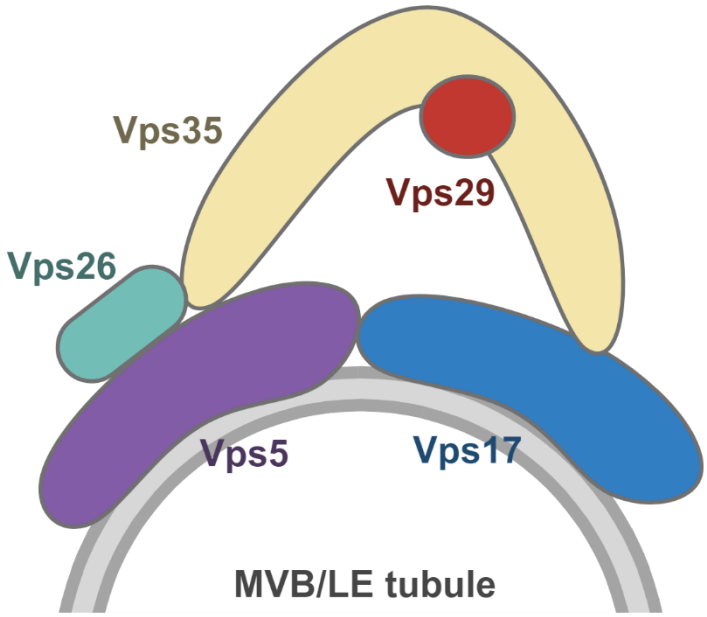

Figure 1.4. Schematic of the retromer complex. The retromer complex is a pentameric complex that forms on multivesicular bodies/late endosomes. It mediates retrograde transport from multivesicular bodies/late endosomes to the trans Golgi network. It is comprised of vacuolar protein sorting (Vps) 5, Vps17, Vps26, Vps29, and Vps35. Vps5 and Vps17 form the SNX-BAR protein dimer and Vps26, Vps29, and Vps35 form the cargo selective complex. LE: late endosomes, MVB: multivesicular bodies. Created using BioRender.com.

The retromer complex mediates the retrograde transport of Vps10 and Atg27 from late endosomes to TGN (Suzuki *et al*., 2019; Suzuki & Emr, 2018). Vps10 is a transmembrane protein receptor for the vacuolar enzymes, carboxypeptidase Y (CPY), bringing it from the TGN to the vacuole (Marcusson *et al*., 1994). In the absence of Vps10, CPY is not able to be delivered to the vacuole but is instead secreted from the cell. This has been measured by a CPY secretion assay, which measures CPY in the media by western blotting (Suzuki *et al*., 2019). This assay can be extended to measure retromer function because retromer dysfunction eliminates Vps10 retrograde transport and consequently has an equivalent phenotype to Vps10 knockout (Suzuki *et al*., 2019). Atg27 is a transmembrane protein involved in biogenesis of Atg9 vesicles, which are necessary for autophagosome biogenesis (Yamamoto *et al*., 2012). Atg27 is delivered to the vacuole by the adaptor protein (AP)-3 pathway—a pathway from TGN to vacuole (Cowles *et al*., 1997). While

Snx4 is involved in its recycling from the vacuole to late endosomes, it is ultimately the retromer complex that recycles Atg27 back to the TGN from late endosomes (Suzuki & Emr, 2018).

Mannose 6-phosphate Receptor Like 1 (Mrl1) is another hydrolase receptor protein, like Vps10. In non-laboratory wildtype strains, Mrl1 distribution and trafficking is regulated by the Vps9 GEF-interacting sorting nexin (VINE) complex, however, this complex is inactive in laboratory strains of *S. cerevisiae* (Shortill *et al*., 2022). Their work shows that the VINE complex performs a similar role to the retromer, with Mrl1 proposed to follow a similar two-step retrograde transport pathway akin to Atg27. In their model, Mrl1 trafficked to the vacuole to deliver hydrolases is recycled first to endosomes in a Snx4-dependent manner, then to the TGN in a VINE complex-dependent manner (Shortill *et al*., 2022). However, as they acknowledge, there is likely redundancy in this recycling pathway because laboratory strains, with inactive VINE complex, show Mrl1 contributing to protease delivery (Whyte & Munro, 2001). Pep4 is a vacuolar hydrolase that requires at least one of Mrl1 and Vps10 for proper sorting, but in the absence of both, Pep4 delivery and maturation are dysfunctional (Whyte & Munro, 2001). These results suggest that the retromer complex may also play a role in the recycling of Mrl1 and the consequent delivery of Pep4 to the vacuole.

1.10 Phosphatidylserine in endocytic trafficking

The negative charge requirement for SNX-BAR proteins binding to membranes alongside the gradient concentration of PS suggests a possible role for PS in retrograde transport along the endocytic pathway. In mammalian cells, PS is important for retrograde transport at recycling endosomes (Uchida *et al*., 2011). However, the role for PS in endocytic trafficking in *S. cerevisiae* is not fully understood. The coincidence of the PS gradient along retrograde transport pathways is described in Figure 1.5.

On the cytosolic leaflet of the PM, both PS and $PI_{3,4}P_2$ are enriched. $PI_{3,4}P_2$ is required for endocytic membrane invagination, however, it is not necessary for endocytic site initiation. In the *cho1Δ* model, cells have defective endocytic patch establishment, showing a role for PS in endocytic site initiation (Sun & Drubin, 2012). Furthermore, a knockout model for Recycling 1 (*rcy1*), which codes a protein that mediates endosome to TGN trafficking, results in enlarged early endosome membrane compartments that are enriched with PS (Sun & Drubin, 2012). These results showed a role for both PS and phosphoinositites in the endocytic pathway.

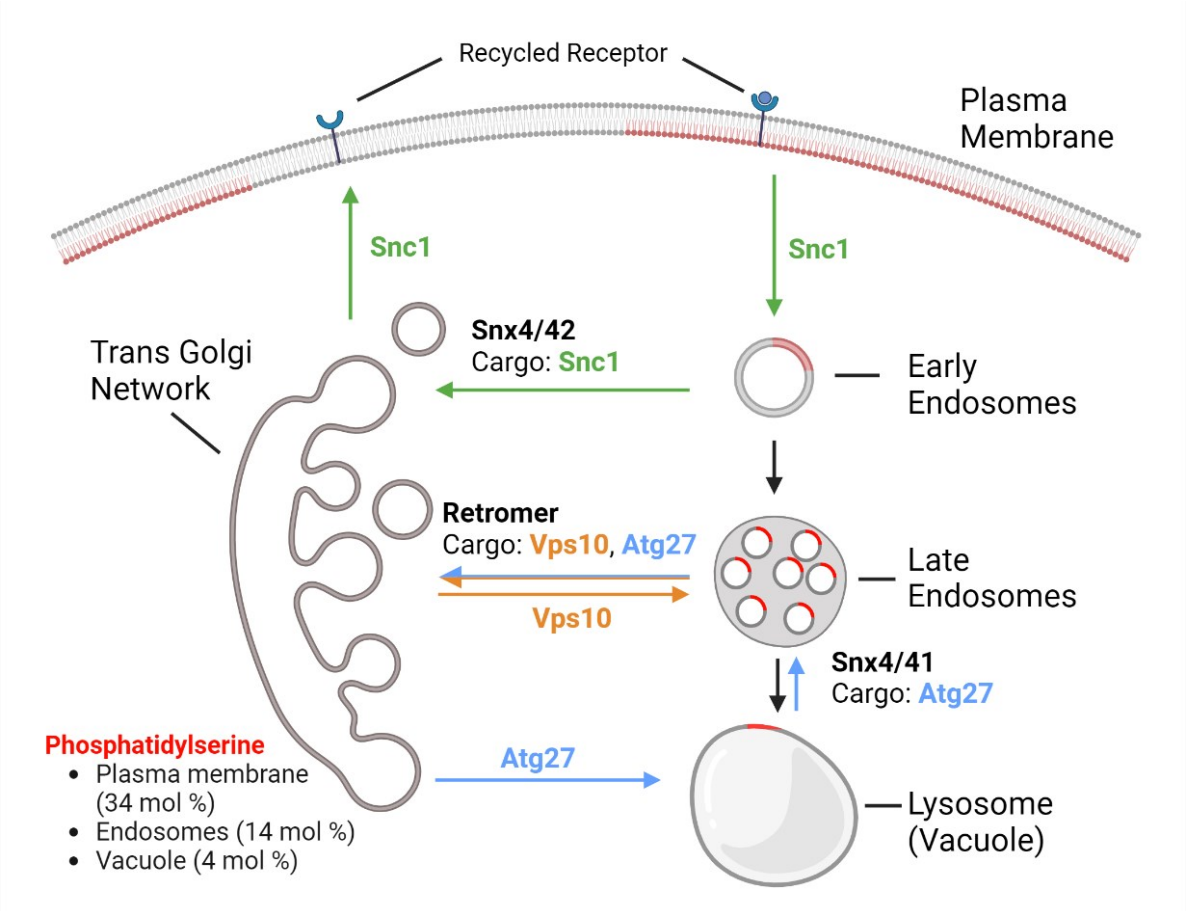

Figure 1.5. Retrograde trafficking pathways along the endocytic pathway with SNX-BAR proteins in *S. cerevisiae*. Retrograde pathways recycle material from endosomes to Golgi. SNX-BAR proteins mediate these pathways, creating a potential role for the unevenly distributed phosphatidylserine (represented in red). Snc1 is recycled from early endosomes to trans Golgi network to PM. Snx4-Snx42 heterodimers mediate this pathway. Late endosomes have cargo retrograde transported to the trans Golgi network by the retromer complex, including Vps10 and Atg27. Atg27 is also transported from the vacuole to late endosomes by Snx4-Snx41 heterodimers. The mol % of phosphatidylserine relative to other phospholipids on each membrane is represented in the bottom left of the figure. Snc1: Suppressor of the Null allele of CAP, Vps10 (Vacuolar protein sorting 10), Snx4/42: Snx4 and Snx42 heterodimer. Created using BioRender.com.

Endocytic trafficking is also regulated by PI_3P. PI_3P is produced by two phosphoinositide 3-kinase (PI3K) complexes. Complex I consists of Vps34, Vps15, Vps30, and Atg14 and is involved in autophagy processes, while complex II consists of Vps34, Vps15, Vps30, and Vps38 and mediates endocytic trafficking. Each complex forms a Y-shape that is centered on the Vps34 C2 domain (Rostislavleva *et al*., 2015). PI3P's role in endocytic trafficking is through regulating the mammalian Rab5 GTPase homologs, Yeast protein two (YPT) 51, 52, and 53 (Singer-Kruger *et al*.,

1994; Gillooly *et al*., 2000). Subsequently, PI3P is transported to the vacuole and degraded by vacuolar hydrolases (Wurmser & Emr, 1998) or converted to $PI_{3,5}P_2$ by the PI3P 5-kinase, Forms Aploid and Binucleate cells (Fab1) (Gary *et al*., 1998). Furthermore, *S. cerevisiae* treated with a PI3K inhibitor, Wortmannin, are also unable to form multivesicular bodies in the endocytic pathway (Fernandez-Morja *et al*., 1999). Consequently, PI3P and Vps34 PI3K complex II act as critical regulators of endocytic processing. The Vps34 complex is further regulated by the lipid membrane characteristics of lipid saturation, membrane curvature, and negative charge. The PI3K complex is more active on unsaturated lipid membranes, and high membrane curvature can compensate for the decrease in activity from lipid saturation. PS, due to its negative charge, can activate either the Vps34 complex or Vps34 alone (Ohashi *et al*., 2021).

Thereby, there are two potential types of interactions by which PS may contribute to endocytic trafficking: interacting with SNX-BAR proteins or activating Vps34 PI3K complex II. Supporting a role for PS in retrograde endocytic transport via SNX-BAR domains, the Snx4-Snx42 dimers preferentially bind to membranes containing PS (Ma *et al*., 2018). Furthermore, *snx4Δ* or *snx42Δ* combined with *psd1Δ* causes PS accumulation in the vacuole and endosomes as well as impaired vacuole homotypic fusion (Ma *et al*., 2018). The role of PS in recycling from early endosomes was described recently by Kashikuma *et al*., 2023. They showed that in *cho1Δ* cells, Snx4 containing puncta accumulate and several cell membrane proteins have defective localisation. Accumulation of Snx4-containing puncta in *cho1Δ* suggests that PS deficiency impairs early endosome to TGN transport, preventing Snx4 from leaving early endosomes. Sterile 2 (Ste2) is the membrane receptor for α-factor mating pheromone that is recycled to the PM. α-factor binding on the PM initiates a signaling cascade for cell polarisation and mating projection formation. c*ho1Δ* cells bind α-factor equivalently to *ste2Δ* cells. Furthermore, Ste2 is mislocalised to the vacuole (Kashikuma *et al*., 2023). This provides an additional explanation for why PS is required for cell polarisation as

described previously (Fairn *et al*., 2011). *cho1Δ* cells are also deficient in the recycling or retrograde transport of several other membrane proteins: Snc1, Canavanine resistance 1 (Can1), and Synthetic lethal with GAP 1 (Wsc1). Each of these proteins were almost entirely mislocalised to the vacuole (Kashikuma *et al*., 2023). The disruption of the recycling pathway from TGN to PM was further characterised by use of the endocytic deficient Snc1 mutant [Snc1(en-)] previously developed (Lewis *et al*., 2000) and by a secretory assay. In *cho1Δ* cells, Snc1(en-) on the PM was decreased to ~76 %, showing that the TGN to PM transport is partially disrupted and the secretory assay showed a decrease in secretion (Kashikuma *et al*., 2023). Together, these results support a role for PS in early endosome to TGN retrograde trafficking and in recycling from the TGN to the PM. Snx4 may play an essential PS-dependent role in each of these functions.

While the role of PS in this pathway is partially characterised, the role of PS in retrograde transport from late endosomes to the TGN via the retromer complex remains largely uninvestigated. This work aims to describe the impact of PS on proteins involved in retrograde transport from late endosomes to the TGN. This work also aims to describe the role of Osh6 and Osh7 in the production and distribution of PS.

CHAPTER 2 Methods

Yeast media and growth

Yeast strains were cultured in either yeast extract-peptone-dextrose (YPD; 1% yeast extract, 2% peptone, and 2% dextrose) media, synthetic complete (SC; 0.2% [or according to supplier instructions] Drop-out mix [BioShop], 2% D-Glucose, and 0.67% Ammonium Sulfate) media, or SC media with Drop-out mix complementary to strain auxotrophies (Selective media/SC-"essential amino acid/nucleoside"). Alternatively, as required resistance to G418 antibiotic would be used at a concentration of 200 μg/ml. Strains with the *cho1Δ* mutation were supplemented with 1 mM Ethanolamine from a 1 M Ethanolamine in stock. To generate plates, 1.7% agar was added to the media. Media was sterilized by autoclaving in all cases. Cells grown in liquid media were typically grown overnight at 30 °C, 230 rpm to early stationary phase. The next day, cultures were diluted 1 in 5 and grown (30 °C, 230 rpm) for 3.5-4.5 hours to reach log phase of growth. Alternatively, log growth phase cells were added to media such that they would reach a desired concentration in log phase using the following formula: $A = A_o e^{kt}$; $k = \ln(2)/T$; A = final concentration; A_o = initial concentration; t = growth time; T = doubling time (~90 minutes or 1.5 hours for WT yeast strains). Additionally, strains were grown on solid agar containing media at either room temperature or 30 °C. These plates could be stored at 4 °C for several months. For long term storage of yeast strains, liquid cultures were mixed with 50% glycerol to a final concentration of 20% glycerol and stored at -80 °C.

Yeast Strains

Table 2.1. List of Strains

Strain	Familiar name	Shorthand	Full Name	Source
DGS001	BY4741	BY4741	*MATa his3Δ1 leu2Δ0 met15Δ0 ura3Δ0*	
DGS002	SEY6210	SEY6210	*MATα leu2-3,112 ura3-52 his3Δ200 trp1Δ901 lys2-801 suc2Δ9*	Scott Emr
DGS003	Delta-	SEY6210;	*MATa leu2-3,112 ura3-52 his3Δ200*	Scott Emr

	Tether	ist2Δ::hisMX6 scs2Δ::TRP1 scs22Δ::hisMX6 tcb1Δ::kanMX6 tcb2Δ::kanMX6 tcb3Δ::hisMX6	*trp1Δ901 lys2-801 suc2Δ9 ist2*Δ::hisMX6 *scs2*Δ::*TRP1 scs22*Δ::hisMX6 *tcb1*Δ::kanMX6 *tcb2*Δ::kanMX6 *tcb3*Δ::hisMX6	
DGS004	Super-tetherΔ	ANDY198; *ice2::NatMX4*	*MAT*a *leu2-3,112 ura3-52 his3Δ200 trp1Δ901 lys2-801 suc2Δ9 ist2*Δ::hisMX6 *scs2*Δ::*TRP1 scs22*Δ::hisMX6 *tcb1*Δ::kanMX6 *tcb2*Δ::kanMX6 *tcb3*Δ::hisMX6 ice2::NatMX4	Chris Beh
DGS005	osh6Δ	SEY6210; *osh6::LEU2*	*MATα leu2-3,112 ura3-52 his3Δ200 trp1Δ901 lys2-801 suc2Δ9 osh6::LEU2*	Chris Beh
DGS006	osh7Δ	SEY6210; osh7::HIS3	*MATα leu2-3,112 ura3-52 his3Δ200 trp1Δ901 lys2-801 suc2Δ9 osh7::HIS3*	Chris Beh
DGS007	osh6/osh7	SEY6210; *osh6::LEU2* osh7::HIS3	*MATα leu2-3,112 ura3-52 his3Δ200 trp1Δ901 lys2-801 suc2Δ9 osh6::LEU2 osh7::HIS3*	Chris Beh
DGS008	cho1Δ	SEY6210; cho1Δ::KanMX	*MATα leu2-3,112 ura3-52 his3Δ200 trp1Δ901 lys2-801 suc2Δ9 cho1Δ::his3*	David Sapp
DGS009	ist2Δ	SEY6210; ist2Δ::HIS3	*MATα leu2-3,112 ura3-52 his3Δ200 trp1Δ901 lys2-801 suc2Δ9 ist2Δ::his3*	David Sapp
DGS010	SEY6210 + GFP-Lact-C2	SEY6210 + prs410-GFP-Lactadherin-C2 domain	*MATα leu2-3,112 ura3-52 his3Δ200 trp1Δ901 lys2-801 suc2Δ9 + prs410-GFP-Lactadherin-C2 domain*	David Sapp
DGS011	Delta-Tether + prs410-GFP-Lact-C2	SEY6210; ist2Δ::hisMX6 scs2Δ::TRP1 scs22Δ::hisMX6 tcb1Δ::kanMX6 tcb2Δ::kanMX6 tcb3Δ::hisMX6 + prs410-GFP-Lactadherin-C2 domain	*MAT*a *leu2-3,112 ura3-52 his3Δ200 trp1Δ901 lys2-801 suc2Δ9 ist2*Δ::hisMX6 *scs2*Δ::*TRP1 scs22*Δ::hisMX6 *tcb1*Δ::kanM`X6 *tcb2*Δ::kanMX6 *tcb3*Δ::hisMX6 + prs410-GFP-Lactadherin-C2 domain	David Sapp
DGS012	Super-tetherΔ + prs410-GFP-Lact-C2	ANDY198; *ice2::NatMX4 + prs410-GFP-Lactadherin-C2 domain*	*MAT*a *leu2-3,112 ura3-52 his3Δ200 trp1Δ901 lys2-801 suc2Δ9 ist2*Δ::hisMX6 *scs2*Δ::*TRP1 scs22*Δ::hisMX6 *tcb1*Δ::kanMX6 *tcb2*Δ::kanMX6 *tcb3*Δ::hisMX6 ice2::NatMX4	David Sapp
DGS013	osh6Δ + prs410-GFP-Lact-C2	SEY6210; *osh6::LEU2 + prs410-GFP-Lactadherin-C2 domain*	*MATα leu2-3,112 ura3-52 his3Δ200 trp1Δ901 lys2-801 suc2Δ9 osh6::LEU2 + prs410-GFP-Lactadherin-C2 domain*	David Sapp
DGS014	osh7Δ +	SEY6210; osh7::HIS3 +	*MATα leu2-3,112 ura3-52 his3Δ200*	David Sapp

	prs410-GFP-Lact-C2	prs410-GFP-Lactadherin-C2 domain	*trp1Δ901 lys2-801 suc2Δ9 osh7::HIS3 + prs410-GFP-Lactadherin-C2 domain*	
DGS015	osh6/osh7 + prs410-GFP-Lact-C2	SEY6210; *osh6::LEU2* osh7::HIS3 + prs410-GFP-Lactadherin-C2 domain	*MATα leu2-3,112 ura3-52 his3Δ200 trp1Δ901 lys2-801 suc2Δ9 osh6::LEU2 osh7::HIS3 + prs410-GFP-Lactadherin-C2 domain*	David Sapp
DGS016	cho1Δ + prs416-GFP-Lact-C2	SEY6210; cho1Δ::KanMX + prs416-GFP-Lactadherin-C2 domain	*MATα leu2-3,112 ura3-52 his3Δ200 trp1Δ901 lys2-801 suc2Δ9 cho1Δ::his3 + prs410-GFP-Lactadherin-C2 domain*	David Sapp
DGS017	ist2Δ + prs416-GFP-Lact-C2	SEY6210; ist2Δ::his3 + prs416-GFP-Lactadherin-C2 domain	*MATα leu2-3,112 ura3-52 his3Δ200 trp1Δ901 lys2-801 suc2Δ9 ist2Δ::his3 + prs410-GFP-Lactadherin-C2 domain*	David Sapp
DGS018	trp1::hghMX	BY4741; trp1::hghMX	*MATa his3Δ1 leu2Δ0 met15Δ0 ura3Δ0 trp1::hghMX*	David Sapp
DGS019	VPH1-mCherry	SEY6210; trp::vph1-mCherry	*MATα leu2-3,112 ura3-52 his3Δ200 trp1Δ901 lys2-801 suc2Δ9 trp::vph1-mCherry*	David Sapp
DGS020	CHS5-mCherry	SEY6210; trp::chs5-mCherry	*MATα leu2-3,112 ura3-52 his3Δ200 trp1Δ901 lys2-801 suc2Δ9 trp::chs5-mCherry*	David Sapp
DGS021	SNF7-mCherry	SEY6210; trp::snf7-mCherry	*MATα leu2-3,112 ura3-52 his3Δ200 trp1Δ901 lys2-801 suc2Δ9 trp::snf7-mCherry*	David Sapp
DGS022	cho1Δ VPH1-mCherry	SEY6210; cho1Δ::his3 trp::vph1-mCherry	*MATα leu2-3,112 ura3-52 his3Δ200 trp1Δ901 lys2-801 suc2Δ9 cho1Δ::his3 trp::vph1-mCherry*	David Sapp
DGS023	cho1Δ CHS5-mCherry	SEY6210; cho1Δ::his3 trp::chs5-mCherry	*MATα leu2-3,112 ura3-52 his3Δ200 trp1Δ901 lys2-801 suc2Δ9 cho1Δ::his3 trp::chs5-mCherry*	David Sapp
DGS024	cho1Δ SNF7-mCherry	SEY6210; cho1Δ::his3 trp::snf7-mCherry	*MATα leu2-3,112 ura3-52 his3Δ200 trp1Δ901 lys2-801 suc2Δ9 cho1Δ::his3 trp::snf7-mCherry*	David Sapp
DGS025	SNX4-GFP	BY4741; SNX4-GFP(S65T)	*MATa his3Δ1 leu2Δ0 met15Δ0 ura3Δ0 SNX4-GFP(S65T):HIS3MX*	C. Boone - from original O'Shea collection
DGS026	SNX41-GFP	BY4741; SNX41-GFP(S65T)	*MATa his3Δ1 leu2Δ0 met15Δ0 ura3Δ0 SNX41-GFP(S65T):HIS3MX*	C. Boone - from original O'Shea collection

DGS027	SNX42-GFP	BY4741; SNX42-GFP(S65T)	*MATa his3Δ1 leu2Δ0 met15Δ0 ura3Δ0 SNX42-GFP(S65T):HIS3MX*	C. Boone - from original O'Shea collection
DGS028	VPS5-GFP	BY4741; VPS5-GFP(S65T)	*MATa his3Δ1 leu2Δ0 met15Δ0 ura3Δ0 VPS5-GFP(S65T):HIS3MX*	C. Boone - from original O'Shea collection
DGS029	VPS10-GFP	BY4741; VPS10-GFP(S65T)	*MATa his3Δ1 leu2Δ0 met15Δ0 ura3Δ0 VPS10-GFP(S65T):HIS3MX*	C. Boone - from original O'Shea collection
DGS030	VPS17-GFP	BY4741; VPS17-GFP(S65T)	*MATa his3Δ1 leu2Δ0 met15Δ0 ura3Δ0 VPS17-GFP(S65T):HIS3MX*	C. Boone - from original O'Shea collection
DGS031	VPS26-GFP	BY4741; VPS26-GFP(S65T)	*MATa his3Δ1 leu2Δ0 met15Δ0 ura3Δ0 VPS26-GFP(S65T):HIS3MX*	C. Boone - from original O'Shea collection
DGS032	VPS29-GFP	BY4741; VPS29-GFP(S65T)	*MATa his3Δ1 leu2Δ0 met15Δ0 ura3Δ0 VPS29-GFP(S65T):HIS3MX*	C. Boone - from original O'Shea collection
DGS033	VPS35-GFP	BY4741; VPS35-GFP(S65T)	*MATa his3Δ1 leu2Δ0 met15Δ0 ura3Δ0 VPS35-GFP(S65T):HIS3MX*	C. Boone - from original O'Shea collection
DGS034	MRL1-GFP	BY4741; MRL1-GFP(S65T)	*MATa his3Δ1 leu2Δ0 met15Δ0 ura3Δ0 MRL1-GFP(S65T):HIS3MX*	C. Boone - from original O'Shea collection
DGS035	ATG27-GFP	BY4741; ATG27-GFP(S65T)	*MATa his3Δ1 leu2Δ0 met15Δ0 ura3Δ0 ATG27-GFP(S65T):HIS3MX*	C. Boone - from original O'Shea collection
DGS036	PEP4-GFP	BY4741; PEP4-GFP(S65T)	*MATa his3Δ1 leu2Δ0 met15Δ0 ura3Δ0 PEP4-GFP(S65T):HIS3MX*	C. Boone - from original O'Shea collection
DGS037	SNX4-GFP CHS5-mCherry	SEY6210; trp::chs5-mCherry SNX4-GFP(S65T)	MATα leu2-3,112 ura3-52 his3Δ200 trp1Δ901 lys2-801 suc2Δ9 trp::chs5-mCherry SNX4-GFP(S65T)	David Sapp
DGS038	SNX42-GFP VPH1-mCherry	SEY6210; trp::vph1-mCherry SNX42-GFP(S65T)	MATα leu2-3,112 ura3-52 his3Δ200 trp1Δ901 lys2-801 suc2Δ9 trp::vph1-mCherry SNX42-GFP(S65T)	David Sapp
DGS039	VPS5-GFP SNF7-mCherry	SEY6210; trp::snf7-mCherry VPS5-GFP(S65T)	MATα leu2-3,112 ura3-52 his3Δ200 trp1Δ901 lys2-801 suc2Δ9 trp::snf7-mCherry VPS5-GFP(S65T)	David Sapp

DGS040	VPS10-GFP VPH1-mCherry	SEY6210; trp::vph1-mCherry VPS10-GFP(S65T)	MATα leu2-3,112 ura3-52 his3Δ200 trp1Δ901 lys2-801 suc2Δ9 trp::vph1-mCherry VPS10-GFP(S65T)	David Sapp
DGS041	VPS17-GFP SNF7-mCherry	SEY6210; trp::snf7-mCherry VPS17-GFP(S65T)	MATα leu2-3,112 ura3-52 his3Δ200 trp1Δ901 lys2-801 suc2Δ9 trp::snf7-mCherry VPS17-GFP(S65T)	David Sapp
DGS042	VPS26-GFP SNF7-mCherry	SEY6210; trp::snf7-mCherry VPS26-GFP(S65T)	MATα leu2-3,112 ura3-52 his3Δ200 trp1Δ901 lys2-801 suc2Δ9 trp::snf7-mCherry VPS26-GFP(S65T)	David Sapp
DGS043	VPS35-GFP SNF7-mCherry	SEY6210; trp::snf7-mCherry VPS35-GFP(S65T)	MATα leu2-3,112 ura3-52 his3Δ200 trp1Δ901 lys2-801 suc2Δ9 trp::snf7-mCherry VPS35-GFP(S65T)	David Sapp
DGS044	MRL1-GFP VPH1-mCherry	SEY6210; trp::vph1-mCherry MRL1-GFP(S65T)	MATα leu2-3,112 ura3-52 his3Δ200 trp1Δ901 lys2-801 suc2Δ9 trp::vph1-mCherry MRL1-GFP(S65T)	David Sapp
DGS045	PEP4-GFP VPH1-mCherry	SEY6210; trp::vph1-mCherry PEP4-GFP(S65T)	MATα leu2-3,112 ura3-52 his3Δ200 trp1Δ901 lys2-801 suc2Δ9 trp::vph1-mCherry PEP4-GFP(S65T)	David Sapp
DGS046	cho1Δ SNX4-GFP CHS5-mCherry	SEY6210; cho1Δ::his3 trp::chs5-mCherry SNX4-GFP(S65T)	MATα leu2-3,112 ura3-52 his3Δ200 trp1Δ901 lys2-801 suc2Δ9 cho1Δ::his3 trp::chs5-mCherry SNX4-GFP(S65T)	David Sapp
DGS047	cho1Δ SNX42-GFP VPH1-mCherry	SEY6210; cho1Δ::his3 trp::vph1-mCherry SNX42-GFP(S65T)	MATα leu2-3,112 ura3-52 his3Δ200 trp1Δ901 lys2-801 suc2Δ9 cho1Δ::his3 trp::vph1-mCherry SNX42-GFP(S65T)	David Sapp
DGS048	cho1Δ VPS5-GFP SNF7-mCherry	SEY6210; cho1Δ::his3 trp::snf7-mCherry VPS5-GFP(S65T)	MATα leu2-3,112 ura3-52 his3Δ200 trp1Δ901 lys2-801 suc2Δ9 cho1Δ::his3 trp::snf7-mCherry VPS5-GFP(S65T)	David Sapp
DGS049	cho1Δ VPS10-GFP VPH1-mCherry	SEY6210; cho1Δ::his3 trp::vph1-mCherry VPS10-GFP(S65T)	MATα leu2-3,112 ura3-52 his3Δ200 trp1Δ901 lys2-801 suc2Δ9 cho1Δ::his3 trp::vph1-mCherry VPS10-GFP(S65T)	David Sapp
DGS050	cho1Δ VPS17-GFP SNF7-mCherry	SEY6210; cho1Δ::his3 trp::snf7-mCherry VPS17-GFP(S65T)	MATα leu2-3,112 ura3-52 his3Δ200 trp1Δ901 lys2-801 suc2Δ9 cho1Δ::his3 trp::snf7-mCherry VPS17-GFP(S65T)	David Sapp
DGS051	cho1Δ VPS26-GFP SNF7-mCherry	SEY6210; cho1Δ::his3 trp::snf7-mCherry VPS26-GFP(S65T)	MATα leu2-3,112 ura3-52 his3Δ200 trp1Δ901 lys2-801 suc2Δ9 cho1Δ::his3 trp::snf7-mCherry VPS26-GFP(S65T)	David Sapp
DGS052	cho1Δ VPS35-GFP SNF7-mCherry	SEY6210; cho1Δ::his3 trp::snf7-mCherry VPS35-GFP(S65T)	MATα leu2-3,112 ura3-52 his3Δ200 trp1Δ901 lys2-801 suc2Δ9 cho1Δ::his3 trp::snf7-mCherry VPS35-GFP(S65T)	David Sapp
DGS053	cho1Δ MRL1-GFP VPH1-	SEY6210; cho1Δ::his3 trp::vph1-mCherry MRL1-GFP(S65T)	MATα leu2-3,112 ura3-52 his3Δ200 trp1Δ901 lys2-801 suc2Δ9 cho1Δ::his3 trp::vph1-mCherry MRL1-GFP(S65T)	David Sapp

	mCherry			
DGS054	cho1Δ PEP4-GFP VPH1-mCherry	SEY6210; cho1Δ::his3 trp::vph1-mCherry PEP4-GFP(S65T)	MATα leu2-3,112 ura3-52 his3Δ200 trp1Δ901 lys2-801 suc2Δ9 cho1Δ::his3 trp::vph1-mCherry PEP4-GFP(S65T)	David Sapp

Yeast chemical transformation

Pelleted log phase yeast cells were washed with LiOAc/TE (0.1 M LiOAc in TE buffer [10 mM Tris, 5 mM EDTA]). Cells were resuspended in 50 µL LiOAc/TE with 5 µL boiled salmon sperm DNA and 1-2 µg plasmid/DNA insert. 300 µL of 40% PEG in LiOAc/TE was gently added and mixed by pipetting. The cells were incubated at 30 °C for 30 minutes followed by 15 minutes at 42 °C. The cells were resuspended in TE, plated, and monitored for growth.

Yeast electroporation transformation

50 mL culture of log phase yeast cells were pelleted at 4 °C. Cells were resuspended in 10 ml pretreatment buffer (100 mM LiAc, 10 mM Tris, 1 mM ETDA, 10 mM DTT) and incubated for 30 minutes at 30 °C at 150 rpm. Cells were kept on ice and washed twice with 25 mL cold sterile H_2O, then washed 2-3 times with 10 mL cold sterile 1 M sorbitol. Cells were resuspended in 500 µL cold sterile 1 M sorbitol. 100 µL of cells with 2 µL boiled salmon sperm DNA, and 5-10 µg linear DNA (to be transformed) were added to a cold 20 mm electroporation cuvette. Cells were pulsed using the BioRad Micropulser Fungi setting (1.5 kV). Immediately after electroporation, the cuvette was transferred to ice and 1 mL of YPD was added. After 10 minutes on ice, the cells were transferred to a microcentrifuge tube and allowed to recover at 30 °C for 1 hour. Cells were pelleted and resuspended in 100 µL 1 M Sorbitol. 50 µL of cells were plated undiluted. 50 µL of 10x and 20x dilutions were also plated as required.

Bacterial DNA transformation

2 µL of plasmid of interest were added to competent DH5α *e. coli*. Cells were incubated on ice for

30 minutes then heatshocked at 42 ºC for 45 seconds. Cells were recovered in 500 µL SOC media for 1 hour at 37 ºC. Culture was spread on LB plate + selection antibiotic (Ampicillin or Kanamycin) and grown overnight at 37 ºC. Then LB + selection antibiotic could be inoculated for miniprep or miraprep. Liquid cultures could be mixed with 50% glycerol to a final concentration of 20% glycerol and stored at –80 °C.

Phospholipid metabolic tracking by [^{3}H]serine

SEY6210, SEY6210 *osh6Δ osh7Δ*, SEY6210 *ist2Δ,* and SEY6210 *cho1Δ* strains were grown overnight in YPD media at 30 ºC at 230 rpm to log phase growth. Three OD_{600} equivalents were harvested and washed three times with SC media (3000 rpm; 5 minutes). Cells were resuspended with 0.5 mL SC media (+ 1 mM ethanolamine for *cho1Δ* strains) and incubated for 30 minutes at 30 ºC. 5 µCi [^{3}H]serine was added to the culture. Cultures were incubated for either 30 or 60 minutes at 30 ºC. Incubation was halted by adding 2 mL 10 mM chilled NaF/NaN_3. Cultures were centrifuged, resuspended in cold water, and transferred to screw-cap tubes. Then they were centrifuged and resuspended in 1 mL chloroform: methanol (C:M; 1:1). Beads were added, and cells were mechanically disrupted by a bead beater (1 minute on, 1 minute on ice, 1 minute on, 1 minute on ice). Samples were transferred to glass test tubes using a Pasteur pipette. Beads were rinsed with 1 mL CM (2:1), and the solution was added to the test tube. 100 µL were removed from each sample for liquid scintillation counting (LSC). 1.5 mL of dH_2O and 1 mL of CM (5:1) were added to the samples. Samples were vortexed for 1 minute and centrifuged (2500 rpm; 10 minutes). 100 µL of the aqueous phase was taken for the total aqueous count in LSC. Subsequently, the aqueous layer and protein interface were aspirated. Samples were washed by adding 1.5 mL dH_2O, vortexing, centrifugation, and the aqueous layer, and any remaining protein interface was aspirated. The organic phase was distributed into 100 µL for LSC, 500 µL for lipid phosphorous determination, and 700 µL for thin layer chromatography (TLC). TLC aliquots could be stored at –20 ºC.

Lipid phosphorous determination

500 µL of organic phase samples from phospholipid metabolic tracking by [^{3}H]serine were dried under N_2 in glass test tubes. 1 mM potassium dihydrogen phosphate in H_2O was distributed as standards in volumes of 0, 5, 10, 20, 40, 60, 80, 100, 120 µL in glass test tubes. 300 µL of H_2O and 150 µL of perchloric acid were added to each sample and standard. Samples and standards were heated at 160 ºC overnight. 700 µL H_2O was added to each sample and standard and cooled at room temperature for 20 minutes. 500 µL of 0.9 % ammonium molybdate was added to each sample and standard, and mixed. 150 µL of 10 % ascorbic acid was added and mixed to each sample and standard. Samples and standards were incubated at 45 ºC for 30 minutes. Absorbance of samples and standards was measured at 820 nm in 1 mL cuvettes. Standards' absorbance was used to create a standard curve. Samples total phosphate was calculated by absorbance using the standard curve.

Thin layer chromatography for phospholipid species

TLC aliquots from phospholipid metabolic tracking by [^{3}H]serine were dried in microcentrifuge tubes by vacuum centrifugation. 20x20cm glass silica plate (60 Å, 250 µm thickness) was scraped to create 1.5 cm wide lanes. Samples were resuspended in 5-10 µL chloroform and spotted on the silica plate. One lane was left blank as a negative control. Three positive control lanes were loaded with 5 µL of one of PC (L-α-phosphatidylcholine [egg, chicken]; 10 mg/mL; Sigma-Aldritch), PS (L-α-phosphatidylserine [brain, procine] [sodium salt]; 10 mg/mL; Sigma-Aldritch), or PE (L-α-phosphatidylethanolamine [liver, bovine], 10 mg/mL; Sigma-Aldritch). TLC plate was run in a large, equilibrated tank containing a piece of filter paper ~20x20 cm and chloroform-methanol-acetic acid-H_2O (25:15:4:2) until the solution reached about 1 cm from the top of the plate. The plate was dried at room temperature and then placed in a container with iodine crystals for lipid staining. Standards were marked on the plate based on the iodine staining. The plates were then scanned using a TLC scanner (5 minutes per lane; blank lane used for background subtraction).

Peaks of radioactivity were detected and paired with phospholipid standards based on migration distance. PS, PE, and PC spots were scraped from each sample lane and moved into scintillation tubes. A scintillation cocktail was added, and vials were mixed before scintillation counts were performed for ^{3}H disintegrations per minute (DPM).

Antibodies

Affinity-purified monoclonal mouse IgG2a anti-GFP antibody, JL-8 was a kind gift from Dr. Chris McMaster or purchased from Takara bio (Lot# A8034133).

Goat Anti-Mouse IgG HRP secondary antibody from Cayman Chemical Company (Batch# 0610381-1).

Gel electrophoresis

Agarose gels were made with 1 % agarose in TAE buffer. Gel solution was microwaved until boiling for ~10-15 seconds. DNA dye (BioBasic Eco-Stain; Thermo Fisher SYBR Safe DNA gel Stain; FroggaBio RedSafe Nucleic Acid Staining Solution) was added as required by manufacturer instructions. The gel was left at room temperature in the molding tray until solidified. Samples were mixed with gel loading dye (New England Biolabs Gel Loading Dye (6x) and run at 90-120 V. Gels were imaged using an Azure 600 digital imager (Azure Biosystems) using UV excitation settings.

Plasmid amplification – Mini-prep

Mini-prep was completed according to the Qiagen Quick-StartProtocol. The concentration of final elutions was measured by nanodrop, and samples could be stored at –20 C.

Plasmid amplification – Maxi-prep

Maxi-preps were completed using the "Mira-prep" protocol as outlined by Pronobis *et al*., 2016. Briefly, 50 mL of LB media with antibiotic selection (Ampicillin [100 μg/mL]/Kanamycin [50

μg/mL]) was inoculated with bacteria containing the plasmid of interest. Cultures were grown overnight at 250 rpm at 37 ºC. Cells were pelleted at 4000 rcf at 4 ºC for 10 minutes. The pellet was resuspended in 2 mL resuspension buffer (Qiagen Buffer P1) containing 100 ug/mL RNase A in a 15 mL falcon tube. 2 mL lysis buffer (Qiagen Buffer P2) was added, and the tube was mixed by inversion. After 3 minutes at room temperature, 2 mL of neutralisation buffer (Qiagen Buffer N3) was added and mixed by inversion. Falcon tubes were centrifuged at 3500 rcf for 5-10 minutes, and the supernatant was distributed into 1.5 mL microcentrifuge tubes. Microcentrifuge tubes were centrifuged at 13200 rcf for 10 minutes. The supernatants were collected and combined, then 1 volume of ≥ 96 % ethanol was added and mixed. This solution was added to ≤ 5 DNA-binding spin columns in sequential aliquots of up to 700 μL. Aliquots were centrifuged at 13200 rcf after the addition of each aliquot for 30 sec. Flow-through was discarded. Columns were washed twice by adding 500 μL of wash buffer (Qiagen Buffer PB), centrifuging at 13200 rcf, and discarding flow-through. Empty columns were centrifuged at 13200 rcf to remove residual wash buffer. Columns were transferred to 1.5 mL microcentrifuge tubes. Plasmids were eluted by 1 minute incubation with 30-35 μL of nuclease-free H_2O followed by centrifugation at 13200 rcf for 2 minutes. Elutions were combined, and concentration was measured using a Nanodrop Microvolume Spectrophotometer. Isolated plasmids were stored -20 ºC.

Plasmid markers

Table 2.2. List of plasmid markers

Name	Yeast selection	Fluorescent tag	Protein	Source
prs410-GFP-Lactadherin-C2 domain	Kanamycin	GFP	Lactadherin-C2 domain	G. Fairn
Prs416-GFP-Lactadherin-C2 domain	Uracil	GFP	Lactadherin-C2 domain	G. Fairn
pFA6a-GFP(F64L,S65T,R80Q,V163A)-His3MX6	Histidine	GFP	N/A	C. McMaster

Organelle markers

Plasmids designed by Zhu *et al*., 2019 were purchased from Addgene and transformed into *E. coli* (DH5α). Plasmids were amplified by miniprep and linearised by 1 hour incubation at 37 ºC with the required restriction enzyme according to Zhu *et al*., 2019. Reactions were performed in 40 µL total volume nuclease-free H_2O with 1X of (10X) FastDigest Buffer (Thermo Fisher Scientific), 20 µL plasmid (~800 ng), and 1 µL restriction enzyme. Reactions were halted by 15 minutes incubation at 65 ºC. Linearized DNA was then transformed into the SEY6210 wildtype or *cho1Δ* strains.

Plasmids for organelle labelling

Table 2.3. List of organelle marker plasmids

Name	**Index**	**Labelled structure**	**Colour**	**Selection marker**	**Restriction enzyme**	**Insert locus**
CHS5-mCherry	ZJOM73	Late Golgi/Early endosome	Red	Trp	AflII	CHS5 promoter
Snf7-mCherry	ZJOM44	Late endosome	Red	Trp	MfeI	SNF7 promoter
VPH1-mCherry	ZJOM65	Vacuole	Red	Trp	PmII	VPH1 promoter

Primers

Table 2.3. List of primers

Ist2Δ forward	5'- TGCGCATAATTTGTTCTTGTAGG -3'
Ist2Δ reverse	5'- CTGTAAGGCCCAAAAGGGCT -3'
Cho1Δ forward	5'- ACCATCTGGCGACAAGCAG -3'
Cho1Δ reverse	5'- GCCATGAAAACCTCTCAAACCTT -3'
Vps5-GFP forward	5'- AAACATTGGAGAGAAGGTATAACCTTACAAA -3'
Vps5-GFP reverse 200 bp	5'-ACTGGACTGAAACGGATATTGAAATG-3'
Vps5-GFP reverse 500 bp	5'- CACAAGAGGTCACTTCTTCTTATTCTATGTC -3'
Vps10-GFP forward	5'- ACGCCAATGACTTATCCAGTTTC -3'
Vps10-GFP reverse ~200 bp	5'- TTTTCCCCATCACAACTGGC -3'
Vps10-GFP reverse 500 bp	5'-AATGAAGTACTATAAATATTAAAGTACGTTAGTAGTTTATTTCTCTT -3'
Vps17-GFP forward	5'- ATACTTCTCAAACCCTTAAAGGGGAC -3'
Vps17-GFP reverse ~200 bp	5'- AACGCATTTGGTCAACAGTGA -3'

Vps17-GFP reverse 500 bp	5'- TATAGAGAAATAGCGGTAGACTTGATAGTGAT -3'
Vps26-GFP forward	5'- TCCGATACGAAATAATGGATGGGT -3'
Vps26-GFP reverse ~200 bp	5'- TTGTTCCCTTGGACAACGCT -3'
Vps26-GFP reverse 500 bp	5'- CATATACATTCGTTTCTTTTTCTCCTCCC -3'
Vps29-GFP forward	5'- AGAATGAGAATGAAAGCAACGTTAAGC -3'
Vps29-GFP reverse 200 bp	5'- AAACACTGCAGTGCTAATTCGG -3'
Vps29-GFP reverse 500 bp	5'- GACACATTGGCGTTTGAGGT -3'
Vps35-GFP forward	5'- TAGGATCGGATGGTACGTATATTCAATTAAAT -3'
Vps35-GFP reverse 200 bp	5'- AGAATAGATTTGTGAGCGCATTGG -3'
Vps35-GFP reverse 500 bp	5'- ATACTTTGATATCATTATCGTTGGAAATAGTACTGTAC -3'
Snx4-GFP forward	5'- TAACGTCATTAACAGGTGAATTAGAAAACG -3'
Snx4-GFP reverse ~200 bp	5'- TGATTACAGGACTTGTTTTGCGA -3'
Snx4-GFP reverse 500 bp	5'- GCAGGGTACGAGAGTATACCG -3'
Snx41-GFP forward	5'- AAGATTGTCTATCAATCTGTATATCAGACATGC -3'
Snx41-GFP reverse 200 bp	5'- TTCTTCAATCTAGGTCTAGCTTTTATTTGTTCTTA -3'
Snx41-GFP reverse 500 bp	5'- TACTACTGACAATTGGTTGATTTTATCATAAAATTTAGAAA -3'
Snx42-GFP forward	5'- CTGAATCATTGGAAGTTACTGAGAATGATTT -3'
Snx42-GFP reverse 200 bp	5'- TGAGTTGGCCATATAGGCATCTC -3'
Snx42-GFP reverse 500 bp	5'- CAAGGCTGACATCGTATGGTG -3'
Pep4-GFP forward	5'- CCAGAGACAATCTACCTGATCTAATTTTCA -3'
Pep4-GFP reverse 200 bp	5'- CGCTATTGGAAAAGGATAAACAAGGAAATTC -3'
Pep4-GFP reverse 500 bp	5'- CGAATTAGAGGTGCTCCGTATGGA -3'
Mrl1-GFP forward	5'- TGAGGTCTTTAGTCAGAGGCAGG -3'
Mrl1-GFP reverse 200 bp	5'- AGTAAAAAAGGAGTAGAAACATTTTGAAGCT -3'
Mrl1-GFP reverse 500 bp	5'- AAAAATGAAACTGAAACTTGAGAAATTGAAGAC -3'
Atg27-GFP forward	5'- ACGCTCTACTGTTTACATTGATATACCTG -3'
Atg27-GFP reverse ~200 bp	5'- TTTATCACATGACGAAACTGTTCTT -3'
Atg27-GFP reverse 500 bp	5'- CAAACATGTCACAGATAGCACAAGAA -3'
HIS3MX6 test forward	5'- ATACTAACGCCGCCATCCA -3'
GFP test reverse	5'- GGTAGTTTTCCAGTAGTG -3'

For *ist2,* primers were designed 508 bp upstream and 3386 downstream from the start codon according to the genomic sequence available on SGD (https://www.yeastgenome.org/). *cho1Δ*

primers were designed 652 bp upstream and 1242 bp downstream from the start of the *cho1* gene according to genomic sequence available on SGD. Primers were designed for amplifying DNA sequences of C-terminally GFP-labelled proteins provided by Dr. Chris Boone's lab (University of Toronto) originally from the O'Shea collection (Huh *et al*., 2003). These strains were initially constructed using the Longtine approach using the pFA6a-GFP(S65T)-HIS3MX6 plasmid (Longtine *et al*., 1998). All primers were designed to have a T_m near 58 ºC. Forward primers for GFP-labelled proteins were designed 200 bp upstream of the protein of interest's stop codon using sequences available on SGD. Two sets of reverse primers were designed, 200 and 500 bp downstream of the protein of interest's stop codon. A forward primer within the sequence of HIS3MX6 was designed to confirm the presence of the HIS3MX6 selection sequence following DNA transformation. A reverse primer within the sequence of GFP was designed to confirm the presence of GFP following DNA transformation. HIS3MX6 and GFP test primers were designed using the pFA6a-GFP(S65T)-HIS3MX6 sequence.

Yeast gDNA extraction

Genomic DNA extraction was completed using the ThermoFisher Scientific Yeast DNA extraction kit and following the manufacturer's instructions. The concentration of purified DNA samples was measured by nanodrop. Samples could be stored at –20 ºC.

Low-fidelity polymerase chain reaction (PCR)

For genotyping, samples were prepared on ice as either 20 or 50 µL reactions. Starting conditions were 2 ng/µL template DNA, 0.5 µM forward primer, 0.5 µM reverse primer, 1X of (2X) Taq FroggaMix (FroggoBio) or 1X of (2X) DreamTaq Green Master Mix (Thermo Fisher Scientific), and nuclease-free water. Samples were heated on a thermocycler using the following steps: initial denaturation at 94 ºC for 3-5 minutes; 35 cycles of 94 ºC (denaturation) for 30 seconds, 58 ºC (annealing) for 30 seconds, and 72 ºC (extension) for at least 1 min/kbp. Template DNA

concentration, annealing temperature, extension time, Samples were run by agarose gel electrophoresis to confirm product generation. Products could be purified by PCR purification and stored at –20 ºC.

High-fidelity PCR

High-fidelity PCR was conducted using Phusion high-fidelity DNA polymerase (Thermo Scientific) or King Kong Pfu DNA polymerase (civic Biosciences). Starting conditions for Phusion high-fidelity DNA polymerase reactions were 2 ng/µL template DNA, 0.5 µM forward primer, 0.5 µM reverse primer, 3 % DMSO, 1X of (5X) Phusion HF Buffer (Thermo Fisher Scientific), 200 µM dNTPs, nuclease-free water, and 0.02 U/µL Phusion High-Fidelity DNA Polymerase. Starting conditions for King Kong Pfu DNA polymerase reactions were 2 ng/µL template DNA, 0.5 µM forward primer, 0.5 µM reverse primer, 3 % DMSO, 1X of (2X) King Kong Buffer, 200 µM dNTPs, and nuclease-free water. Samples were heated on a thermocycler using the following steps: initial denaturation at 94 ºC for 3-5 minutes; 35 cycles of 94 ºC (denaturation) for 30 seconds, 58 ºC (annealing) for 30 seconds, and 72 ºC (extension) for at least 1 min/kbp. Samples were run by agarose gel electrophoresis to confirm product generation. Products could be purified by PCR purification and stored at –20 ºC.

Gel extraction

DNA samples were run on 0.8 or 1 % agarose gels with extended lanes using low voltage (70-80 V). The band of interest was identified and cut out of the gel. The gel slice was placed in a 0.5 mL microcentrifuge tube with a hole in the bottom. This tube was placed in a 1.5 mL microcentrifuge tube and stored at –20 ºC for at least 30 minutes. Samples were centrifuged at high speed for 10 minutes. Supernatant was moved to a new tube and 10 % 3 M Na-acetate pH 5.2 was added alongside 2 volumes 100 % ethanol. Samples were incubated at –20 ºC for 30 minutes. Samples were run through DNA binding columns 3 times and washed with wash buffer. Empty column was

spun again and DNA was eluted by nuclease-free H_2O. Samples could be stored at –20 ºC.

PCR purification

PCR purification was completed using the Luna Nanotech PuroSPIN PCR Product Purification Kit and following the manufacturer's product manual. The concentration of purified DNA samples was measured by Nanodrop. Samples were stored at –20 ºC.

Yeast protein extraction

On ice, 5 mL overnight yeast cultures were resuspended in 200 µL of nuclease-free H_2O with 1X of (10X) RIPA buffer, 1 tablet/50 mL protease inhibitors (cOmplete ULTRA Tablets, EDTA-Free; Rocha), and 1 mM PMSF. Samples were transferred to 1.5 mL microcentrifuge tubes and 0.5 mm glass beads (Cole-Parmer) were added. Cells were homogenized for 1 minute using BioSpec Mini-Beadbeater. Tubes containing lysates were moved to ice for 3 minutes before homogenization for 1 minute using the same machine. Lysates were returned to ice for several minutes before centrifugation at 14000 rcf at 4 ºC for 10 min. The supernatant was transferred to new microcentrifuge tubes and samples were stored at –20 ºC.

Bradford assay

Bovine Serum Albumin (BSA) standards of the following concentrations were made by serial dilutions: 2 mg/mL, 1.5 mg/mL, 1 mg/mL, 0.75 mg/mL, 0.5 mg/mL, 0.25 mg/mL, 0.125 mg/mL, and 0 mg/mL in PBS. Standards were stored at –20 ºC. 5 µL of standards and protein samples diluted in PBS were added to a 96-well plate in duplicate. 250 µL of Bradford Reagent was added to each sample. The plate was mixed by a shaker for 30 seconds and then incubated for 5-45 minutes at room temperature. Absorbance was measured at 595 nm and BSA standards were used to calculate the protein concentration of samples.

Western blot - immunoblotting

Protein samples were mixed with 1X of (2X) Laemmli buffer and 5 % β-mercaptoethanol and boiled for 5 minutes. Gel electrophoresis was run on samples using SurePAGE, Bis-Tris 4-12 % gels with Tris-MOPS running buffer. 3 µL Precision Plus Protein All Prestained Protein Standards was loaded as a protein ladder. Proteins were transferred to PVDF membranes using the Trans-Blot Turbo Transfer System (BioRad) according to the manufacturer's instruction manual for 1.5 mm gels. For fluorescence and chemiluminescence imaging an Azure 600 was used. Total protein was visualized using No-Stain Protein Labeling Reagent (Thermo Fisher Scientific) according to manufacturer instructions. Total protein was measured using the Azure 600 (Protein stain Ex/Em: 472/595 nm; protein ladder Ex/Em: 628/735 nm). Membranes were blocked with 5 % skim milk in TBST for 1 hour at room temperature (or overnight at 4 ºC) and then incubated with primary antibody in 5 % skim milk in TBST for 1.5 hour (or overnight at 4 ºC). Membranes were washed 5 times for 5 minutes with TBST and incubated for 1 hour with secondary antibody in 5 % skim milk in TBST. Membranes were washed again 5 times for 5 minutes each. Membranes were imaged using the Azure 600. For horse radish peroxidase (HRP) secondary antibodies, membranes were rinsed with Radiance Plus Femtogram HRP substrate (Azure Biosystems) for 1-2 minutes and then imaged with 30 sec, 1 minute, and 5 minutes exposure times for chemiluminescence.

Stripping buffer

For PVDF/nitrocellulose membrane stripping, a stripping buffer of 10 % SDS, 0.5 M Tris HCl pH 6.8, 0.8 % β-mercaptoethanol in H_2O was used. Membranes were stripped for 1 hour and washed with TBST. Membranes could then be reprobed by immunoblotting.

PS distribution assay

SEY6210 (Wild type) WT, *osh6Δosh7Δ*, *ist2Δ*, and *cho1Δ* cells were transformed with plasmids expressing GFP-Lact-C2. Cells were grown overnight in YPD at 30 ºC and back inoculated 1 in 5 the next day. Cells were grown for 4-5 hours before washing twice with 2 % glycerol 1 mM

ethanolamine in PBS. Circular coverslips were pretreated with ~0.2 % Concanavalin A in PBS for at least 10 minutes. 5 µL of resuspended cells were added to the coverslip and centrifuged at 1200 rcf for 1 minute. Coverslips were loaded in a round chamber and cells were covered in PBS. Cells were imaged by spinning disk confocal microscopy.

Endocytosis assay

SEY6210 WT and *cho1Δ* cells with organelle markers Chs5-mCherry, Snf7-mCherry, or Vph1-mCherry were grown overnight in YPD at 30 ºC and back inoculated 1 in 5 the next day. Cells were grown for 4-5 hours before washing twice SC media and resuspending in SC media with 1 mM Ethanolamine and 10 µM SynaptoGreen C4. Cells were incubated at 0 ºC for 30 minutes. Circular coverslips were pretreated with ~0.2 % Concanavalin A in PBS for at least 10 minutes. Cells were removed from ice and imaged at 0, 10, 20, 40, and 60 minutes. For imaging, cells were washed once and then centrifuged at 1200 rcf for 1 minute at 4 ºC on prepared coverslips. Coverslips were loaded in a round chamber and cells were covered in PBS. Cells were imaged by spinning disk confocal microscopy.

Bud Scar assay

SEY6210 Vph1-mCherry and SEY6210 *cho1*D Vph1-mCherry strains were grown overnight in YPD at 30 ºC and back inoculated 1 in 5 the next day. Cells were grown for 4-5 hours before washing twice with 2 % glycerol 1 mM ethanolamine in PBS. The pellet was then resuspended in 2 % glycerol 1 mM ethanolamine 100 µg/mL Wheat Germ Agglutinin CF®405S conjugate (Biotium; #29027; lot#: 22W0718-1192) in PBS and incubated for 10 minutes in the dark. 5 µL of resuspended cells were added to the coverslip and centrifuged at 1200 rcf for 1 minute. Coverslips were loaded in a magnetic chamber and cells were covered in PBS. Cells were imaged by spinning disk confocal microscopy.

GFP colocalisation assay

Yeast strains were grown overnight in YPD at 30 ºC. Cultures were backinoculated and grown for 4 hours at 30 ºC. Circular coverslips were pretreated with ~0.2 % Concanavalin A in PBS for at least 10 minutes. Cultures were washed with either PBS, SC media, or 2 % glucose 1 mM ethanolamine in PBS. Cultures were resuspended in either PBS, SC media or 2 % glucose 1 mM ethanolamine in PBS for imaging. 5 µL of resuspended cells were added to the coverslip and centrifuged at 1200 rcf for 1 minute. Coverslips were loaded in a round chamber and cells were covered in PBS. Cells were imaged by spinning disk confocal microscopy.

Microscope Specifications

Intelligent Imaging Innovation (3i) Marianas™ spinning-disc confocal microscopy is based on the Zeiss Axio Observer 7 Advanced Microscope with Definite Focus 3. Epifluorescence viewing and imaging of samples used pE-340Fura Illumination System (CoolLED) with GFP, mCherry or Fura2 filter cubes (Chroma). The system incorporates a Yokogawa CSU-W1 T2 Super-Resolution Spinning Disk Confocal, 50 µm and SoRa Disks with a magnification changer (1x, 2.8x, and 4x) for confocal and super-resolution imagining. The system has a Plan-Apochromat 20x /0.8NA and a C Plan-Apochromat 63x/1.4NA Oil Objective (Zeiss). The system uses 4 lasers controlled by a LaserStack v4 with single-mode optical fibres for 405 nm (150 mW), 488 nm (200 mW), 561 nm (140 mW), 638 nm (200 mW). Samples were collected using appropriate single bandpass filters or a quad-band filter (440/521/607/700 nm). Images were acquired with a Hamamatsu ORCA Fusion BT sCMOS Camera with 2304 x 2304 pixels and a pixel size of 6.5 µm controlled with SlideBook software (3i). Acquisition settings and capture were controlled by SlideBook Software v2023 (Intelligent Imaging Innovations).

Image analysis

Image analysis was completed using Fiji software (Schindelin *et al*., 2012). ImageJ Macros were

used to assist with this process (Figure 2.1). All images were filtered (Figure 2.1a). For colocalisation experiments, images were converted to maximum Z-projections and colocalisation was measured using JaCOP (Bolte & Cordelières, 2006) (Figure 2.1b,c). Object counts were obtained by the "3D Object Counter" tool in Fiji for the colocalisation experiments. For the bud scar imaging assay, bud scar counts and vacuole categorization/counts were completed manually. For

a. Filter

```
run("Subtract Background...", "rolling=50 sliding stack");
run("Despeckle", "stack");
```

b. Max Intensity Projections

```
run("Duplicate...", "title=GFP-mcherry duplicate channels=2-3");
run("Duplicate...", "title=GFP duplicate channels=1");
selectImage("GFP-mcherry");
run("Duplicate...", "title=mcherry duplicate channels=2");
selectImage("GFP");
run("Z Project...", "projection=[Max Intensity]");
selectImage("mcherry");
run("Z Project...", "projection=[Max Intensity]");
```

c. Colocalisation Measurements

```
imageCalculator("AND create", "Mask","MAX_GFP");
selectImage("Result of Mask");
selectImage("Mask");
selectImage("GFP");
selectImage("Mask");
selectImage("Result of Mask");
rename("GFP mask");
imageCalculator("AND create", "Mask","MAX_mcherry");
selectImage("Result of Mask");
selectImage("Mask");
selectImage("GFP");
selectImage("Mask");
selectImage("Result of Mask");
rename("Mask mcherry");
run("JACoP ");
```

d. Creating PM and Intracellular Regions

```
run("Duplicate...", "title=threshold");
setAutoThreshold("Otsu dark 16-bit no-reset");
//run("Threshold...");
//setThreshold(22, 255);
setOption("BlackBackground", true);
run("Convert to Mask");
run("Fill Holes");
//setTool("wand");
doWand(65, 65);
roiManager("Add");
run("Options...", "iterations=6 count=1 black edm=8-bit do=Erode");
//setTool("wand");
doWand(62, 71);
roiManager("Add");
```

Figure 2.1. ImageJ macros used for image analysis

measuring the PM/intracellular intensity ratio in the PS distribution assay, intracellular signal and total signal were assessed (Figure 2.1 d). PM signal was calculated by subtracting intracellular

signal from total signal. PM signal and intracellular signal were divided by their respective area to calculate average intensity in each region. Then PM/intracellular intensity signal was calculated.

Data analysis

All data analysis was completed using RStudio software with R version 4.3.2. Plots were created using the ggplot2 package. When sufficient sample sizes were available, ANOVA was completed, and significance was tested using the significance tests described in the respective figures. Statistical analysis was completed using RStudio software.

CHAPTER 3 Distribution of Phosphatidylserine by Osh6 and Osh7

3.1 Introduction

Phospholipids are the major building blocks for cellular membranes, participating in many aspects of cellular structure and function. Their internal organisation within the cellular environment requires regulation of lipid transport. Consequently, the mechanisms by which phospholipids are transported are essential to cellular function. PS is the most abundant negatively charged phospholipid (Vance *et al*., 2008), is accumulated in the PM and found mainly in the cytosolic leaflet and has important roles in cellular functions.

The distribution of PS has been studied in *S. cerevisiae* as a single-cell eukaryotic model organism. In yeast, PS comprises 34 mol % of the PM, 13 mol % of secretory vesicles' membranes, and only 4 mol % of vacuoles' membranes (Zinser *et al*., 1991). Furthermore, PS on the PM is nearly entirely on the intracellular leaflet (Mioka *et al*., 2014). PS also accumulates in bud necks, the bud cortex, and mating projections (Fairn *et al*., 2011). Furthermore, PS is important in the processes of cell division and mating. The Cdc42 complex is necessary for the initiation of these cellular functions, however, in the absence of PS its own polar localisation is impaired (Fairn *et al*., 2011). PS within the cell also contributes to endocytic trafficking pathways (Kashikuma *et al*., 2023; Ma *et al*., 2018).

The mechanisms of PS metabolism and trafficking control the distribution of PS that is necessary for it to contribute to these cellular functions. In yeast, PS is synthesised in the ER by Cho1 from CDP-DAG and serine (Vance, 1990). PS can then be converted to PE by either Psd1 or Psd2 in the inner mitochondrial membrane or TGN/endosomal compartments, respectively (Bürgermeister *et al*., 2004; Calzada *et al*., 2019). Subsequently, PE can be converted by a multistep process to PC in the cytosol. Importantly, for PS to be converted to PE, it must be transported from the ER to either the mitochondria or TGN/endosomes.

Transport of PS between organelles occurs by either vesicular transport or at membrane contact sites. For polarisation to bud necks, bud cortexes, and mating projections, PS is transported by secretory vesicles (Fairn *et al*., 2011). PS transport from ER to mitochondria and directly from ER to PM occurs at membrane contact sites. The ERMES complex acts as a protein tether between the ER and PS and is the site where PS is transported from the ER to the mitochondria, where it is decarboxylated into PE by Psd1 (Nguyen *et al*., 2012). Most PS ends up on the PM by transport across membrane contact sites between the cortical ER and the PM. Lipid transfer proteins Osh6 and Osh7 transport PS from the ER to the PM (Maeda *et al*., 2013). The membrane contact sites where PS transfer from ER to PM occurs are maintained by the tether protein, Ist2. Ist2 is required to localise Osh6 to ER-PM contact sites and to efficiently transport PS to the PM (D'Ambrosio *et al*., 2020). Furthermore, knockout of Osh6 and Osh7 or Ist2 results in decreased steady-state levels of PS (D'Ambrosio *et al*., 2020). In *osh6Δosh7Δ* cells, studies have shown conflicting results describing the distribution of PS measured by the Lact-C2 probe. Maeda *et al*., 2013 showed that PS is delocalised from the PM and adheres to intracellular membrane structures. Other studies showed phenotypic heterogeneity, with some cells having normal PS distributions and others having the phenotype described by Maeda *et al*., 2013 (D'Ambrosio *et al*., 2020; Yang, unpublished). It is possible that alternative mechanisms of PS transport can compensate in the absence of Osh6 and Osh7 through vesicular transport (Fairn *et al*., 2011) or through Snx4-mediated recycling of PS from early endosomes to the PM (Ma *et al*., 2018). The interplay between these mechanisms and lipid transfer proteins is unclear.

The distribution of PS within the cell is important for cellular function; however, the literature lacks explanations for the mechanisms by which this occurs. This work aims to examine further the role of ER-PM contact sites in PS transport to the PM.

3.2 Results

PS distribution in cells with impaired ER-PM PS transfer

The distribution of PS in cells with impaired ER-PM PS transfer was investigated by constructing *ist2Δ* and *cho1Δ* in an SEY6210 genetic background. The *osh6Δosh7Δ* strain was provided courtesy of C. Beh (Simon Fraser University). WT, *osh6Δosh7Δ*, *ist2Δ*, and *cho1Δ* strains were transformed with a plasmid expressing the PS-probe, Lact-C2-GFP. Cells were imaged by spinning disk confocal microscopy and fluorescence intensity was measured in the PM and intracellular space (Figure 3.1a). The ratio of PM/intracellular fluorescent signal was assessed (Figure 3.1b). The *osh6Δosh7Δ* cells had no change in intensity ratio relative to WT, however, *ist2Δ* showed a partial decrease, while *cho1Δ* (which lack PS) had a mean value less than one, indicating more signal in the intracellular space than PM.

Metabolic tracking of [^{3}H]serine in cells with impaired ER-PM PS transfer

Serine follows a linear metabolic pathway beginning with an introduction into PS by Cho1, then conversion to PE, and then PC. The production and degradation of phospholipids can be assessed by tracking serine metabolism. To understand how the transfer of PS from ER to PM affects PS metabolism, phospholipid metabolic tracking of [^{3}H]serine was performed (Figure 3.2). WT, *osh6Δosh7Δ*, and *ist2Δ* cells were assessed using disintegrations per minute (DPM)/total DPM of phospholipids measured (Figure 3.2b). At 30 minutes, PS is significantly decreased in *osh6Δosh7Δ* relative to WT ($p = 0.032$) and *ist2Δ* trends the same way. Concomitantly, PE was significantly increased in *osh6Δosh7Δ* relative to WT ($p = 0.0132$) and, again, *ist2Δ* trends the same way ($p = 0.12$). There is also an increase in PC between 30 minutes and 60 minutes ($p = 0.024$) that is not observed in WT, and once again, *ist2Δ* trends the same way ($p = 0.0575$).

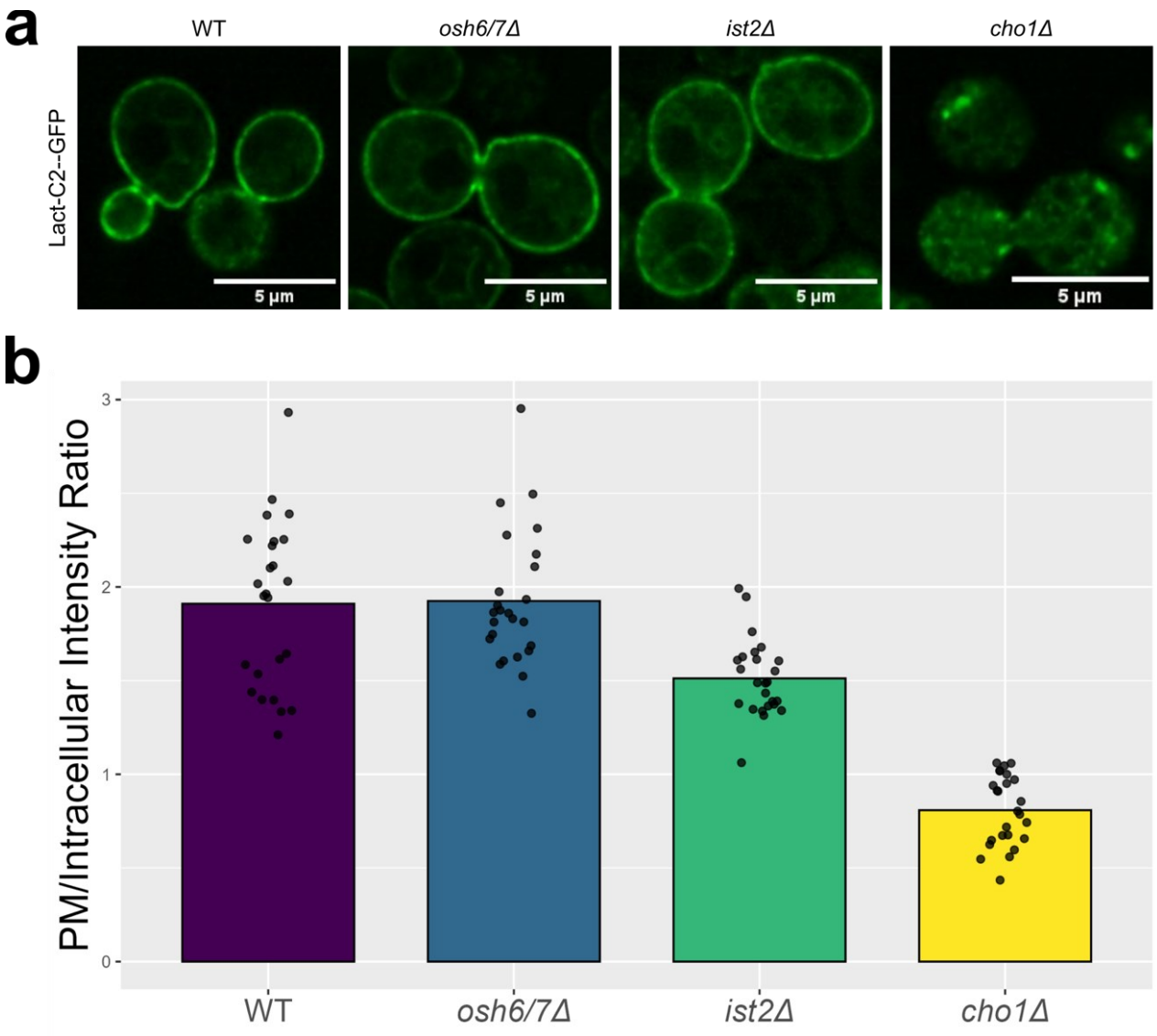

Figure 3.1. PS distribution in mutants with deficient PS trafficking or production. **a**. Spinning disk confocal microscopy representative images of WT, *osh6Δosh7Δ*, *ist2Δ*, and *cho1Δ* cells expressing Lact-C2-GFP probe for PS. **b.** Fluorescence intensity ratio of PM/Intracellular signal from microscopy. Fluorescence intensity was calculated as total signal/area measured for the PM and intracellular space, respectively, from (**a**). Barplots represent mean values and points represent individual cell values. n = 1, 25 cells each.

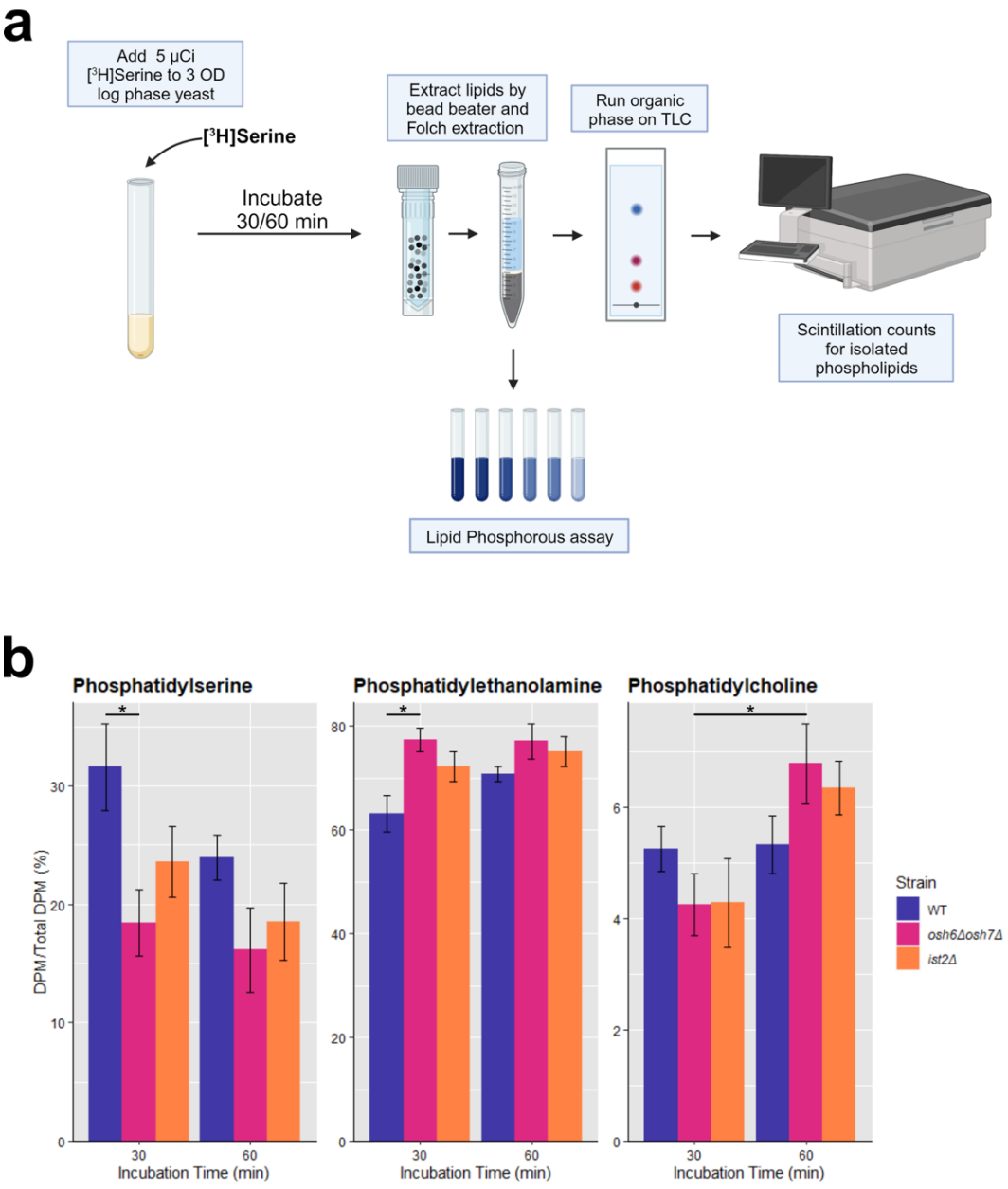

Figure 3.2. Phospholipid metabolic tracking by [^{3}H]Serine in mutants with deficient PS trafficking. **a**. Workflow for following metabolism of serine using radioisotope tracking. Cells were incubated with [^{3}H]serine for 30 or 60 minutes. Lipids were extracted from the cells and separated by TLC. DPM for each phospholipid was measured by a scintillation counter. Lipid phosphorous assay data was not used. **b**. Percent DPM of phospholipid/total DPM of all phospholipids assayed at 30 and 60 minutes for WT, *osh6Δosh7Δ*, and *ist2Δ*. Error bars represent standard error. Statistical analysis was completed using Dunnett test for WT versus mutant comparisons and Student's T test for same strain between timepoint analysis. n = 5; *: p = <0.05. OD: optical density; TLC: thin layer chromatography; DPM: disintegrations per minute. Created using BioRender.com.

3.3 Conclusions

The distribution of PS is dependent on degradation in mitochondria, ER-PM transport, and vesicular trafficking. When the ER-PM transport proteins, Osh6 and Osh7 are removed, PS is still able to be transported to the PM. Furthermore, the loss of Osh6 and Osh7 also alters the metabolism of PS, reducing total PS and changing the proportions of its degradation products. ER-PM transport is an important mechanism for regulating PS, however, compensatory mechanisms are available to ensure that PS production and distribution is not altered too severely.

CHAPTER 4 Phosphatidylserine in Endocytic Trafficking

4.1 Introduction

Endocytosis is a key functional process in eukaryotic cells by which external molecules are internalised into membrane-limited vesicles. The endocytic pathway extends to a trafficking network within the cell that transports both anterograde towards the vacuole and retrograde towards the TGN. Following the anterograde route, clathrin-coated pits form and "pinch-off," from early endosomes. Gradually, early endosomes progress toward the cell's interior and transition into late endosomes or multivesicular bodies. Subsequently, late endosomes deliver their cargo to the vacuole or lysosomes. Retrograde transport occurs from both early and late endosomes toward the TGN with both sources requiring SNX-BAR proteins (Hettema *et al*., 2003). SNX-BAR proteins form an oligomeric matrix around the lipid membrane, facilitating membrane tubulation (van Weering *et al*., 2010; Gopaldass *et al*., 2023). These SNX-BAR proteins are essential for this cellular process and bind preferentially to negatively charged and curved membranes (Peter *et al*., 2004). This coincides with a decrease in proportion relative to other phospholipids of the most abundant negatively charged phospholipid, PS in lipid membranes along the endocytic pathway from the PM to the vacuole.

The relationship between SNX-BAR proteins and negatively charged phospholipids has been focused on PI3P, the classical binding partner for the PX domain, a characteristic component of SNX-BAR proteins. There is substantial support for the role of PS in retrograde trafficking from early endosomes to TGN. For instance, *rcy1Δ* cells are deficient in endosome to TGN transport, resulting in an accumulation of PS in early endosomes (Sun & Drubin, 2012). This is consistent with PS being a cargo of retrograde transport carriers transiting from the endosomes to TGN. This notion was further supported by *snx4Δ psd1Δ* cells having increased cytoplasmic PS compared to WT or *psd1Δ* at the expense of the PM's PS (Ma *et al*., 2018). However, *snx4Δ* alone did not

significantly differ from WT, suggesting two mutations impacting different pathways were required. Interestingly, similar analysis by our own research group showed an increased proportion of *snx4Δ* cells characterized by altered PS distribution relative to WT controls (Yang, unpublished). Most evidence so far supports PS acting through SNX-BAR proteins (Ma *et al*., 2018, Kashikuma *et al*., 2023).

An in vitro assay displayed a direct interaction between PS and SNX-BAR domain proteins. More Snx4-Snx42 heterodimer bound to liposomes containing higher proportions of PS (Ma *et al*., 2018). Furthermore, the addition of Snx4-Snx42 resulted in the formation of membrane tubules in 30% PS-containing liposomes but not liposomes without PS (Ma *et al*., 2018). These data support a functional interaction between PS-containing membranes and Snx4-Snx42 heterodimers. The role of PS in early endosome to TGN transport has been more clearly determined recently. *cho1Δ* cells were shown to accumulate Snx4-containing puncta and have several membrane receptor proteins that mislocalise to the vacuole: Ste2, Snc1, Can1, and Wsc1 (Kashikuma *et al*., 2023). These data support a model of dysfunctional retrograde endocytic trafficking in the absence of PS and that Snx4 and its homologs cannot support transport from endosomes to the TGN in the absence of PS. As a result, proteins typically recycled from the early endocytic pathway accumulate in the vacuole in the absence of PS.

There is less support for the role of PS in retrograde transport from late endosomes to TGN. This pathway is mediated by the retromer complex, which contains the SNX-BAR proteins Vps5 and Vps17. There is no evidence differentiating the proportion of PS in late endosomes specifically, compared to the vacuole (Zinser *et al*., 1991), and Vps5-Vps17 heterodimer binding to liposomes was not significantly affected by PS concentration (Ma *et al*., 2018). It is possible that the *in vitro* model used to investigate Vps5-Vps17 binding to liposomes was missing necessary components of

the cellular environment, such as the other retromer components, Vps26, Vps29 and Vps35. However, previous work from our research group showed that knockout strains for retromer component proteins, Vps26, Vps29, and Vps35 results in a subtle alteration in PS distribution in most of the cells and impaired Vps10 trafficking. (Yang, unpublished). Vps10 is a receptor protein that shuttles carboxypeptidase Y (CPY) precursor from the TGN to the vacuole. After being transported to the late endosomes, Vps10 is recycled to the TGN by the retromer complex in retrograde transport for continued function. In *cho1Δ* cells, Vps10 colocalises with the vacuole and CPY is secreted from the cell instead of delivered to the vacuole (Yang, unpublished).

The role of PS in endocytic trafficking is not well understood. While there is some evidence for early endosome to TGN retrograde transport, the retromer-mediated, late endosome to TGN pathway is not well studied. This work aims to investigate the role of PS in late endosome to TGN retrograde transport and to replicate data showing a role for PS in early endosome to TGN retrograde transport.

4.2 Results

Construction of WT and *cho1Δ* strains with mCherry endocytic organelle markers

To study the role of PS in endocytic trafficking pathways, *S. cerevisiae* from the SEY6210 genetic background was used. WT and *cho1Δ* strains were each transformed with mCherry organelle markers for either early endosomes (Chs5-mCherry), late endosomes (Snf7-mCherry), or vacuoles (Vph1-mCherry) (Figure 4.1a). These organelle markers were created and transformed based on the validated set created by Zhe *et al*., 2019. The fluorescent chimeric proteins are inserted as linear DNA into the genome and expressed under the endogenous promoter as a second copy. Both the Chs5-mCherry and Snf7-mCherry markers appear as small puncta in the cell in the WT and *cho1Δ* strains (Figure 4.1b), as expected for their respective organelles (Zhu *et al*., 2019). The Vph1-

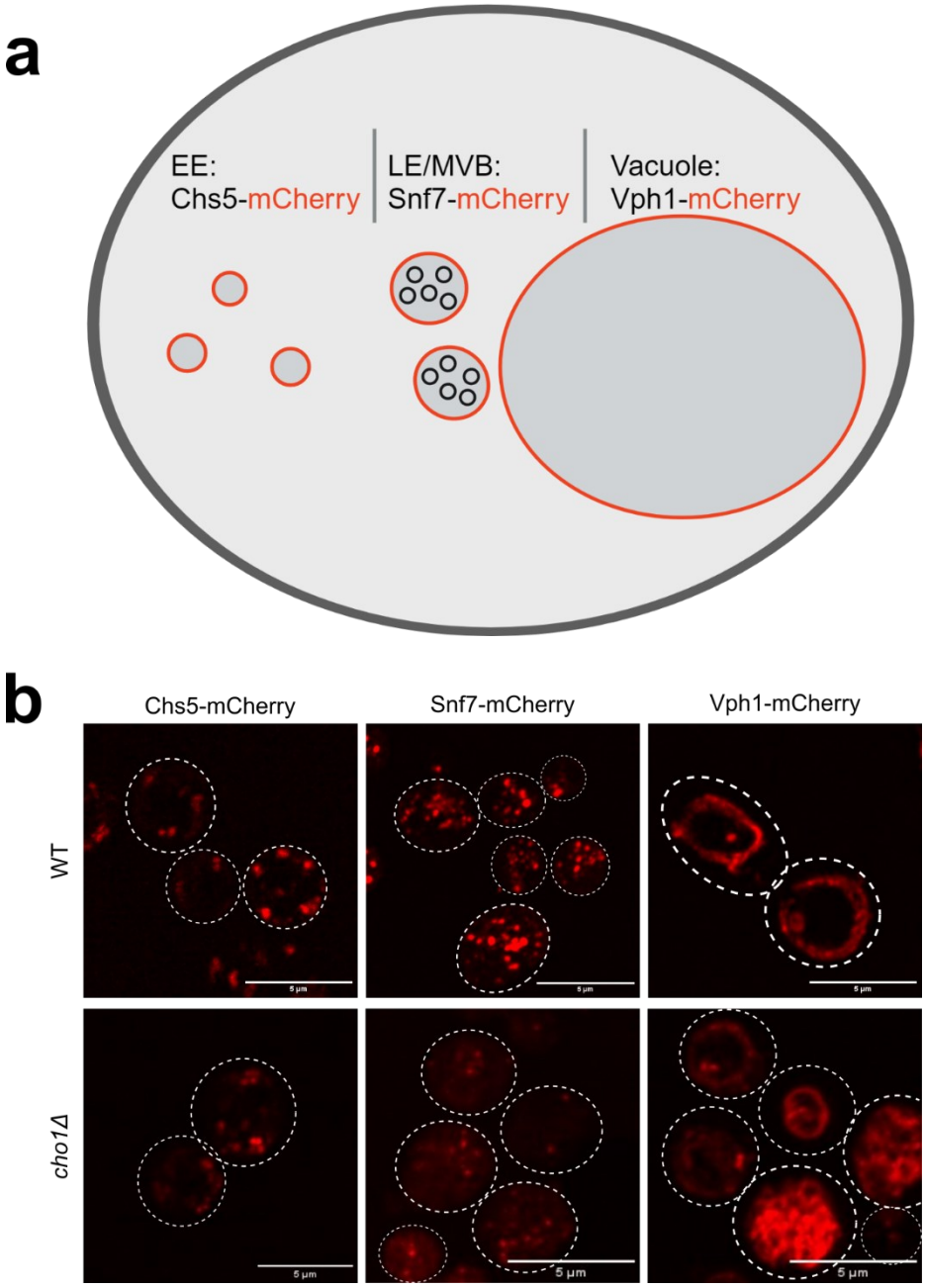

Figure 4.1. mCherry organelle markers transformed into WT and *cho1Δ* strains. **a**. Diagram of fluorescently labelled organelles in the endocytic pathway. Early endosomes are labelled by Chs5-mCherry. Late endosomes/multivesicular bodies are labelled by Snf7-mCherry. Vacuoles are labelled by Vph1-mCherry. **b**. Spinning disk confocal max intensity Z-projections of WT and *cho1Δ* strains in SEY6210 background. Each strain was labelled for organelles along the endocytic pathway described (**a**). Dotted lines indicate the cell perimeters. EE: early endosome; LE: late endosome; MVB: multivesicular body. Created using BioRender.com.

mCherry in the WT presents as a circular outline in an individual Z-slice (not shown), but forms part of a sphere projected on a 2D plane when observed as a maximum intensity projection (Figure

4.1b). This is the expected form of the vacuole in *S. cerevisiae* (Zhu *et al*., 2019). The *cho1Δ* cells display a varied phenotype. Some cells present with regular circular/spherical vacuoles, while others present as a cluster (Figure 4.1b).

The architecture of the organelle markers in the transformed cells supports successful transformation into each strain (Figure 4.1b). The structure of Vph1-mCherry in the *cho1Δ* strain is expected (Yang, unpublished); Figure 4.1b).

To validate the organelle structures as components of the endocytic pathway, pulse-chase of SynaptoGreen C4 (Figure 4.2) was performed in WT and *cho1Δ* strains with mCherry organelle markers. SynaptoGreen C4 is equivalent to FM1-43, a green fluorescence analog of the widely used endocytic tracer, FM4-64 (Vida & Emr, 1995). At 0 minutes, the WT and *cho1Δ* strains both present with SynaptoGreen C4 on the cell surface and in puncta near the cell surface, which may represent clathrin coated vesicles or early endosomes taking up SynaptoGreen C4 (Figure 4.2a). In WT and *cho1Δ* strains expressing Chs5-mCherry, the localisation of Chs5-mCherry was disrupted (data not shown). In the early time points (0 and 10 minutes), the WT cells internalize more of the dye, while the dye remains on the cell surface for longer in the *cho1Δ* cells (Figure 4.2a). In the WT cells at 10, 20, and 40 minutes and in the *cho1Δ* cells at 20, and 40 minutes, most of the dye is internalised in puncta within the cells. At 60 minutes, most of the dye is on the vacuole surface or in vacuole-adjacent puncta in both WT and *cho1Δ* cells, however, there is also a large proportion of the dye that is not clearly localised to subcellular structures at this timepoint in both strains (Figure 4.2a). Comparison of the localisation of SynaptoGreen C4 and mCherry organelle markers shows colocalised puncta in both WT and *cho1Δ* strains expressing Snf7-mCherry at 60 minutes (Figure 4.2b). Similar comparison of WT and *cho1Δ* expressing Vph1-mCherry at 60 minutes shows

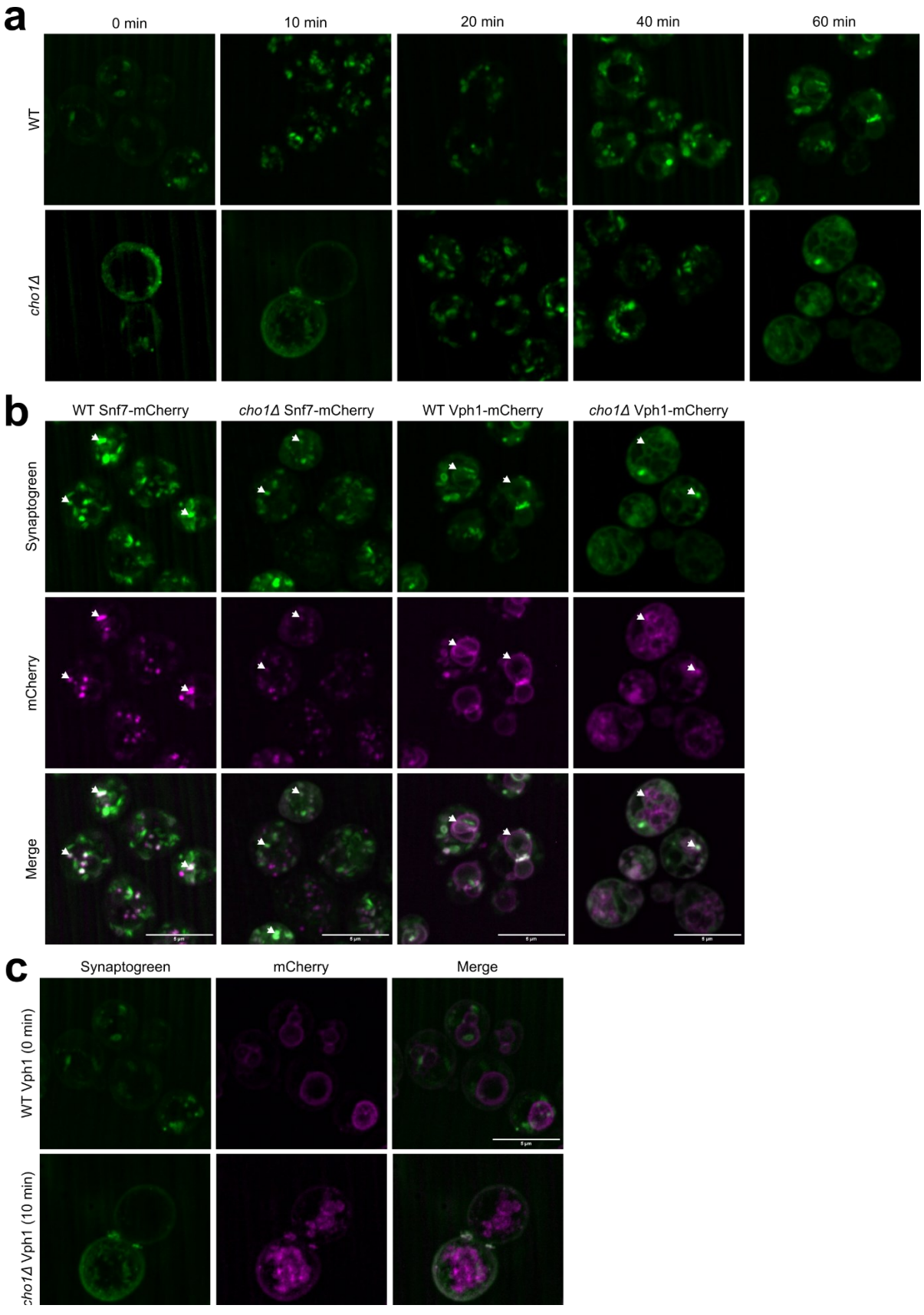
a
0 min
10 min
20 min
40 min
60 min
WT
cho1Δ
b
WT Snf7-mCherry
cho1Δ Snf7-mCherry
WT Vph1-mCherry
cho1Δ Vph1-mCherry
Synaptogreen
mCherry
Merge
c
Synaptogreen
mCherry
Merge
WT Vph1 (0 min)
cho1Δ Vph1 (10 min)

Figure 4.2. Pulse-chase of SynaptoGreen C4 internalisation through the endocytic pathway in WT and *cho1Δ* strains. **a**. Spinning disc confocal imaging of SynaptoGreen C4 pulse chase in WT and *cho1Δ* strains from SEY6210 background with Vph1-mCherry. Following staining, cells were imaged at 0, 10, 20, 40, and 60 minutes. The panels show SynaptoGreen C4 at each time point. **b**. Colocalisation of late endosomes or vacuoles with SynaptoGreen in WT and *cho1Δ* strains at 60 minutes in pulse chase. Late endosomes are identified by Snf7-mCherry expression. Vacuoles are identified by Vph1-mCherry expression. Points showing colocalised SynaptoGreen C4 and mCherry-tagged organelles are indicated by arrowheads. **c**. WT Vph1-mCherry and *cho1Δ* Vph1-mCherry with expected regular vacuole structure before complete internalisation of SynaptoGreen C4. **n.b.** Some images are used in multiple sections of the figure.

colocalisation of SynaptoGreen C4 at low intensity to Vph1-mCherry containing structures (Figure 4.2b). The Vph1-mCherry structures in WT and *cho1Δ* strains at early time points (Figure 4.2c) resemble those found without SynaptoGreen C4 (Figure 4.1b), however, at 60 minutes SynaptoGreen C4 pulse-chase in *cho1Δ* cells, the Vph1-mCherry-containing structures may be further disrupted in comparison with *cho1Δ* Vph1-mCherry alone or at early timepoints (Figure 4.1b, Figure 4.2b,c).

The *cho1Δ* cells exhibit defects in endocytic site formation; however, PS is not necessary for endocytic membrane invagination (Sun & Drubin. 2012). This may result in delayed endocytosis of SynaptoGreen C4, as was observed (Figure 4.2a). After internalisation, the SynaptoGreen C4 is internalised into puncta representing early endosomes and, subsequently, late endosomes (Emr & Vida, 1995). The assessment of early endosomes marked by Chs5-mCherry was not possible due to mislocalisation of Chs5-mCherry when SynaptoGreen C4 was added. This result was unexpected because when the organelle marker was initially validated, it showed a punctate distribution of Chs5-mCherry following incubation with FM4-64 using a similar concentration (16 μM FM4-64 vs. 10 μM SynaptoGreen C4). Furthermore, functional analysis by Zhu *et al*., 2019 of the Chs5-mCherry marker did not show any defects. (Zhu *et al*., 2019). This discrepancy may be due to structural differences between FM4-64 and SynaptoGreen C4 or the use of a different genetic background *S. cerevisiae* strain (TN124 [*MAT*a *leu2 ura3 trp1 pho8Δ60 pho13Δ::LEU2*] versus

SEY6210). The SynaptoGreen C4 transitions from a punctate distribution to a combination of punctate, cytosolic, and vacuolar localisation at 60 minutes (Figure 4.2a). The distribution may have localised more specifically to the vacuole with a longer incubation period. A four-hour incubation period was used previously in the original pulse-chase experiment characterising FM4-64 internalisation, while after 60 minutes, the distribution was more varied (Vida & Emr, 1995). Colocalisation of both Snf7-mCherry and Vph1-mCherry with SynaptoGreen C4 was observed (Figure 4.2b). This supports these organelle markers as components of the endocytic pathway. The increased disruption of Vph1-mCherry in *cho1Δ* Vph1-mCherry cells at 60 minutes can likely be explained by the disruption caused by SynaptoGreen C4, as the WT Vph1-mCherry and *cho1Δ* Vph1-mCherry cells at early time points have architecture consistent with cells untreated with SynaptoGreen C4 (Figure 4.1b). Together, these results support that endocytic compartments are successfully labelled with mCherry markers for late endosomes and vacuoles in WT and *cho1Δ* cells.

Construction of WT and *cho1Δ* strains with organelle markers and GFP-tagged endocytic trafficking proteins

To examine the role of PS in retrograde transport pathways, the WT and *cho1Δ* strains with mCherry labelled markers for endocytic organelles were used to introduce genomically tagged GFP-fusions of proteins involved in retrograde transport. Initially, transformation of GFP-tags was attempted using PCR of pFA6a-GFP(F64L,S65T,R80Q,V163A)-HIS3MX6 using the Longtine *et al*., 1998 method. However, this was unsuccessful due to low transformation efficiency, especially in the *cho1Δ* strains (data not shown). Subsequently, C-terminal GFP(S65T)-labelled strains were acquired from the O'Shea GFP collection (Huh *et al*., 2003), courtesy of the C. Boone research group. Snx4-GFP, Snx41-GFP, Snx42-GFP, Vps5-GFP, Vps17-GFP, Vps26-GFP, Vps29-GFP,

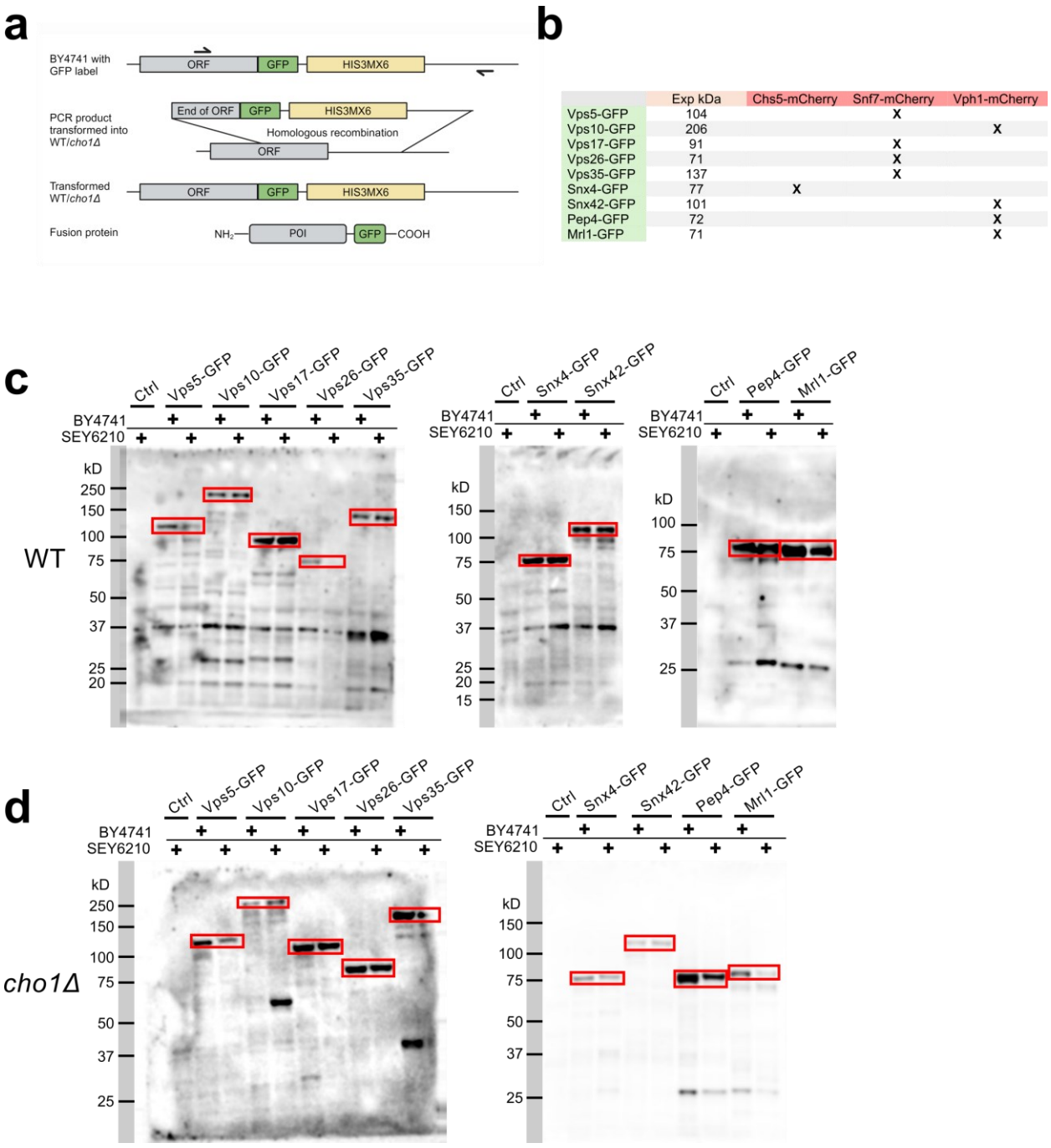

Figure 4.3. GFP-tagging of proteins involved in endocytic trafficking. **a**. Schematic of genomic tagging method. **b**. Table of GFP-tagged strains that were produced in the SEY6210 background. Proteins of interest were tagged in both WT and *cho1Δ* strains containing mCherry labels for organelle markers. The expected size of the GFP-tagged proteins is based on the known protein size plus 28 kDa for GFP. **c,d**. Chemiblots of anti-GFP Western blots of WT and *cho1Δ* strains transformed with a GFP tag. The first lane of each membrane contains a negative control strain (WT Vph1-mCherry) that does not express GFP. Each transformed strain (SEY6210

Vps35-GFP, Atg27-GFP, Mrl1-GFP, Pep4-GFP. Atg27-GFP and Vps29-GFP displayed diffuse

GFP signal similar to soluble GFP and were not used (data not shown). The rest of the GFP-tagged

strains were used as templates for transforming the GFP-tags into WT and *cho1Δ* strains with mCherry-tagged organelles (Figure 4.3a). These transformations result in C-terminal genomic GFP-tags of the endogenous protein of interest. The strains created in both WT and *cho1Δ* are described in Figure 4.3b and their expected size is listed. Immunoblots using anti-GFP antibodies show little to no signal in negative control lanes (WT Vph1-mCherry) (Figure 4.3c,d). The largest band in every lane of both transformed and positive control lanes in WT and *cho1Δ* is within a small range of the expected size of the chimeric protein, except for WT Snf7-mCherry Vps26-GFP, which does not have the expected band (Figure 4.3b-d). Several smaller bands occur among several different GFP-tagged strains and in both transformed strains and positive control strains. The most frequent lesser bands are at ~37 kDa, ~28 kDa, and ~18 kDa (Figure 4.3c,d). There is also a bright band between 50-75 kDa in *cho1Δ* Vph1-mCherry Vps10-GFP (Figure 4.3d).

These Western blots support successful transformation of GFP in WT and *cho1Δ* for each of the described strains except WT Snf7-mCherry Vps26-GFP (Figure 4.3). Furthermore, PCR amplification followed by agarose gel electrophoresis was used to verify each transformation, which was positive for all strains, including WT Snf7-mCherry Vps26-GFP, supporting successful transformation (data not shown). Many smaller bands identified are most likely degradation products containing the GFP fragment. The band at ~28 kDa may represent GFP alone, while larger bands may contain some of the original protein fragment, and smaller bands contain a portion of GFP that the monoclonal antibody is specific to (Figure 4.3c,d). The bright band between 50-75 kDa in *cho1Δ* Vph1-mCherry Vps10-GFP may be a degradation product or an unexpected recombination event, which may result in GFP signal that does not represent Vps10-GFP in this strain (Figure 4.3d).

<u>Colocalisation of endocytic proteins with organelle markers in WT and *cho1Δ* strains</u>

Analysis of the WT and *cho1Δ* strains expressing GFP-tagged proteins related to the endocytic pathway and mCherry organelle markers was performed to describe the role of PS in endocytic trafficking. The impact of *cho1Δ* on colocalisation of GFP and mCherry from spinning disk confocal microscopy maximum intensity Z-projections and 3D object counts of GFP were assessed in each strain. For each strain, colocalisation was measured by Mander's and Pearson's coefficients, with M1 representing the proportion of GFP signal overlapping with mCherry signal, M2 representing the proportion of mCherry signal overlapping with GFP signal. Pearson's coefficient was measured for the total cell area (Mander's *et al*., 1993). For this data, Mander's coefficients can be used to measure correlation of relevant structures, however, Pearson's coefficient is biased by negative space and background fluorescence (Dunn *et al*., 2011), making it unreliable for assessing correlation unless comparing between groups.

Snx4 is a SNX-BAR protein that forms heterodimeric complexes with other SNX-BAR proteins, Snx41 and Snx42. Snx4-Snx42 heterodimer is important for retrograde transport from early endosomes to TGN, while Snx4-Snx41 is important for transporting Atg27 from the vacuole to endosomes (Ma *et al*., 2016; Hettema *et al*., 2003). Snx4-GFP does not correlate highly with Chs5-mCherry in the WT or *cho1*Δ based on Mander's and the Pearson's coefficients have similar values (Figure 4.4a,b). The Snx4-GFP object count per cell is similar between groups, trending toward more puncta in WT, however, this trend is inverted when accounting for cell area. (Figure 4.4c). In the WT and *cho1Δ* Snx42-GFP Vph1-mCherry strains, there is an increase in M1 in the *cho1Δ* relative to WT. The object count per cell and per cell area also decreased in *cho1Δ* relative to WT (Figure 4.4d-f).

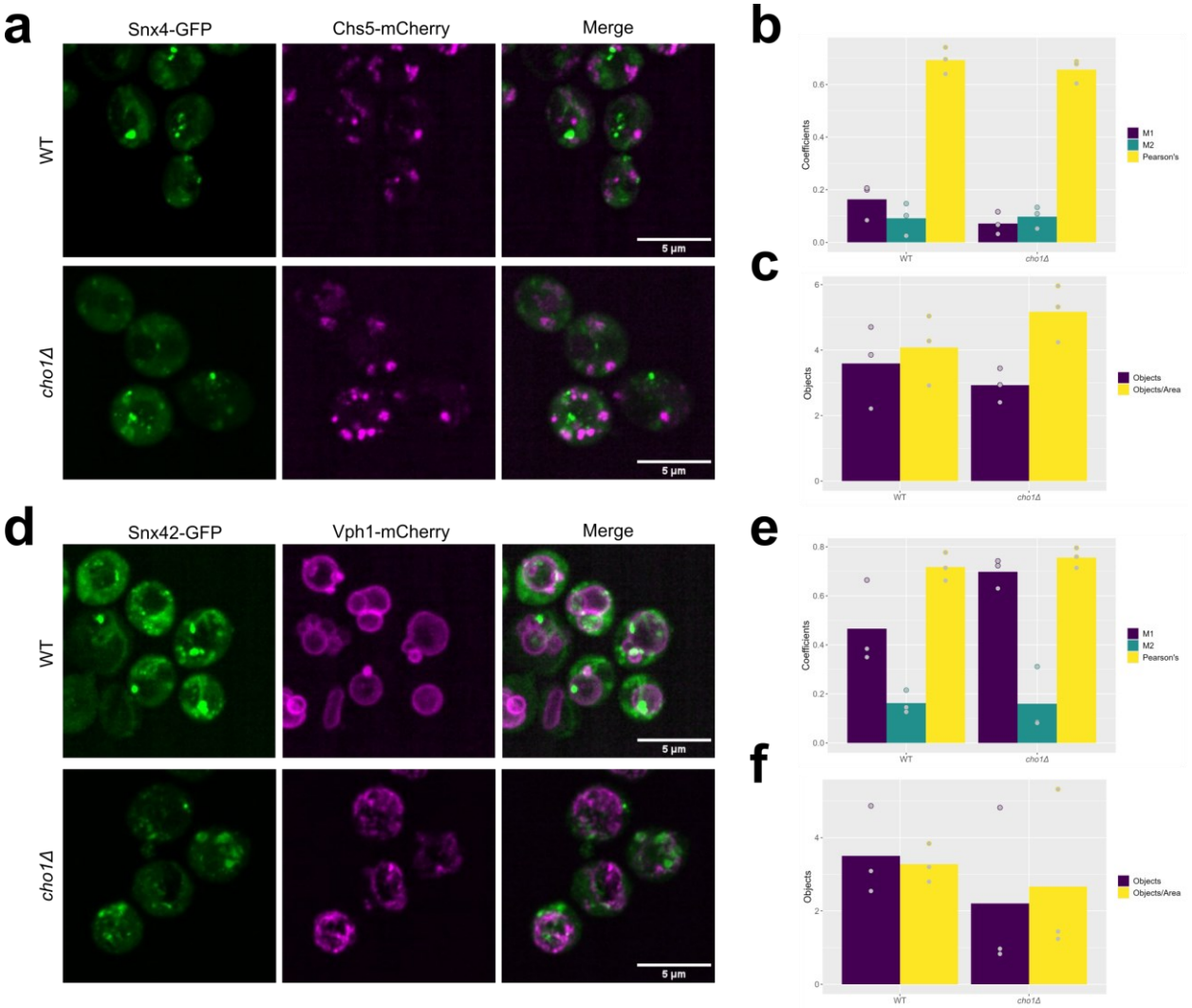

Figure 4.4. Snx4 and Snx42 colocalisation assay. Colocalisation and puncta/object count of WT and *cho1Δ* strains with GFP-tagged SNX-BAR proteins and mCherry-tagged early endosomes (Chs5) or vacuoles (Vph1). **a**,**d**. Spinning disc confocal images of WT and *cho1Δ* with GFP-tagged Snx4 (**a**) or Snx42 (**b**). **b**, **e**. Colocalisation coefficients for Mander's and Pearson's tests of maximum Z projections from WT and *cho1Δ* with GFP-tagged Snx4 (**b**) or Snx42 (**e**). M1 represents proportion of protein of interest (GFP) overlapping with organelle (mCherry) and vice versa for M2. Pearson's test uses the area of the whole cell. **c**, **f**. 3D object counts for WT and *cho1Δ* with GFP-tagged Snx4 (**c**) or Snx42 (**f**). The barplots represent objects/cell, while the right barplots represent objects/area (arbitrary units). Student's T-test statistical analysis between strains. n = 3, 25 cells in each sample; *: p = <0.05.

The increase in the M1 coefficient in *cho1Δ* relative to WT for Snx42-GFP is most likely due to the disruption of the vacuole resulting in both taking up a larger portion of the cell, increasing the overlap for Mander's coefficients (Figure 4.4d,e). Snx42 is not expected to localise to the vacuole (Ma *et al*., 2018; Hettema *et al*., 2003) and visual inspection of the structures does not show

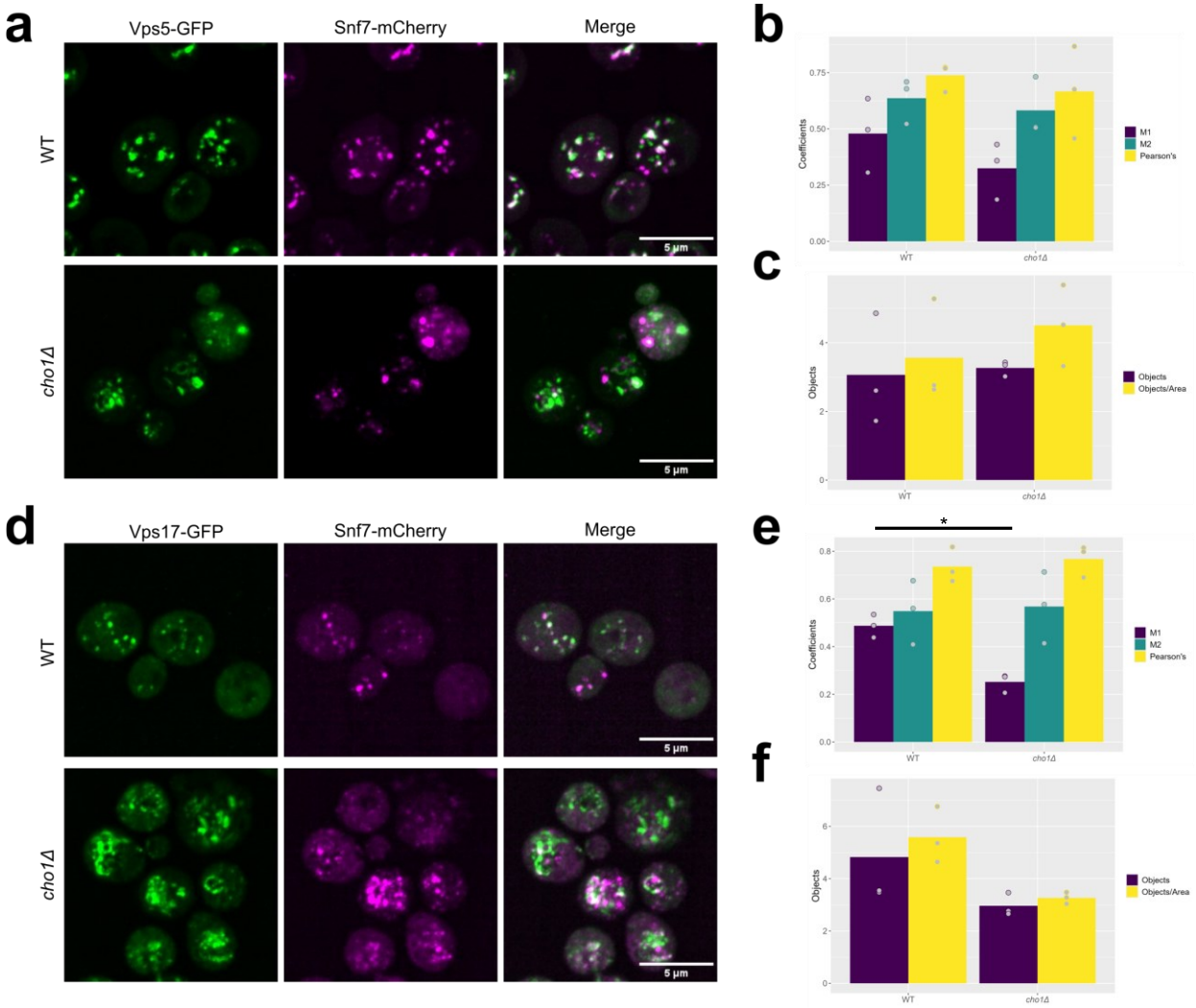

Figure 4.5. Vps5 and Vps17 colocalisation assays. Colocalisation and puncta/object count of WT and *cho1Δ* strains with GFP-tagged retromer component proteins and mCherry-tagged late endosomes (Snf7). **a**,**d**. Spinning disc confocal images of WT and *cho1Δ* with GFP-tagged Vps5 (**a**) or Vps17 (**b**). **b**, **e**. Colocalisation coefficients for Mander's and Pearson's tests of maximum Z projections from WT and *cho1Δ* with GFP-tagged Vps5 (**b**) or Vps17 (**e**). M1 represents proportion of protein of interest (GFP) overlapping with late endosomes (mCherry) and vice versa for M2. Pearson's test uses the area of the whole cell. **c**, **f**. 3D object counts for WT and *cho1Δ* with GFP-tagged Vps5 (**c**) or Vps17 (**f**). The barplots represent objects/cell, while the right barplots represent objects/area (arbitrary units). Student's T-test statistical analysis between strains. n = 3, 25 cells in each sample; *: p = <0.05.

colocalisation (Figure 4.4d).

Similarly, microscopy was used to investigate the role of PS in retromer-mediated retrograde transport from late endosomes to TGN. Analogous to early endosomes to TGN retrograde transport, the retromer complex includes SNX-BAR proteins Vps5 and Vps17 and creates a protein matrix

around the membrane, resulting in membrane tubulation, scission, and trafficking (Hurley & Johannes, 2019; Liu *et al*., 2012).

WT Vps5-GFP Snf7-mCherry has a high correlation between Vps5-GFP and Snf7-mCherry, supported by Manders coefficients (Figure 4.5a,b). The *cho1Δ* Vps5-GFP Snf7-mCherry has lower M1, M2, and Pearson's coefficients than the WT (Figure 4.5b). Additionally, the objects per cell and cell area increase in the *cho1Δ* cells (Figure 4.5c) Together, this may suggest an increase in Vps5-GFP puncta that are not on Snf7-mCherry-containing endosomes, which is supported by the phenotype observed in representative images (Figure 4.5a). The distribution of Vps5's SNX-BAR counterpart, Vps17-GFP, is more disrupted in the *cho1Δ* cells than Vps5-GFP (Figure 4.5d). The decrease in M1 ($p = 0.003$) and increase in M2 between WT and *cho1Δ* could be explained by the disrupted localisation of Vps17-GFP resulting in larger puncta and more total area in the cell with Vps17-GFP (Figure 4.5d,e). There is also a non-significant decrease in the object counts per cell and per area between WT and *cho1Δ* Snf7-mCherry Vps17-GFP (Figure 4.5d,f). The absence of PS causes abnormal distribution of SNX-BAR components of the retromer complex and an increase in Vps5-GFP puncta, but a decrease in Vps17-GFP puncta.

Two retromer cargo selective complex proteins, Vps26 and Vps35 were also imaged. The cargo selective complex comprising Vps26, Vps29, and Vps35 joins the SNX-BAR retromer components to tubulate late endosomes for retrograde transport and mediates cargo selection (Seaman, 2012). Vps26-GFP distribution is disrupted in *cho1Δ* cells (Figure 4.6a). The number of Vps26-GFP

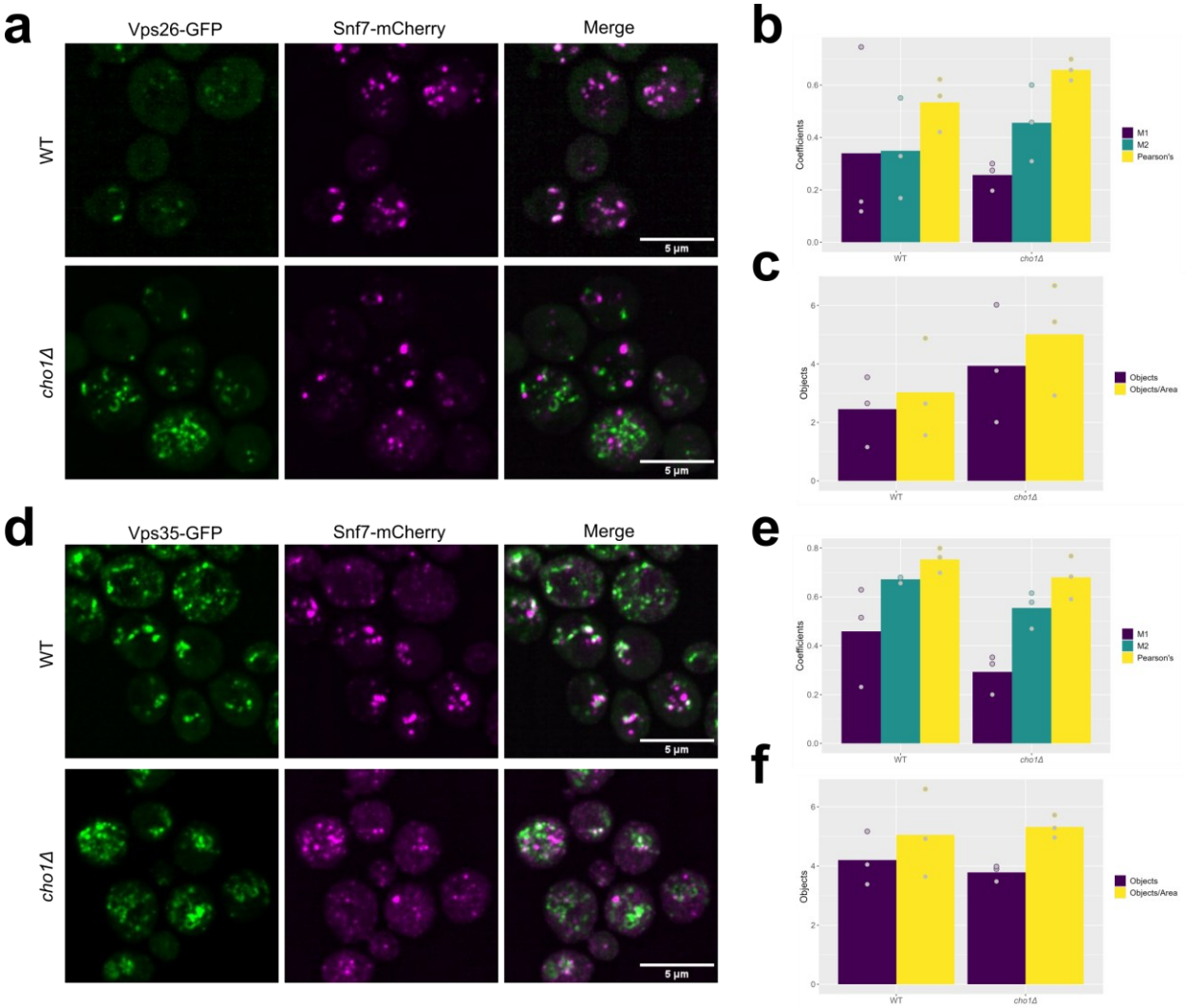

Figure 4.6. Vps26 and Vps35 colocalisation assays. Colocalisation and puncta/object count of WT and *cho1Δ* strains with GFP-tagged retromer component proteins and mCherry-tagged late endosomes (Snf7). **a**,**d**. Spinning disc confocal images of WT and *cho1Δ* with GFP-tagged Vps26 (**a**) or Vps35 (**b**). **b**, **e**. Colocalisation coefficients for Mander's and Pearson's tests of maximum Z projections from WT and *cho1Δ* with GFP-tagged Vps26 (**b**) or Vps35 (**e**). M1 represents proportion of protein of interest (GFP) overlapping with late endosomes (mCherry) and vice versa for M2. Pearson's test uses the area of the whole cell. **c**, **f**. 3D object counts for WT and *cho1Δ* with GFP-tagged Vps26 (**c**) or Vps35 (**f**). The barplots represent objects/cell, while the right barplots represent objects/area (arbitrary units). Student's T-test statistical analysis between strains. n = 3, 25 cells in each sample; *: p = <0.05.

puncta increases, and there is large variability in the Mander's coefficients between between samples in Vps26-GFP and Snf7-mCherry (Figure 4.6a-c). One sample showed very high correlation my the M1 coefficient in WT WT Snf7-mCherry Vps26 cells, with nearly all of the Vps26-GFP on late endosomes, however, the other samples showed low correlation between

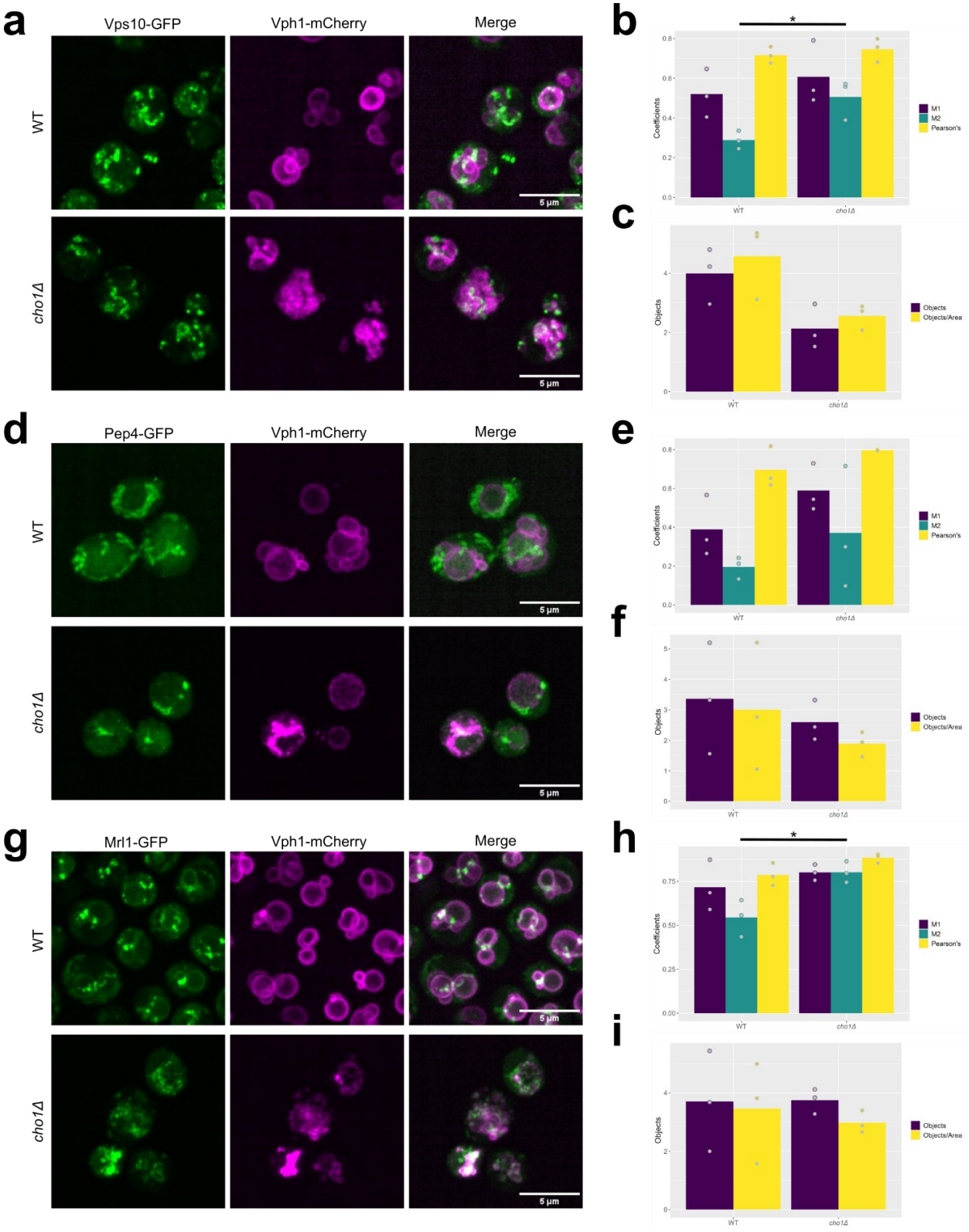
a
Vps10-GFP
Vph1-mCherry
Merge
WT
cho1Δ
5 µm
b
*
Coefficients
M1
M2
Pearson's
WT
cho1Δ
c
Objects
Objects/Area
d
Pep4-GFP
e
f
g
Mrl1-GFP
h
i

Figure 4.7. Vps10, Pep4, and Mrl1 colocalisation assays. Colocalisation and puncta/object count of WT and *cho1Δ* strains with GFP-tagged endocytic trafficking receptor and cargo proteins and mCherry-tagged vacuoles (Vph1). **a**,**d**. Spinning disc confocal images of WT and *cho1Δ* with GFP-tagged Vps26 (**a**) or Vps35 (**b**). **b**, **e**. Colocalisation coefficients for Mander's and Pearson's tests of maximum Z projections from WT and *cho1Δ* with GFP-tagged Vps26 (**b**) or Vps35 (**e**). M1 represents proportion of protein of interest (GFP) overlapping with late endosomes (mCherry) and vice versa for M2. Pearson's test uses the area of the whole cell. **c**, **f**. 3D object counts for WT and *cho1Δ* with GFP-tagged Vps26 (**c**) or Vps35 (**f**). The barplots represent objects/cell, while the right barplots represent objects/area (arbitrary units). Student's T-test statistical analysis between strains. n = 3, 25 cells in each sample; *: p = <0.05.

Vps26-GFP and Snf7-mCherry in WT (Figure 4.6b). In the *cho1Δ* cells, the correlation coefficiennts show that most of the Vps26-GFP is not localised to Snf7-mCherry-containinng late endosomes (Figure 4.6b,c). Vps35-GFP results show a decrease in all correlation coefficients between WT and *cho1Δ* cells, , which is supported by overlap of punctate structures in WT images (Figure 4.6d,e). Again, the punctate distribution of Vps35-GFP is disrupted in the *cho1Δ* cells, corresponding to a decrease in M1 and M2, though there is less of a discernible decrease in object counts (Figure 4.6e,f). Without PS, components of the retromer cargo selective complex are abnormally distributed and the number of Vps26-GFP puncta increases.

To observe the functionality of the retromer complex in *cho1Δ* strains, hydrolase receptor proteins, Vps10 and Mrl1, were assessed. Vps10 is a retromer cargo protein (Suzuki *et al*., 2019; Suzuki & Emr, 2018); however, the mechanism by which Mrl1 is transported is less clear, particularly in laboratory strains of *S. cerevisiae*, which do not have an active VINE complex (Shorthill *et al*., 2022). Additionally, Pep4, which is proposed as cargo for each of these receptor proteins (Whyte & Munro, 2001), was assessed. Vps10-GFP is primarily localized as puncta at the periphery of the vacuole, which may represent late endosomes in both WT and *cho1Δ* (Figure 4.7a). The significant increase ($p = 0.0482$) in M2 in *cho1Δ* compared to WT may be caused by a combination of vacuole deformation and a decrease in Vps10-GFP puncta (Figure 4.7a-c). Mrl1-GFP object count is similar between WT and *cho1Δ*. (Figure 4.7i). This suggests that Mrl1-GFP is not being degraded in the

vacuole. Mrl1-GFP also colocalises well to the periphery of the vacuole in WT, while the significant increase ($p = 0.0311$) in M2 in *cho1Δ* may be a consequence of Mrl1-GFP accumulation on the vacuole periphery or a consequence of vacuole deformation (Figure 4.7g,h). In WT, Pep4-GFP localizes to the vacuole periphery rather than in the vacuole as expected (Figure 4.7d). However, acidic environments quench GFP fluorescence (Shinoda *et al*., 2018), which may prevent visualization of Pep4-GFP in the vacuole (Figure 4.7d). In the *cho1Δ* cells, M1, M2,, and Pearson's coefficients increased and the Pep4-GFP object count decreases, which may cause the change in correlation coefficients (Figure 4.7e,f). Retromer cargo protein, Vps10-GFP, and Pep4-GFP have fewer puncta, while Mrl1-GFP puncta remain consistent in the absence of PS. This suggests that Vps10 and Mrl1 do not have equivalent mechanisms for the transport of Pep4. The retromer cargo proteins have altered distributions in the *cho1Δ*, however, PS deficiency could be causing this phenotype by retromer dysfunction or because of the disrupted vacuole architecture in *cho1Δ*.

Effect of replicative age on vacuole morphology in WT and *cho1Δ*

The *cho1Δ* cells were observed to have a mixed phenotype of vacuole morphologies. Some cells have one or more distinct vacuole structures (Figure 4.8a bottom right), while the majority have a vacuole "cluster" (Figure 4.8a bottom left, bottom middle). To test if these morphologies are a consequence of replicative age, the number of bud scars were counted as a biomarker for replicative cell age (Powell *et al*., 2003) and vacuole morphology was assessed in WT and *cho1Δ* cells (Figure 4.8). WT cells also have variety in vacuole morphology, with one or more vacuole structures per cell, however, they do not have vacuole "clusters" as seen in the *cho1Δ* cells (Figure 4.8a). In both WT and *cho1Δ*, the number of bud scars trended upward in cells with more vacuole structures (>=4 includes vacuole "clusters" in *cho1Δ*), with a significant increase in bud scars of WT cells with 1 or fewer vacuoles compared to 4 or more ($p = 0.0016$) (Figure 4.8b). In the *cho1Δ*, two of three

replicates had 100% of cells with vacuole "clusters," suggesting that the precise growth conditions may impact the integrity of the vacuole in *cho1Δ* cells. The replicative age of *S. cerevisiae* cells has a significant effect on the vacuole architecture; however, this data does not support it as a primary cause of vacuole deformation in the *cho1Δ* cells.

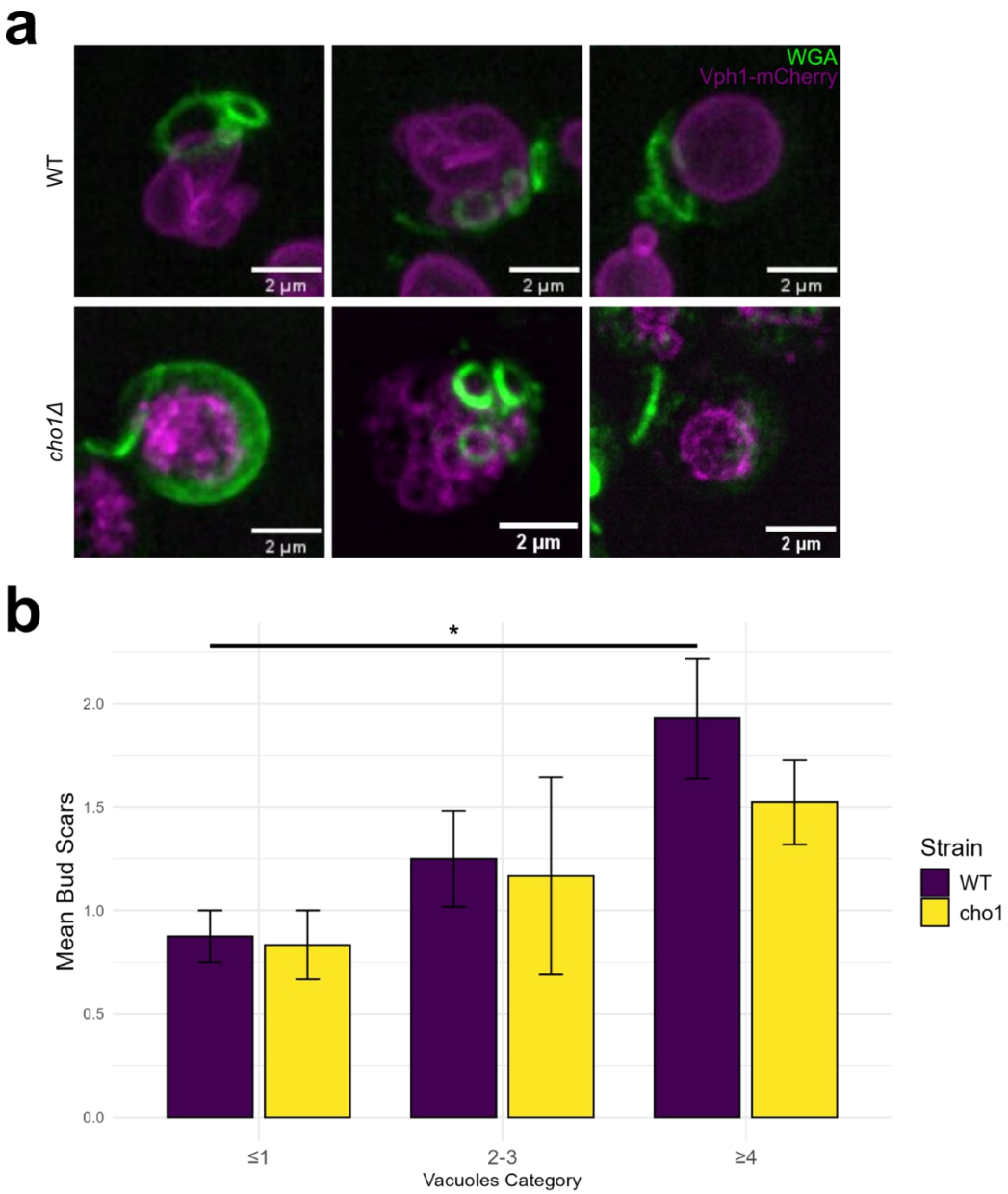

Figure 4.8. Association of Vacuole phenotype with replicative age. **a**. Spinning disc confocal representative images of WT and *cho1Δ* Vph1-mCherry cells stained with WGA-405, marker for bud scars. **b**. Bud scar count per cell categorised by the number of vacuole structures are present. "Cluster" vacuole phenotypes observed in the *cho1Δ* cells were counted as >=4. Statistical analysis was performed by Tukey's test using RStudio software. p = 0.0016. n = 3, 25 cells per replicate.

4.3 Conclusions

WT and *cho1Δ* strains containing organelle markers and fluorescent tags for proteins involved in endocytic trafficking were successfully constructed and validated. In the absence of PS, the distribution of endocytic trafficking proteins is altered showing a role for PS in their localisation. The morphology of the endocytic

proteins' distribution, as well as the number of puncta are dependent on PS in the cell. Additionally, the vacuole morphology of PS-deficient cells is also altered, however, replicative age did not explain this effect.

CHAPTER 5 Discussion

5.1 Distribution of PS by Osh6 and Osh7

This work contributes to the characterisation the role of lipid transfer proteins, Osh6 and Osh7, in controlling PS distribution and metabolism. Previous work has investigated their role. However, some of the results are conflicting (Maeda *et al*., 2013, D'Ambrosio *et al*., 2020; Yang, unpublished). In Maeda *et al*., 2013, described the *osh6Δosh7Δ* phenotype as PS being localised to both the PM and internal cellular structures, however, D'Ambrosio *et al*., 2020 showed that they phenotype is diverse and only a small percentage of cells had a difference in PM/intracellular PS ratio, measured by the Lact-C2-GFP probe. Similarly, previous work from our research group showed that a subset of *osh6Δosh7Δ* cells exhibit the phenotype described by Maeda *et al*., 2013 (Yang, unpublished). This work examined the phenotype by measuring the relative distribution of PS in the PM versus the intracellular space (Figure 3.1). Considering Maeda *et al*., 2013 provided no quantitation and only showed a single cell, given the work of D'Ambrosio *et al*., 2020 and our lab, it could be that the penetrance of this altered PS distribution is very low. This is an important distinction since the Maeda *et al*., 2013 paper suggests that Osh6 and Osh7 have a very prominent role in transferring PS to the PM. However, despite the *osh6Δosh7Δ* cells having a ~50% reduction in total cellular PS (Maeda *et al*., 2013; D'Ambrosio *et al*., 2020) the PS that remains seems to traffic normally demonstrating the existence of alternative pathways.

In addition to compensatory PS distribution mechanisms, *osh6Δosh7Δ* affects the total PS in the cell. Lipidomics assays showed decreased PS in the ER, PM, and the whole cell of *osh6Δosh7Δ* cells relative to WT (Maeda *et al*., 2013; D'Ambrosio *et al*., 2020).

The previous lipidomics studies did not provide a mechanism to explain why PS levels are lower in the *osh6Δosh7Δ* cells. We hypothesized two potential mechanisms. First, a build-up of PS in the ER could feedback inhibit the Cho1 enzyme, slowing the synthesis of PS. Second, PS could be more

rapidly transported to the mitochondria or TGN for decarboxylation by Psd1 or Psd2, respectively. In tracking the incorporation of serine into phospholipids the label is incorporated at a similar rate across the 3 cell types. This largely rules out the first possibility. The decrease in PS and increase in PE at 30 minutes in *osh6Δosh7Δ* cells is consistent with an increase in PS conversion to PE by Psd1 or Psd2 (Figure 3.2b). Though not significant, these results are mirrored by a trend in the *ist2Δ* strain. Since Osh6/7 are the PS transporters and Ist2 helps localize them to contact sites, it is likely that the absence of Ist2 makes the job of Osh6/7 harder and thus slows transport, while in the *osh6Δosh7Δ* cells, the proteins are missing, and this pathway is completely abolished. Osh6 and Osh7 have been shown not to have a significant role in PS transport to the mitochondria (Maeda *et al*., 2013) and thus I suspect that the two non-vesicular transport pathways ER to PM and ER to mitochondria may compete for ER resident PS. In the absence of Osh6 and Osh7 the ER-mitochondria pathway is no longer substrate limited and accelerated the transport and decarboxylation of the PS. The levels of PC in *osh6Δosh7Δ* cells ($p = 0.024$) and *ist2Δ* ($p = 0.0575$) also increase between 30 and 60 minutes which supports the notion of increased flux from PS to PE and subsequent methylation to form PC. Notably, while not significant, PC at 60 minutes in *osh6Δosh7Δ* and *ist2Δ* is greater than in WT (Figure 3.2). Additionally, these data show that PS levels have reached equilibrium at 30 minutes because there is no change in ^{3}H-PS levels between 30 and 60 minutes (Figure 3.2). An earlier timepoint may have captured the rates of PS synthesis before reaching equilibrium. Together, these data support the literature, showing that PS levels are decreased in *osh6Δosh7Δ* and *ist2Δ* strains. They also suggest that an increase in decarboxylation of PS may be the cause of the reduced PS levels.

The lipid transfer proteins are important contributors to the distribution and metabolism of PS in *S. cerevisiae.* This work shows that PS distribution in cells with impaired ER to PM PS transfer can still deliver PS to the PM by alternative mechanisms which have not yet been identified. This data

also shows that PS levels are reduced when PS cannot be transferred directly from the ER to PM, which may result from increased PS decarboxylation rates or decreased PS synthesis rates.

5.2 PS IN RETROGRADE ENDOCYTIC TRAFFICKING

This work examines the role of PS in retrograde transport pathways along the endocytic pathway. Proteins involved in retrograde transport pathways were tagged genomically to characterise their distribution in WT and *cho1Δ* cells relative to fluorescently labelled endocytic compartments. By using spinning disk confocal microscopy combined with genomic fluorescent tags, this work more accurately characterises the distribution of these proteins than previous work by our research group that used overexpressed fluorescent proteins from plasmids (Yang, unpublished).

Early endosomes, late endosomes, and vacuoles were successfully labelled with mCherry by Chs5-mCherry, Snf7-mCherry, and Vph1-mCherry (Figure 4.1), respectively, which are validated organelle markers (Zhu *et al*., 2019). This was completed in WT and *cho1Δ* strains, which had punctate distributions for early and late endosomes. The vacuole morphology in *cho1Δ* was also as expected based on previous work. Data from our research group has shown that *cho1Δ* cells have a deformed vacuole by FM4-64 staining and electron microscopy (Fairn, unpublished; Yang, unpublished). They also showed that this strain's vacuole has reduced acidity and V-ATPase activity (Yang & Fairn, unpublished). The disrupted phenotype described by these data is consistent with what was observed here by microscopy.

The organelle markers were validated as participants of the endocytic pathway by a pulse-chase experiment following the endocytosis of SynaptoGreen C4 in WT and cho1Δ (Figure 4.2). While these results showed some abnormal distribution of organelle markers in strains with Chs5-mCherry (data not shown) and later timepoints of strains with Vph1-mCherry (Figure 4.2b), these are likely due to interaction with the SynaptoGreen C4 dye as these distributions are only seen with the

presence of the stain. This data helps to validate Snf7-mCherry and Vph1-mCherry as components of the endocytic pathway, demarking late endosomes and vacuoles, respectively (Figure 4.2). Chs5-mCherry was previously validated by the endocytic tracker stain, FM4-64, as an early endosome (Zhu *et al*., 2019), and it has the expected punctate distribution of early endosomes (Figure 4.1). Together, these results support the organelle markers Chs5-mCherry, Snf7-mCherry, and Vph1-mCherry as their anticipated organelles within the endocytic pathway.

With the organelle markers characterised and validated, genomic C-terminal GFP tags were added to proteins involved in retrograde transport that may be affected by PS-deficiency. Using genomic DNA from the O'Shea collection (Huh *et al*., 2003) WT and *cho1Δ* strains with mCherry organelle markers were constructed and validated by western blot (Figure 4.3), PCR and gel electrophoresis (data not shown), and microscopy (Figure 4.4-4.7). These results support the successful transformation of the listed strains (Figure 4.3b), except western blot data for WT Snf7-mCherry Vps26-mCherry and *cho1Δ* Vph1-mCherry Vps10-GFP. These two exceptions are still supported as successful transformations by microscopy and PCR and gel electrophoresis data. Despite the discrepancy, these results validate the GFP strains across several methods, besides two outliers that still appear usable for microscopy analysis.

The WT and *cho1Δ* strains labelled with GFP and mCherry were then used for spinning disk confocal microscopy analysis to examine the effects of PS-deficiency on retrograde endocytosis. The role of PS in early endosome to TGN retrograde transport has been described recently (Kashikuma *et al*., 2023; Yang, unpublished). It was shown that PS is necessary for the recycling of membrane receptor proteins, Snc1 (Yang, unpublished; Kashikuma *et al*., 2023), Can1, and Wsc1 (Kashikuma *et al*., 2023). An *in vitro* liposome binding assay also showed that the SNX-BAR protein heterodimer, Snx4-Snx42, binds more with higher PS concentration (Ma *et al*., 2018).

Furthermore, Snx4-GFP puncta accumulated in *cho1Δ* cells (Kashikuma *et al*., 2023), however, in *cho1Δ* Chs5-mCherry Snx4-GFP our data shows no change in Snx4-GFP puncta relative to WT (Figure 4.4c). This contrasts the model described by Kashikuma *et al*., 2023 in which PS-dependent retrograde transport from early endosomes to TGN is halted in *cho1Δ* cells resulting in Snx4 accumulation in early endosomes. Interestingly, our data for Snx42-GFP does not support this model, with a decrease in Snx42-GFP puncta (Figure 4.3f). Snx42-GFP may be a more reliable marker for early endosomes to TGN retrograde transport because Snx4 is also involved in vacuole to late endosome transport in a heterodimer with Snx41 (Hettema *et al*., 2003). In our Snx4-GFP analysis, there is also an unexpectedly low correlation between Snx4-GFP and Chs5-mCherry, as both are expected to localise to early endosomes (Ma *et al*., 2018; Zhu *et al*., 2019). While Zhu *et al*., 2019 validated Chs5-mCherry with internalisation of FM4-64 and other early endosome markers, they conflate late TGN and early endosomes. Chs5 is a component of the exomer complex, with a role in the export of specific proteins from TGN to PM (Sanchatjate &Schekman, 2006; Trautwein *et al*., 2006) which may be distinct from Snx4-residing early endosomes. While there are few changes in Snx4-GFP in WT and *cho1Δ*, the characteristics of Snx42-GFP count support the hypothesis that early endosome to TGN retrograde transport is PS-dependent in a SNX-BAR mediated process.

The role of PS in late endosome to TGN transport is less well studied. This process is also mediated by SNX-BAR proteins Vps5 and Vps17. They form a heterodimer that comprises the SNX-BAR dimer in the retromer complex (Hurley & Johannes, 2019). The retromer complex is also comprised of Vps26, Vps29, and Vps35, forming the cargo selective complex portion (Seaman, 2012). A role for PS in this pathway is supported by data showing retromer dysfunction in *cho1Δ* cells. It was shown that in *cho1Δ* cells, retromer cargo Vps10 is mislocalised to the vacuole, instead of being recycled to the TGN by the retromer complex. Furthermore, CPY, the protein cargo of Vps10 is

secreted in *cho1Δ* cells rather than being transported to the vacuole by Vps10 (Yang, unpublished). This is a consequence of Vps10 not being recycled by retromer to the TGN. Retromer dysfunction in *cho1Δ* cells implicates a role for PS in retrograde transport from late endosomes to TGN.

The mechanism by which PS contributes to retromer-mediated retrograde transport is uncertain. It may facilitate SNX-BAR protein binding to the late endosome membrane, influence lipid membrane kinetics, or regulate Vps34-medited initiation of trafficking (Ohashi *et al*., 2021). In fact, the literature suggests that retromer membrane binding is not PS dependent (Ma *et al*., 2018) and that both the SNX-BAR dimer and the cargo selective complex of retromer bind lipid membranes in a PI3P-dependent manner (Purushothaman *et al*., 2017). Furthermore, tubulation depends on the retromer complex. However, 5.35 mol% PS was used to make the vesicle (Purushothaman *et al*., 2017). PS may be necessary to facilitate increased membrane curvature during tubulation, as it is necessary for the production of spontaneous curvature (Hirama *et al*., 2017a). Vps34 is a PI3K kinase, which produces PI3P, part of complex II for endocytosis. In *vps30* or *vps38*, which are complex II protein components, Vps10 is mislocalised to vacuolar membranes and Vps5 and Vps17 are redistributed to the cytoplasm (Burda *et al*., 2002). This shows that Vps34 is necessary for retromer function. Furthermore, Vps34 or complex II can be activated by the negative charge of PS alone (Ohashi *et al*., 2021). Together, these data support several possible roles for PS in retromer-mediated retrograde transport.

In the localisation studies, Vps5 and, especially, Vps17 are mislocalised in the *cho1Δ* strains, no longer colocalising well with late endosomes. These proteins lose their distinct punctate distribution in the *cho1Δ*, suggesting dysfunction of the retromer complex. The accumulation of Vps5-GFP puncta in the *cho1Δ* could also support retromer dysfunction with Vps5-GFP binding to late endosomes without retrograde transport occurring, although the decreased correlation with late endosomes does not support this (Figure 4.5). Similarly, retromer's cargo selective complex

components have abnormal morphology in *cho1Δ* and Vps26-GFP puncta accumulate in *cho1Δ* cells (Figure 4.6). Together these data support the hypothesis that PS is necessary for normal localisation of retromer components and some of the retromer components accumulate without PS. The disruption of the vacuole and late endosomes architecture in *cho1Δ* may prevent retromer-mediated retrograde transport because of larger scale disruption to the cell structure rather than because of PS-dependent mechanisms. The vacuole disruption may be caused by alteration of the phospholipid composition. Ma *et al*., 2018 proposed that an increased PS/PE ratio decreased vacuole fusion competence in PE-deficient cells. In *cho1Δ* cells PS is almost completely eliminated and PE is decreased to about 17% of WT phospholipid proportions (Fairn *et al*., 2011).

The function of the retromer complex was assessed by localisation studies of retromer cargo proteins. Retromer cargo protein, Vps10-GFP, had a decrease in puncta in *cho1Δ* cells, which may be caused by retromer dysfunction resulting in mislocalisation of Vps10-GFP to the vacuole, causing degradation (Figure 4.7c). A possible retromer cargo protein, Mrl1-GFP did not show the same effect, with little change in the number of Mrl1-GFP puncta in *cho1Δ* compared to WT, however, it did show an increase in localisation to the vacuole. (Figure 4.7i). This may suggest an increase in degradation occurring at the vacuole or simply reduced recycling from the vacuole resulting in an accumulation of Mrl1 at the vacuole. Mrl1 has also been shown to be recycled from the vacuole to endosomes by Snx4, while the mechanism by which it is recycled from endosomes to TGN has not been shown (Shortill *et al*., 2022). Consequently, PS-deficiency may also be affecting Mrl1 transport from the vacuole to late endosomes, which may play a role in increased Mrl1-GFP localisation to the vacuole and Vps10-GFP puncta decrease in *cho1Δ*. Pep4 is a cargo of both Vps10 and Mrl1, so if they are not recycled, Pep4-GFP may be secreted to be mislocalised or secreted like CPY (Yang, unpublished; Suzuki *et al*., 2019), however, if at least one of Vps10 or Mrl1 are functionally recycled, Pep4-GFP would be localised to the vacuole, like in WT (Whyte & Munro,

2001). Pep4-GFP puncta count decrease in *cho1Δ* cells but colocalisation with Vph1-mCherry increases. This may show increased delivery to the vacuole and coincident increased degradation or it may be a result of reduced quenching effects on the GFP. There may be improved visualisation of Pep4-GFP due to the increased pH of the vacuole in *cho1Δ* cells (Farin, unpublished) reducing the quenching effect on GFP in the typically acidic environment of the vacuole (Shinoda *et al*., 2018). These data show that *cho1Δ* cells have mislocalised retromer components and altered number of puncta for several of them. *cho1Δ* cells also have aberrant localisation of retromer cargo proteins and their cargo protein, Pep4-GFP. Together, these data support the hypothesis that *cho1Δ* cells have dysfunctional retromer-mediated retrograde transport. However, the broad disruption of endocytic architecture in the cell may be preventing retrograde transport by itself.

Current data do support a role for PS in retrograde transport by either modulating membrane curvature dynamics to facilitate budding (Hirama *et al*., 2017a) or by activating Vps34 (Ohashi *et al*., 2021). There is evidence opposing a direct role for PS in influencing membrane binding of SNX-BAR proteins, Vps5 and Vps17. Vps5 and Vps17 do not bind to PS-containing vesicles without PI3P (Purushothaman *et al*., 2017), bind to liposomes in a PS concentration-dependent manner, nor localize to endosomes without functional Vps34 complex II. While it is possible that PS secondarily influences Vps5 and Vps17 binding to late endosomes in the cellular environment, our data further supports that PS is not necessary for this process. Despite some alteration to their distribution in *cho1Δ* cells, they still localise to punctate structures that partially correlate with late endosomes.

The “cluster” vacuole phenotype found in a large proportion of *cho1Δ* cells was investigated to identify if *cho1Δ* cells transition into this state as a function of their replicative age, as measured by the biomarker, bud scars. In WT cells, those with more vacuole structures had a greater mean

replicative age. In the *cho1Δ* cells, this was observed as a trend, however, growth condition factors may have a larger effect on the "cluster" vacuole phenotype, because in two of the biological replicates 100% of the cells analysed had this phenotype (Figure 4.8b; data not shown). This shows that it is possible that further analysis of the *cho1Δ* strains may identify growth conditions that reduce the "cluster" vacuole phenotype and better facilitate the use of this strain for studying the effects of PS-deficiency. Other methods that reduce the negative phenotype associated with chronic PS-deficiency are available. A temperature-sensitive mutant could be isolated, the *CHO1* promoter could be replaced by an inducible promoter, or PS could be sequestered by inducible overexpression of tandem Lact-C2 (Hirama *et al*., 2017b).

The retrograde transport systems in *S. cerevisiae* are dependent on PS in the cell for proper function, however, it remains unclear the mechanism by which PS is involved in retromer-mediated retrograde transport. The evidence presented here is consistent with PS having a role that is not through direct binding of Vps5 and Vps17. The *cho1Δ* model of PS-deficiency may have too severe of a cell-wide defect to discern a mechanism by which retromer-mediated transport is regulated by PS. Alternative models in *S. cerevisiae* could be developed to answer this question more clearly.

BIBLIOGRAPHY

Atkinson K, Fogel S, Henry SA. Yeast mutant defective in phosphatidylserine synthesis. *J Biol Chem*. 1980;255(14):6653-6661.

Behnia R, Munro S. Organelle identity and the signposts for membrane traffic. *Nature*. 2005;438(7068):597-604. doi:10.1038/nature04397

Bevers EM, Tilly RH, Senden JM, Comfurius P, Zwaal RF. Exposure of endogenous phosphatidylserine at the outer surface of stimulated platelets is reversed by restoration of aminophospholipid translocase activity. *Biochemistry*. 1989;28(6):2382-2387. doi:10.1021/bi00432a007

Birge RB, Boeltz S, Kumar S, et al. Phosphatidylserine is a global immunosuppressive signal in efferocytosis, infectious disease, and cancer. *Cell Death Differ*. 2016;23(6):962-978. doi:10.1038/cdd.2016.11

Bürgermeister M, Birner-Grünberger R, Nebauer R, Daum G. Contribution of different pathways to the supply of phosphatidylethanolamine and phosphatidylcholine to mitochondrial membranes of the yeast Saccharomyces cerevisiae. *Biochim Biophys Acta*. 2004;1686(1-2):161-168. doi:10.1016/j.bbalip.2004.09.007

Burri L, Lithgow T. A complete set of SNAREs in yeast. *Traffic*. 2004;5(1):45-52. doi:10.1046/j.1600-0854.2003.00151.x

Calzada E, Avery E, Sam PN, *et al*. Phosphatidylethanolamine made in the inner mitochondrial membrane is essential for yeast cytochrome bc_1 complex function. *Nat Commun*. 2019;10(1):1432. Published 2019 Mar 29. doi:10.1038/s41467-019-09425-1

Carman GM, Henry SA. Phospholipid biosynthesis in the yeast Saccharomyces cerevisiae and interrelationship with other metabolic processes. *Prog Lipid Res*. 1999;38(5-6):361-399. doi:10.1016/s0163-7827(99)00010-7

Chi RJ, Harrison MS, Burd CG. Biogenesis of endosome-derived transport carriers. *Cell Mol Life Sci*. 2015;72(18):3441-3455. doi:10.1007/s00018-015-1935-x

Cho W, Stahelin RV. Membrane-protein interactions in cell signaling and membrane trafficking. *Annu Rev Biophys Biomol Struct*. 2005;34:119-151. doi:10.1146/annurev.biophys.33.110502.133337

Cowles CR, Odorizzi G, Payne GS, Emr SD. The AP-3 adaptor complex is essential for cargo-selective transport to the yeast vacuole. *Cell*. 1997;91(1):109-118. doi:10.1016/s0092-8674(01)80013-1

D'Ambrosio JM, Albanèse V, Lipp NF, *et al*. Osh6 requires Ist2 for localization to ER-PM contacts and efficient phosphatidylserine transport in budding yeast. *J Cell Sci*. 2020;133(11):jcs243733. Published 2020 Jun 4. doi:10.1242/jcs.243733

Dunn KW, Kamocka MM, McDonald JH. A practical guide to evaluating colocalization in biological microscopy. *Am J Physiol Cell Physiol*. 2011;300(4):C723-C742. doi:10.1152/ajpcell.00462.2010

Fadok VA, de Cathelineau A, Daleke DL, Henson PM, Bratton DL. Loss of phospholipid asymmetry and surface exposure of phosphatidylserine is required for phagocytosis of apoptotic cells by macrophages and fibroblasts. *J Biol Chem*. 2001;276(2):1071-1077. doi:10.1074/jbc.M003649200

Fairn GD, Hermansson M, Somerharju P, Grinstein S. Phosphatidylserine is polarized and required for proper Cdc42 localization and for development of cell polarity. *Nat Cell Biol*. 2011;13(12):1424-1430. Published 2011 Oct 2. doi:10.1038/ncb2351

Fernandez-Borja M, Wubbolts R, Calafat J, *et al*. Multivesicular body morphogenesis requires phosphatidyl-inositol 3-kinase activity. *Curr Biol*. 1999;9(1):55-58. doi:10.1016/s0960-9822(99)80048-7

Frost A, Perera R, Roux A, *et al*. Structural basis of membrane invagination by F-BAR domains. *Cell*. 2008;132(5):807-817. doi:10.1016/j.cell.2007.12.041

Gall WE, Geething NC, Hua Z, *et al*. Drs2p-dependent formation of exocytic clathrin-coated vesicles in vivo. *Curr Biol*. 2002;12(18):1623-1627. doi:10.1016/s0960-9822(02)01148-x

Gary JD, Wurmser AE, Bonangelino CJ, Weisman LS, Emr SD. Fab1p is essential for PtdIns(3)P 5-kinase activity and the maintenance of vacuolar size and membrane homeostasis. *J Cell Biol*. 1998;143(1):65-79. doi:10.1083/jcb.143.1.65

Gillooly DJ, Morrow IC, Lindsay M, *et al*. Localization of phosphatidylinositol 3-phosphate in yeast and mammalian cells. *EMBO J*. 2000;19(17):4577-4588. doi:10.1093/emboj/19.17.4577

Gopaldass N, De Leo MG, Courtellemont T, *et al*. Retromer oligomerization drives SNX-BAR coat assembly and membrane constriction. *EMBO J*. 2023;42(2):e112287. doi:10.15252/embj.2022112287

Gould SB. Membranes and evolution. *Curr Biol*. 2018;28(8):R381-R385. doi:10.1016/j.cub.2018.01.086

Haas A, Scheglmann D, Lazar T, Gallwitz D, Wickner W. The GTPase Ypt7p of Saccharomyces cerevisiae is required on both partner vacuoles for the homotypic fusion step of vacuole inheritance. *EMBO J*. 1995;14(21):5258-5270. doi:10.1002/j.1460-2075.1995.tb00210.x

Hancock JF, Paterson H, Marshall CJ. A polybasic domain or palmitoylation is required in addition to the CAAX motif to localize p21ras to the plasma membrane. *Cell*. 1990;63(1):133-139. doi:10.1016/0092-8674(90)90294-o

Hettema EH, Lewis MJ, Black MW, Pelham HR. Retromer and the sorting nexins Snx4/41/42 mediate distinct retrieval pathways from yeast endosomes. *EMBO J*. 2003;22(3):548-557. doi:10.1093/emboj/cdg062

Hirama T, Das R, Yang Y, *et al*. Phosphatidylserine dictates the assembly and dynamics of caveolae in the plasma membrane. *J Biol Chem*. 2017**b**;292(34):14292-14307. doi:10.1074/jbc.M117.791400

Hirama T, Lu SM, Kay JG, *et al*. Membrane curvature induced by proximity of anionic phospholipids can initiate endocytosis. *Nat Commun*. 2017**a**;8(1):1393. Published 2017 Nov 9. doi:10.1038/s41467-017-01554-9

Holthuis JC, Menon AK. Lipid landscapes and pipelines in membrane homeostasis. *Nature*. 2014;510(7503):48-57. doi:10.1038/nature13474

Huh WK, Falvo JV, Gerke LC, *et al*. Global analysis of protein localization in budding yeast. *Nature*. 2003;425(6959):686-691. doi:10.1038/nature02026

Hurley JH, Johannes L. Retro Styles for Vesicle Coats. *Biochemistry*. 2019;58(6):433-434. doi:10.1021/acs.biochem.8b01271

Kamińska A, Enguita FJ, Stępień EŁ. Lactadherin: An unappreciated haemostasis regulator and potential therapeutic agent. *Vascul Pharmacol*. 2018;101:21-28. doi:10.1016/j.vph.2017.11.006

Kashikuma R, Nagano M, Shimamura H, *et al*. Role of phosphatidylserine in the localization of cell surface membrane proteins in yeast. *Cell Struct Funct*. 2023;48(1):19-30. doi:10.1247/csf.22081

Kennedy EP, Weiss SB. The function of cytidine coenzymes in the biosynthesis of phospholipides. *J Biol Chem*. 1956;222(1):193-214.

Lemmon MA. Membrane recognition by phospholipid-binding domains. *Nat Rev Mol Cell Biol*. 2008;9(2):99-111. doi:10.1038/nrm2328

Leventis PA, Grinstein S. The distribution and function of phosphatidylserine in cellular membranes. *Annu Rev Biophys*. 2010;39:407-427. doi:10.1146/annurev.biophys.093008.131234

Lewis MJ, Nichols BJ, Prescianotto-Baschong C, Riezman H, Pelham HR. Specific retrieval of the exocytic SNARE Snc1p from early yeast endosomes. *Mol Biol Cell*. 2000;11(1):23-38. doi:10.1091/mbc.11.1.23

Liu TT, Gomez TS, Sackey BK, Billadeau DD, Burd CG. Rab GTPase regulation of retromer-mediated cargo export during endosome maturation. *Mol Biol Cell*. 2012;23(13):2505-2515. doi:10.1091/mbc.E11-11-0915

Lolicato F, Nickel W, Haucke V, Ebner M. Phosphoinositide switches in cell physiology - From molecular mechanisms to disease. *J Biol Chem*. 2024;300(3):105757. doi:10.1016/j.jbc.2024.105757

Longtine MS, McKenzie A 3rd, Demarini DJ, *et al*. Additional modules for versatile and economical PCR-based gene deletion and modification in Saccharomyces cerevisiae. *Yeast*. 1998;14(10):953-961. doi:10.1002/(SICI)1097-0061(199807)14:10<953::AID-YEA293>3.0.CO;2-U

Ma M, Burd CG. Retrograde trafficking and plasma membrane recycling pathways of the budding yeast Saccharomyces cerevisiae. *Traffic*. 2020;21(1):45-59. doi:10.1111/tra.12693

Ma M, Burd CG, Chi RJ. Distinct complexes of yeast Snx4 family SNX-BARs mediate retrograde trafficking of Snc1 and Atg27. *Traffic*. 2017;18(2):134-144. doi:10.1111/tra.12462

Ma M, Kumar S, Purushothaman L, *et al*. Lipid trafficking by yeast Snx4 family SNX-BAR proteins promotes autophagy and vacuole membrane fusion. *Mol Biol Cell*. 2018;29(18):2190-2200. doi:10.1091/mbc.E17-12-0743

Maeda K, Anand K, Chiapparino A, *et al*. Interactome map uncovers phosphatidylserine transport by oxysterol-binding proteins. *Nature*. 2013;501(7466):257-261. doi:10.1038/nature12430

Manders EMM, Verbeek FJ, Aten JA. Measurement of co-localization of objects in dual-colour confocal images. *J Microsc*. 1993;169(3):375-382. doi:10.1111/j.1365-2818.1993.tb03313.x

Marcusson EG, Horazdovsky BF, Cereghino JL, Gharakhanian E, Emr SD. The sorting receptor for yeast vacuolar carboxypeptidase Y is encoded by the VPS10 gene. *Cell*. 1994;77(4):579-586. doi:10.1016/0092-8674(94)90219-4

Maxfield FR, McGraw TE. Endocytic recycling. *Nat Rev Mol Cell Biol*. 2004;5(2):121-132. doi:10.1038/nrm1315

Maxfield FR, Yamashiro DJ. Endosome acidification and the pathways of receptor-mediated endocytosis. *Adv Exp Med Biol*. 1987;225:189-198. doi:10.1007/978-1-4684-5442-0_16

Melero A, Boulanger J, Kukulski W, Miller EA. Ultrastructure of COPII vesicle formation in yeast characterized by correlative light and electron microscopy. *Mol Biol Cell*. 2022;33(13):ar122. doi:10.1091/mbc.E22-03-0103

Mioka T, Fujimura-Kamada K, Tanaka K. Asymmetric distribution of phosphatidylserine is generated in the absence of phospholipid flippases in Saccharomyces cerevisiae. *Microbiologyopen*. 2014;3(5):803-821. doi:10.1002/mbo3.211

Mulgrew-Nesbitt A, Diraviyam K, Wang J, *et al*. The role of electrostatics in protein-membrane interactions. *Biochim Biophys Acta*. 2006;1761(8):812-826. doi:10.1016/j.bbalip.2006.07.002

Natarajan P, Wang J, Hua Z, Graham TR. Drs2p-coupled aminophospholipid translocase activity in yeast Golgi membranes and relationship to in vivo function. *Proc Natl Acad Sci U S A*. 2004;101(29):10614-10619. doi:10.1073/pnas.0404146101

Nguyen TT, Lewandowska A, Choi JY, *et al*. Gem1 and ERMES do not directly affect phosphatidylserine transport from ER to mitochondria or mitochondrial inheritance. *Traffic*. 2012;13(6):880-890. doi:10.1111/j.1600-0854.2012.01352.x

Nothwehr SF, Bruinsma P, Strawn LA. Distinct domains within Vps35p mediate the retrieval of two different cargo proteins from the yeast prevacuolar/endosomal compartment. *Mol Biol Cell*. 1999;10(4):875-890. doi:10.1091/mbc.10.4.875

Nothwehr SF, Ha SA, Bruinsma P. Sorting of yeast membrane proteins into an endosome-to-Golgi pathway involves direct interaction of their cytosolic domains with Vps35p. *J Cell Biol*. 2000;151(2):297-310. doi:10.1083/jcb.151.2.297

Ohashi Y, Tremel S, Williams RL. Unsaturation, curvature and charge: effects of membrane parameters on PIK3C3/VPS34-containing complexes. *Autophagy*. 2021;17(3):823-825. doi:10.1080/15548627.2021.1872190

Ostrowicz CW, Meiringer CT, Ungermann C. Yeast vacuole fusion: a model system for eukaryotic endomembrane dynamics. *Autophagy*. 2008;4(1):5-19. doi:10.4161/auto.5054

Peter BJ, Kent HM, Mills IG, *et al*. BAR domains as sensors of membrane curvature: the amphiphysin BAR structure. *Science*. 2004;303(5657):495-499. doi:10.1126/science.1092586

Pomorski T, Lombardi R, Riezman H, Devaux PF, van Meer G, Holthuis JC. Drs2p-related P-type ATPases Dnf1p and Dnf2p are required for phospholipid translocation across the yeast plasma membrane and serve a role in endocytosis. *Mol Biol Cell*. 2003;14(3):1240-1254. doi:10.1091/mbc.e02-08-0501

Powell CD, Quain DE, Smart KA. Chitin scar breaks in aged Saccharomyces cerevisiae. *Microbiology (Reading)*. 2003;149(Pt 11):3129-3137. doi:10.1099/mic.0.25940-0

Pronobis MI, Deuitch N, Peifer M. The Miraprep: A Protocol that Uses a Miniprep Kit and Provides Maxiprep Yields. *PLoS One*. 2016;11(8):e0160509. Published 2016 Aug 3. doi:10.1371/journal.pone.0160509

Purushothaman LK, Arlt H, Kuhlee A, Raunser S, Ungermann C. Retromer-driven membrane tubulation separates endosomal recycling from Rab7/Ypt7-dependent fusion. *Mol Biol Cell*. 2017;28(6):783-791. doi:10.1091/mbc.E16-08-0582

Quinville BM, Deschenes NM, Ryckman AE, Walia JS. A Comprehensive Review: Sphingolipid Metabolism and Implications of Disruption in Sphingolipid Homeostasis. *Int J Mol Sci*. 2021;22(11):5793. Published 2021 May 28. doi:10.3390/ijms22115793

Ray J, Sapp DG, Fairn GD. Phosphatidylinositol 3,4-bisphosphate: Out of the shadows and into the spotlight. *Curr Opin Cell Biol*. Published online May 21, 2024. doi:10.1016/j.ceb.2024.102372

Rostislavleva K, Soler N, Ohashi Y, *et al*. Structure and flexibility of the endosomal Vps34 complex reveals the basis of its function on membranes. *Science*. 2015;350(6257):aac7365. doi:10.1126/science.aac7365

Sanchatjate S, Schekman R. Chs5/6 complex: a multiprotein complex that interacts with and conveys chitin synthase III from the trans-Golgi network to the cell surface. *Mol Biol Cell*. 2006;17(10):4157-4166. doi:10.1091/mbc.e06-03-0210

Sapmaz A, Erson-Bensan AE. EGFR endocytosis: more than meets the eye. *Oncotarget*. 2023;14:297-301. Published 2023 Apr 10. doi:10.18632/oncotarget.28400

Schuh AL, Audhya A. The ESCRT machinery: from the plasma membrane to endosomes and back again. *Crit Rev Biochem Mol Biol*. 2014;49(3):242-261. doi:10.3109/10409238.2014.881777

Seaman MN, Marcusson EG, Cereghino JL, Emr SD. Endosome to Golgi retrieval of the vacuolar protein sorting receptor, Vps10p, requires the function of the VPS29, VPS30, and VPS35 gene products. *J Cell Biol*. 1997;137(1):79-92. doi:10.1083/jcb.137.1.79

Seaman MN, McCaffery JM, Emr SD. A membrane coat complex essential for endosome-to-Golgi retrograde transport in yeast. *J Cell Biol*. 1998;142(3):665-681. doi:10.1083/jcb.142.3.665

Seaman MN. The retromer complex - endosomal protein recycling and beyond. *J Cell Sci*. 2012;125(Pt 20):4693-4702. doi:10.1242/jcs.103440

Shevchenko A, Simons K. Lipidomics: coming to grips with lipid diversity. *Nat Rev Mol Cell Biol*. 2010;11(8):593-598. doi:10.1038/nrm2934

Schindelin J, Arganda-Carreras I, Frise E, *et al*. Fiji: an open-source platform for biological-image analysis. *Nat Methods*. 2012;9(7):676-682. Published 2012 Jun 28. doi:10.1038/nmeth.2019

Shinoda H, Shannon M, Nagai T. Fluorescent Proteins for Investigating Biological Events in Acidic Environments. *Int J Mol Sci*. 2018;19(6):1548. Published 2018 May 23. doi:10.3390/ijms19061548

Shortill SP, Frier MS, Wongsangaroonsri P, Davey M, Conibear E. The VINE complex is an endosomal VPS9-domain GEF and SNX-BAR coat. *Elife*. 2022;11:e77035. Published 2022 Aug 8. doi:10.7554/eLife.77035

Sikorski RS, Hieter P. A system of shuttle vectors and yeast host strains designed for efficient manipulation of DNA in Saccharomyces cerevisiae. *Genetics*. 1989;122(1):19-27. doi:10.1093/genetics/122.1.19

Singer-Krüger B, Stenmark H, Düsterhöft A, *et al*. Role of three rab5-like GTPases, Ypt51p, Ypt52p, and Ypt53p, in the endocytic and vacuolar protein sorting pathways of yeast. *J Cell Biol*. 1994;125(2):283-298. doi:10.1083/jcb.125.2.283

Steinman RM, Mellman IS, Muller WA, Cohn ZA. Endocytosis and the recycling of plasma membrane. *J Cell Biol*. 1983;96(1):1-27. doi:10.1083/jcb.96.1.1

Sun Y, Drubin DG. The functions of anionic phospholipids during clathrin-mediated endocytosis site initiation and vesicle formation. *J Cell Sci*. 2012;125(Pt 24):6157-6165. doi:10.1242/jcs.115741

Suzuki SW, Chuang YS, Li M, Seaman MNJ, Emr SD. A bipartite sorting signal ensures specificity of retromer complex in membrane protein recycling. *J Cell Biol*. 2019;218(9):2876-2886. doi:10.1083/jcb.201901019

Suzuki SW, Emr SD. Membrane protein recycling from the vacuole/lysosome membrane. *J Cell Biol*. 2018;217(5):1623-1632. doi:10.1083/jcb.201709162

Trautwein M, Schindler C, Gauss R, Dengjel J, Hartmann E, Spang A. Arf1p, Chs5p and the ChAPs are required for export of specialized cargo from the Golgi. *EMBO J*. 2006;25(5):943-954. doi:10.1038/sj.emboj.7601007

Uchida Y, Hasegawa J, Chinnapen D, *et al*. Intracellular phosphatidylserine is essential for retrograde membrane traffic through endosomes. *Proc Natl Acad Sci U S A*. 2011;108(38):15846-15851. doi:10.1073/pnas.1109101108

Vance JE, Steenbergen R. Metabolism and functions of phosphatidylserine. *Prog Lipid Res*. 2005;44(4):207-234. doi:10.1016/j.plipres.2005.05.001

Vance JE. Phosphatidylserine and phosphatidylethanolamine in mammalian cells: two metabolically related aminophospholipids. *J Lipid Res*. 2008;49(7):1377-1387. doi:10.1194/jlr.R700020-JLR200

Vance JE. Phospholipid synthesis in a membrane fraction associated with mitochondria. *J Biol Chem*. 1990;265(13):7248-7256.

van Weering JR, Verkade P, Cullen PJ. SNX-BAR proteins in phosphoinositide-mediated, tubular-based endosomal sorting. *Semin Cell Dev Biol*. 2010;21(4):371-380. doi:10.1016/j.semcdb.2009.11.009

Vida TA, Emr SD. A new vital stain for visualizing vacuolar membrane dynamics and endocytosis in yeast. *J Cell Biol*. 1995;128(5):779-792. doi:10.1083/jcb.128.5.779

Wenk MR. The emerging field of lipidomics [published correction appears in Nat Rev Drug Discov. 2005 Sep;4(9):725]. *Nat Rev Drug Discov*. 2005;4(7):594-610. doi:10.1038/nrd1776

Whyte JR, Munro S. A yeast homolog of the mammalian mannose 6-phosphate receptors contributes to the sorting of vacuolar hydrolases. *Curr Biol*. 2001;11(13):1074-1078. doi:10.1016/s0960-9822(01)00273-1

Wurmser AE, Emr SD. Phosphoinositide signaling and turnover: PtdIns(3)P, a regulator of membrane traffic, is transported to the vacuole and degraded by a process that requires lumenal vacuolar hydrolase activities. *EMBO J*. 1998;17(17):4930-4942. doi:10.1093/emboj/17.17.4930

Xu P, Baldridge RD, Chi RJ, Burd CG, Graham TR. Phosphatidylserine flipping enhances membrane curvature and negative charge required for vesicular transport. *J Cell Biol*. 2013;202(6):875-886. doi:10.1083/jcb.201305094

Yamamoto H, Kakuta S, Watanabe TM, *et al*. Atg9 vesicles are an important membrane source during early steps of autophagosome formation. *J Cell Biol*. 2012;198(2):219-233. doi:10.1083/jcb.201202061

Yang Y, Lee M, Fairn GD. Phospholipid subcellular localization and dynamics. *J Biol Chem*. 2018;293(17):6230-6240. doi:10.1074/jbc.R117.000582

Yang Y. Investigating the roles of anionic phospholipids in endocytic trafficking in mammalian and *S. cerevisiae* cells. Unpublished.

Yeung T, Gilbert GE, Shi J, Silvius J, Kapus A, Grinstein S. Membrane phosphatidylserine regulates surface charge and protein localization. *Science*. 2008;319(5860):210-213. doi:10.1126/science.1152066

Zhu J, Zhang ZT, Tang SW, *et al*. A Validated Set of Fluorescent-Protein-Based Markers for Major Organelles in Yeast (Saccharomyces cerevisiae). *mBio*. 2019;10(5):e01691-19. Published 2019 Sep 3. doi:10.1128/mBio.01691-19

Zerial M, McBride H. Rab proteins as membrane organizers [published correction appears in Nat Rev Mol Cell Biol 2001 Mar;2(3):216]. *Nat Rev Mol Cell Biol*. 2001;2(2):107-117. doi:10.1038/35052055

Zinser E, Paltauf F, Daum G. Sterol composition of yeast organelle membranes and subcellular distribution of enzymes involved in sterol metabolism. *J Bacteriol*. 1993;175(10):2853-2858. doi:10.1128/jb.175.10.2853-2858.1993

Zinser E, Sperka-Gottlieb CD, Fasch EV, Kohlwein SD, Paltauf F, Daum G. Phospholipid synthesis and lipid composition of subcellular membranes in the unicellular eukaryote Saccharomyces cerevisiae. *J Bacteriol*. 1991;173(6):2026-2034. doi:10.1128/jb.173.6.2026-2034.1991